Quantum Phenomena in Molecular Graphene Device and Metal-Organic Coordination Frameworks

Xiaobo Wang

Supervisor: Prof. Nian LIN

Department of Physics, The Hong Kong University of Science and Technology, Clear Water Bay, Hong Kong

OUTLINE

Introduction one

Functionalizing of graphene and decoupling of 2D-MOF using graphene substrate

Part 1 The Spin Resonant Scattering of Epitaxial Iron Phthalocyanine Molecules on Graphene on h-BN device

Part 2 $\mathbf{Cu_2(C_6O_6)}$ Metal-Organic Monolayer Grown on Silicon Carbide Epitaxial Graphene

Introduction two

Orbital design of 2D-MOFs with complex orbital symmetry

Part 3 Two-Dimensional Metal-Organic Fe-porphyrin Coordination framework Exhibiting Mixed Spin States

Part 4 Two-Dimensional Metal Organic Framework with p-Orbital Honeycomb Kagome Lattice

Introduction

Introduction one

Functionalizing of graphene and decoupling of 2D-MOFs using graphene substrate

Theoretical predicted quantum phenomena in 2D-MOFs

Organic topological insulator

$Ni_3C_{12}S_{12}$

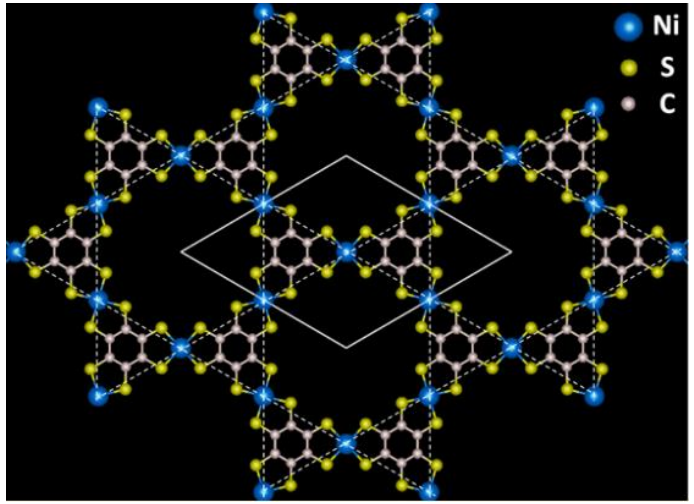

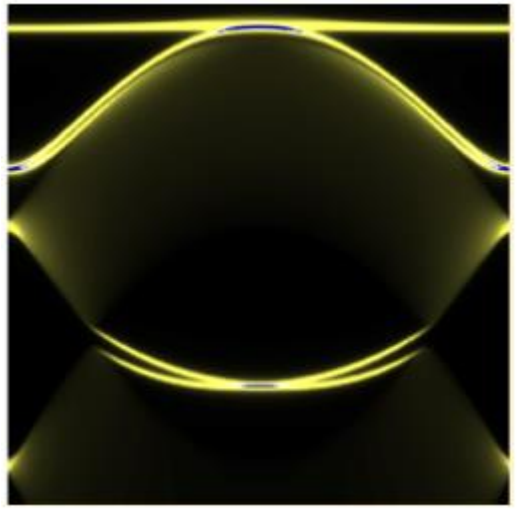

Nano Lett. 2013, 13, 2842−2845

Organic topological Chern insulator

$Mn_2C_{18}H_{12}$

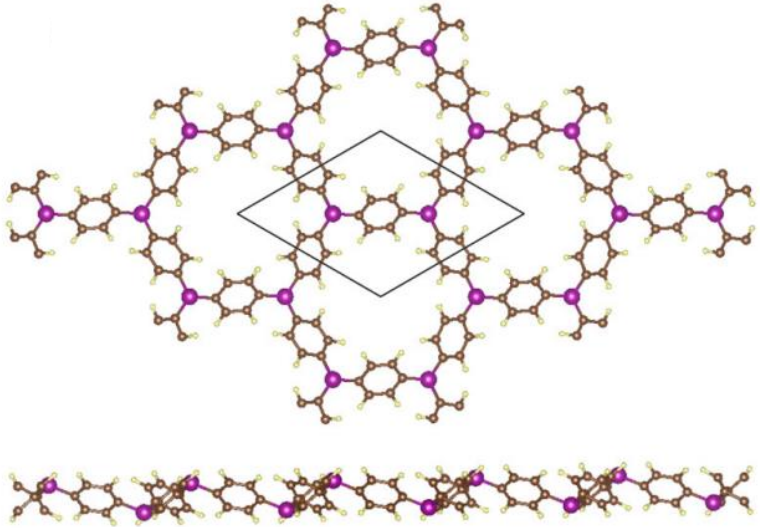

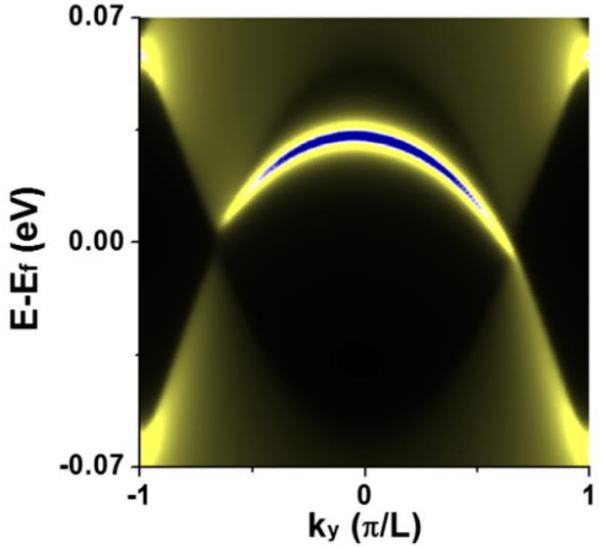

PRL 110, 196801 (2013)

Organic 2D superconductivity

Cu-BHT

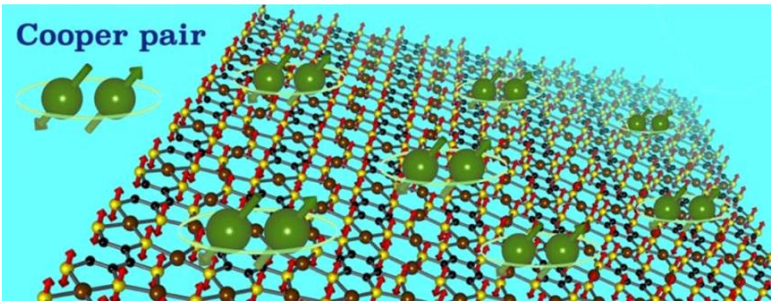

2D s-wave $T_c = 4.43K$

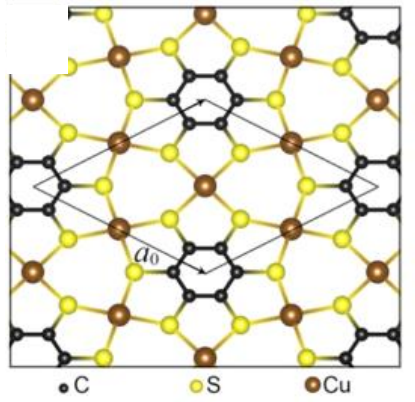

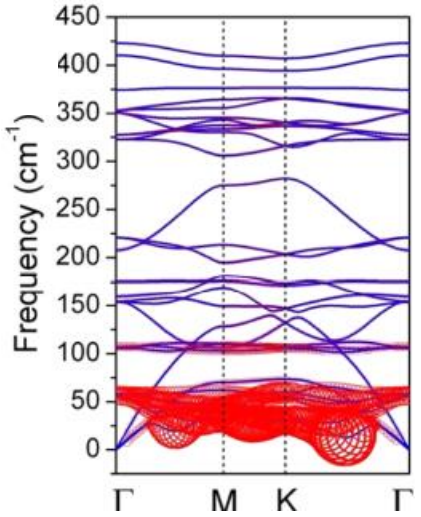

Nano Lett. 2017, 17, 6166−6170

Synthesis of two-dimensional metal organic frameworks (2D-MOFs)

Synthetic strategies for 2D-MOFs

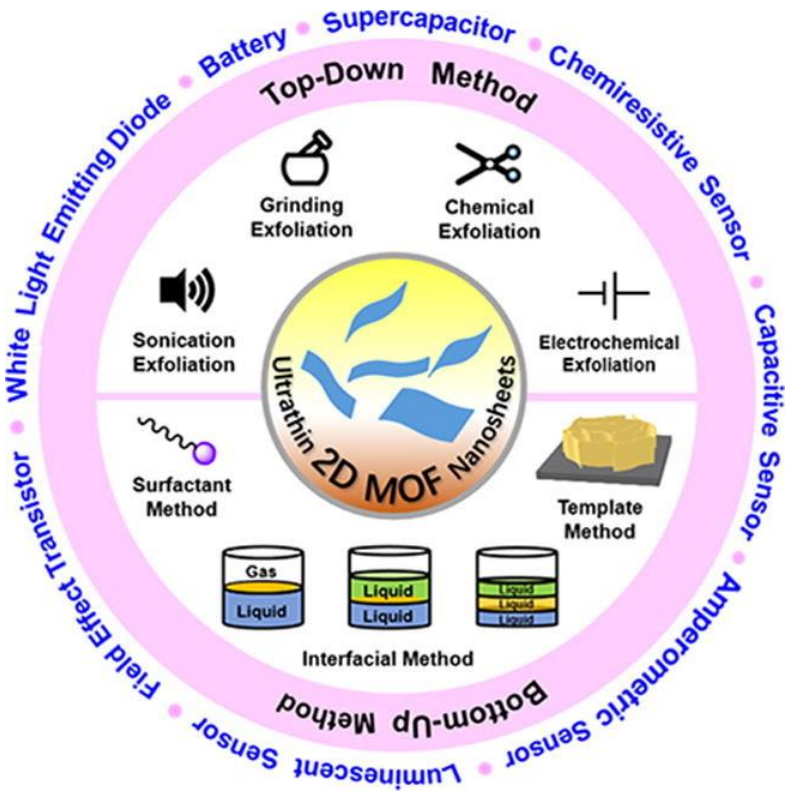

Top-down and bottom-up approaches to 2D MOFs synthesis

Difficult to obtain single-layer 2D-MOF structure

On surface synthesis of single-layer 2D-MOFs

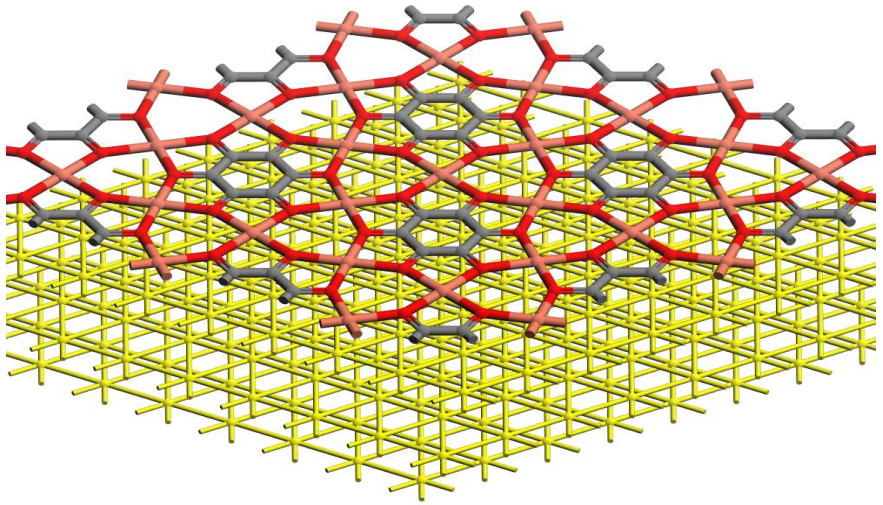

advantages

Effective surface catalysis and surface confinement

Obtain single-layer 2D-MOF structure

Chin. J. Chem., **2018**, 36, 754 − 764

Synthesis of two-dimensional metal organic frameworks (2D-MOFs)

Synthetic strategies for 2D-MOFs

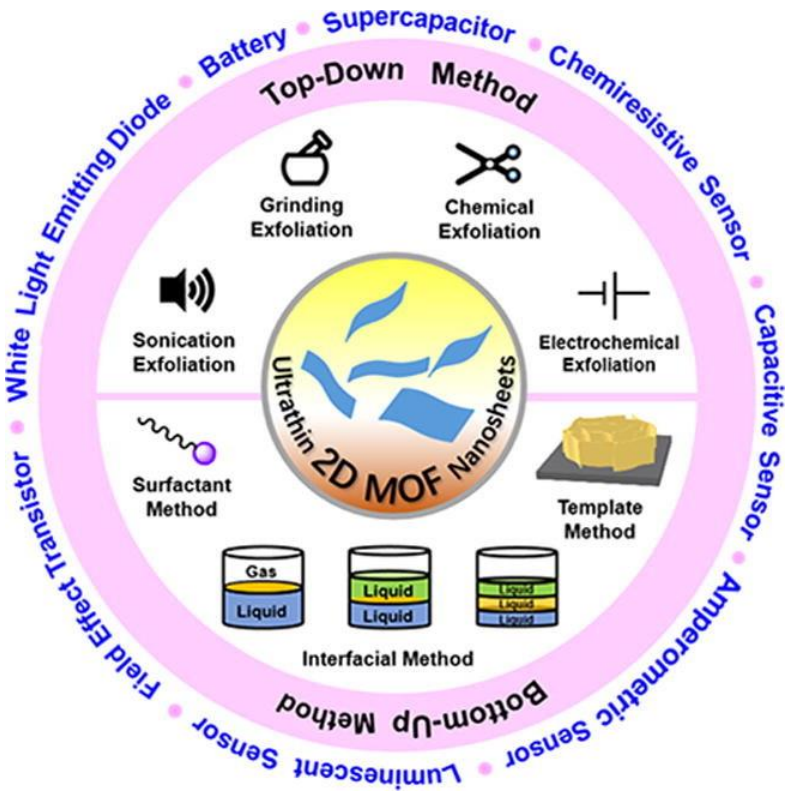

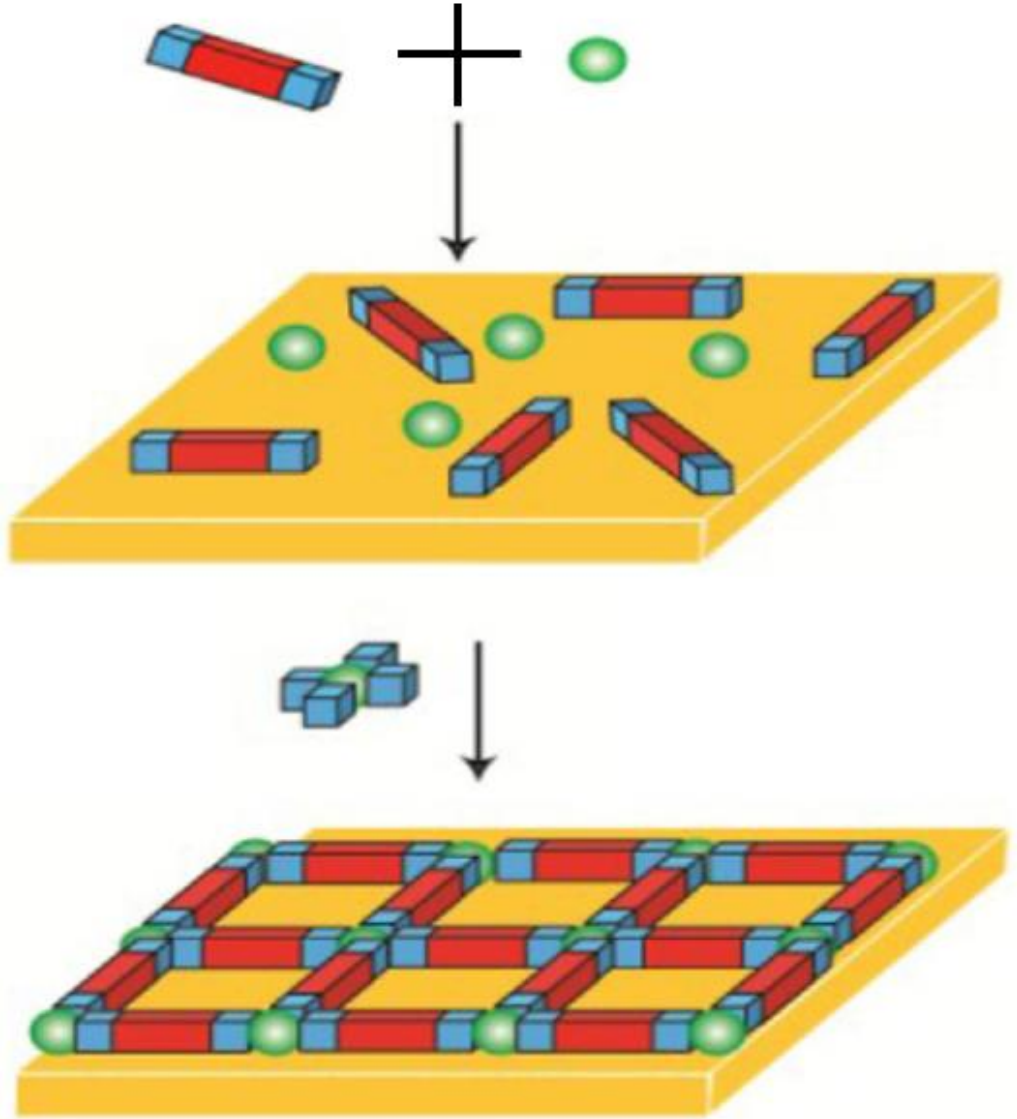

Top-down and bottom-up approaches to 2D MOFs synthesis

Difficult to obtain single-layer 2D-MOF structure

Chin. J. Chem., **2018**, 36, 754 − 764

Decoupling of 2D-MOFs

Most of 2D-MOFs grown on metal substrates

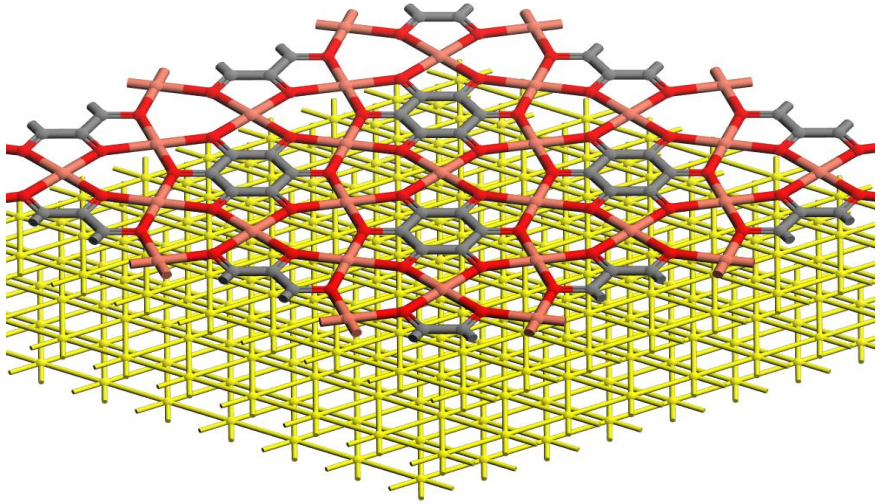

Screen effect **Smearing**

Intrinsic electronic properties of MOF are absent

Weak coupling substrate

Graphene

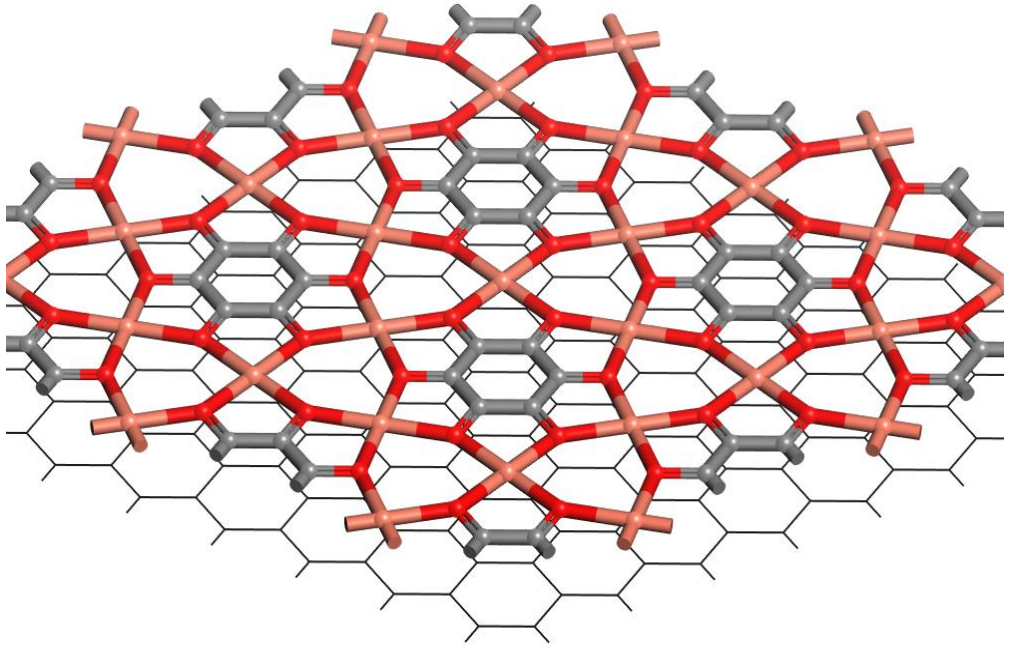

Intrinsic electronic properties are preserved

Motivation of fabricating organic/graphene heterostructure

Decoupling of the 2D-MOF structure

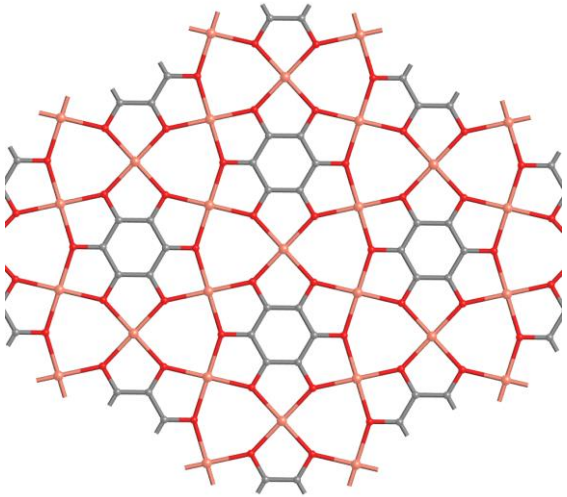

Close to free-standing 2D-MOF

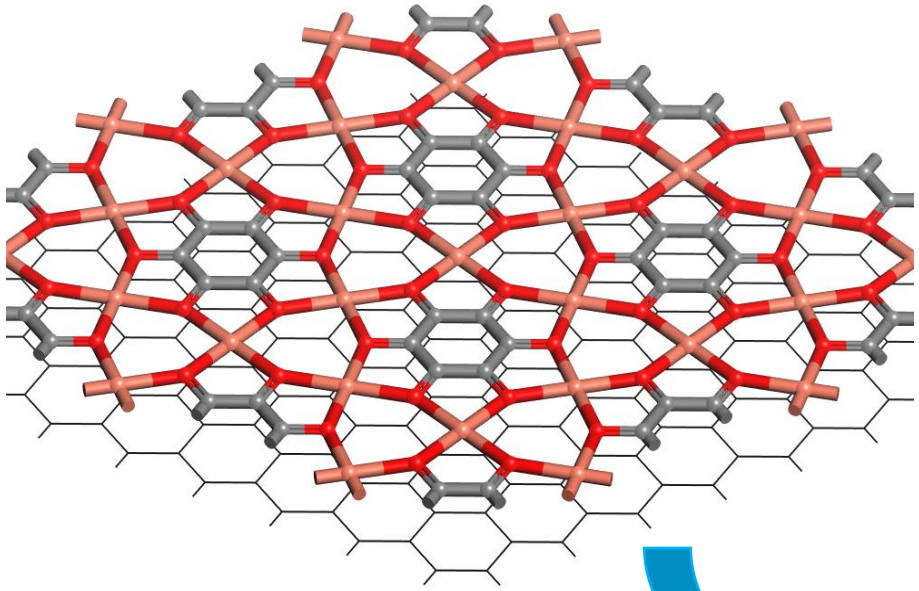

Functionalized Graphene

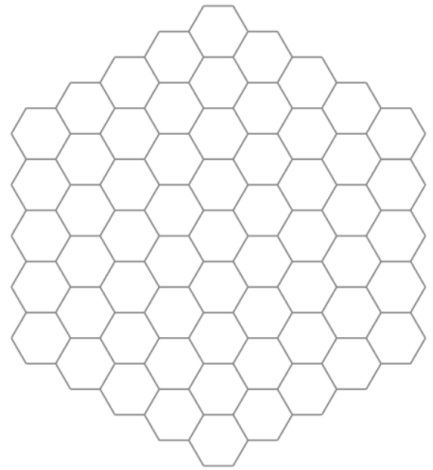

Functionalizing of graphene

Graphene

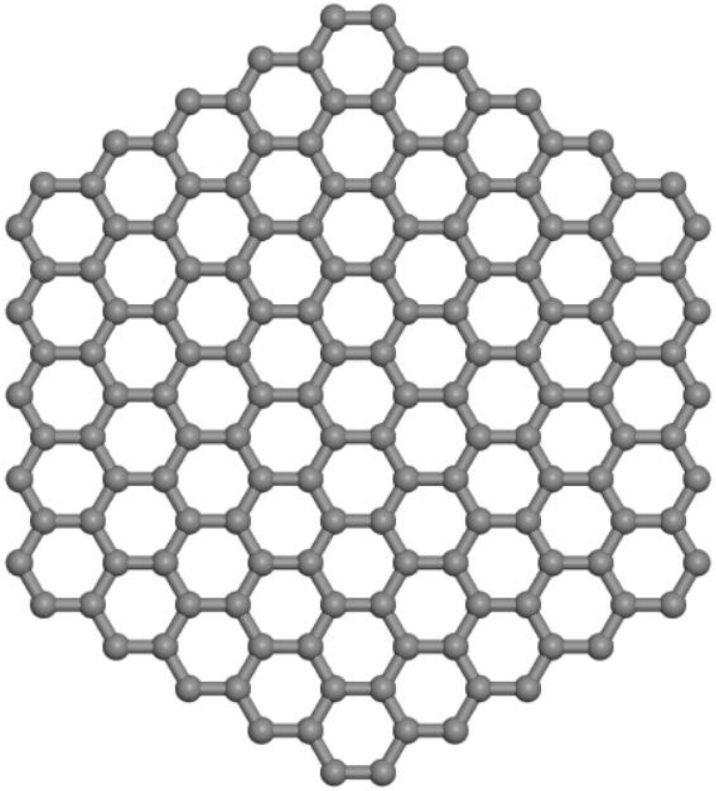

Graphene lattice

Weak SOC

gapless

~μeV

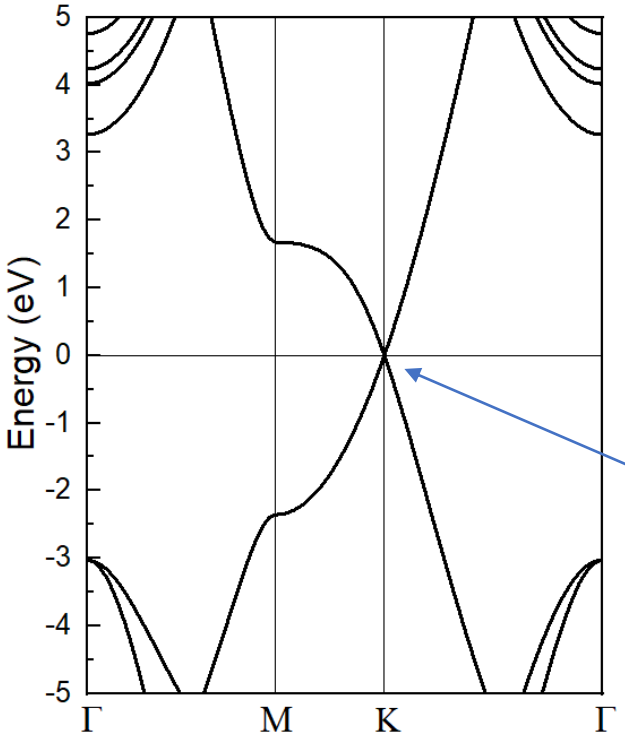

$$H_\kappa(k) = \kappa v_F k \cdot \sigma_\kappa$$

Dirac cone

Graphene band strucutre

Without magnetism

Time-reversal symmetry

Functionalizing of graphene

Theoretical predicted material in realizing quantum anomalous Hall effect

3d metal adatoms on graphene

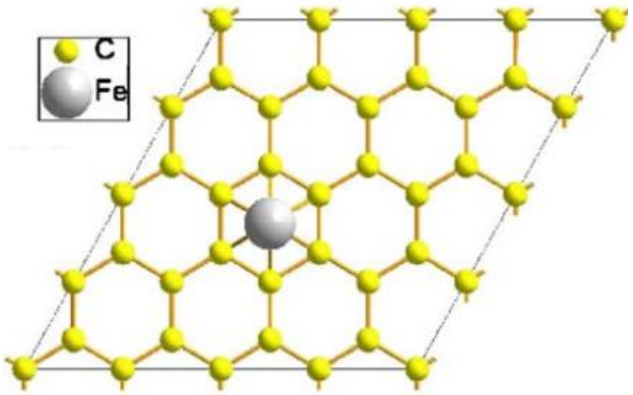

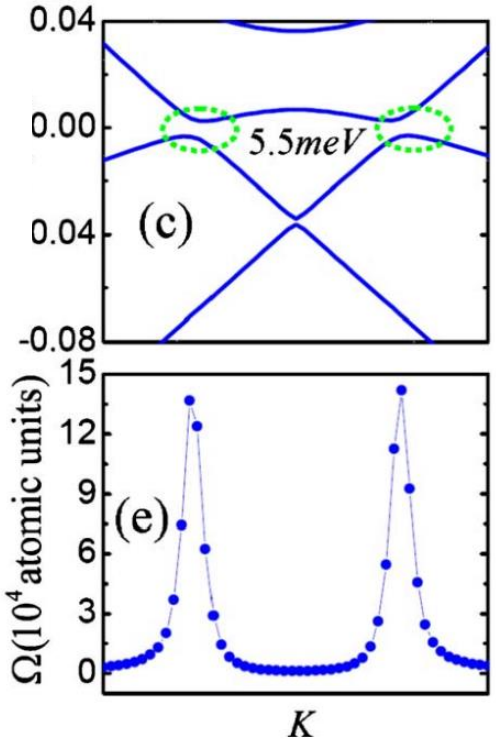

Difficulty → Metal cluster on graphene

PRB 82, 161414 (2010)

Effective spin doping using molecules

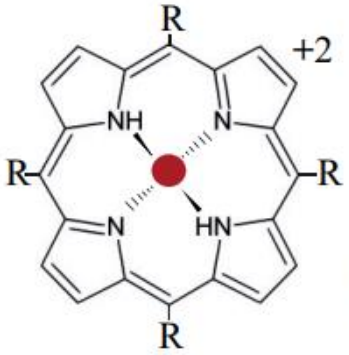

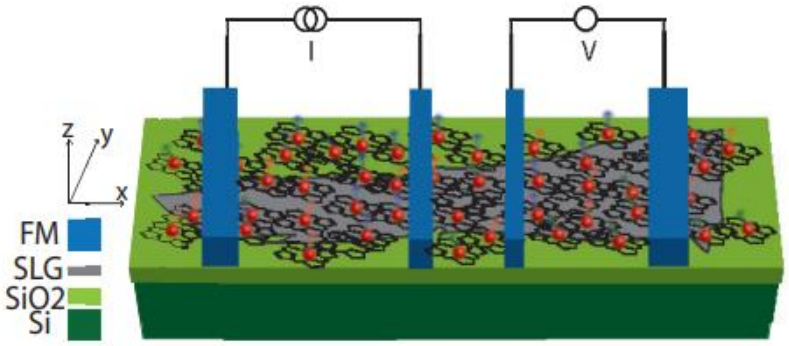

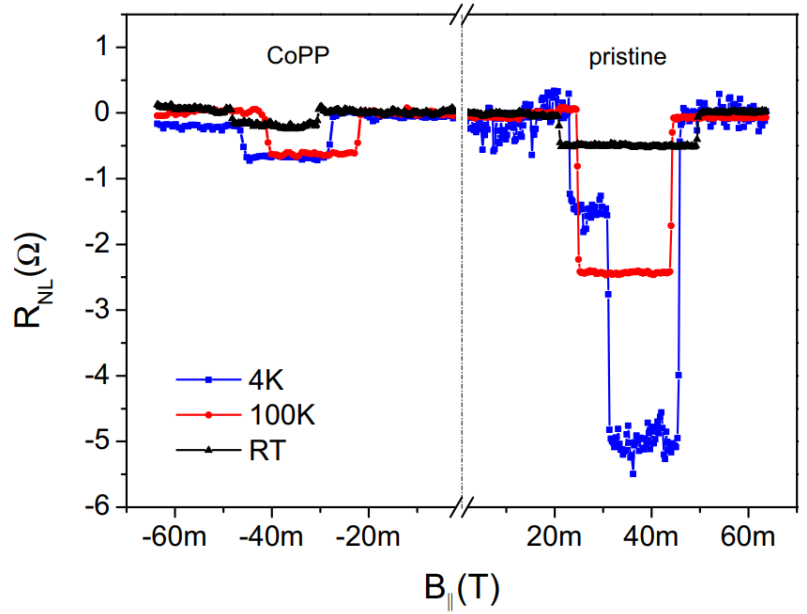

PRB 92, 115442 (2015)

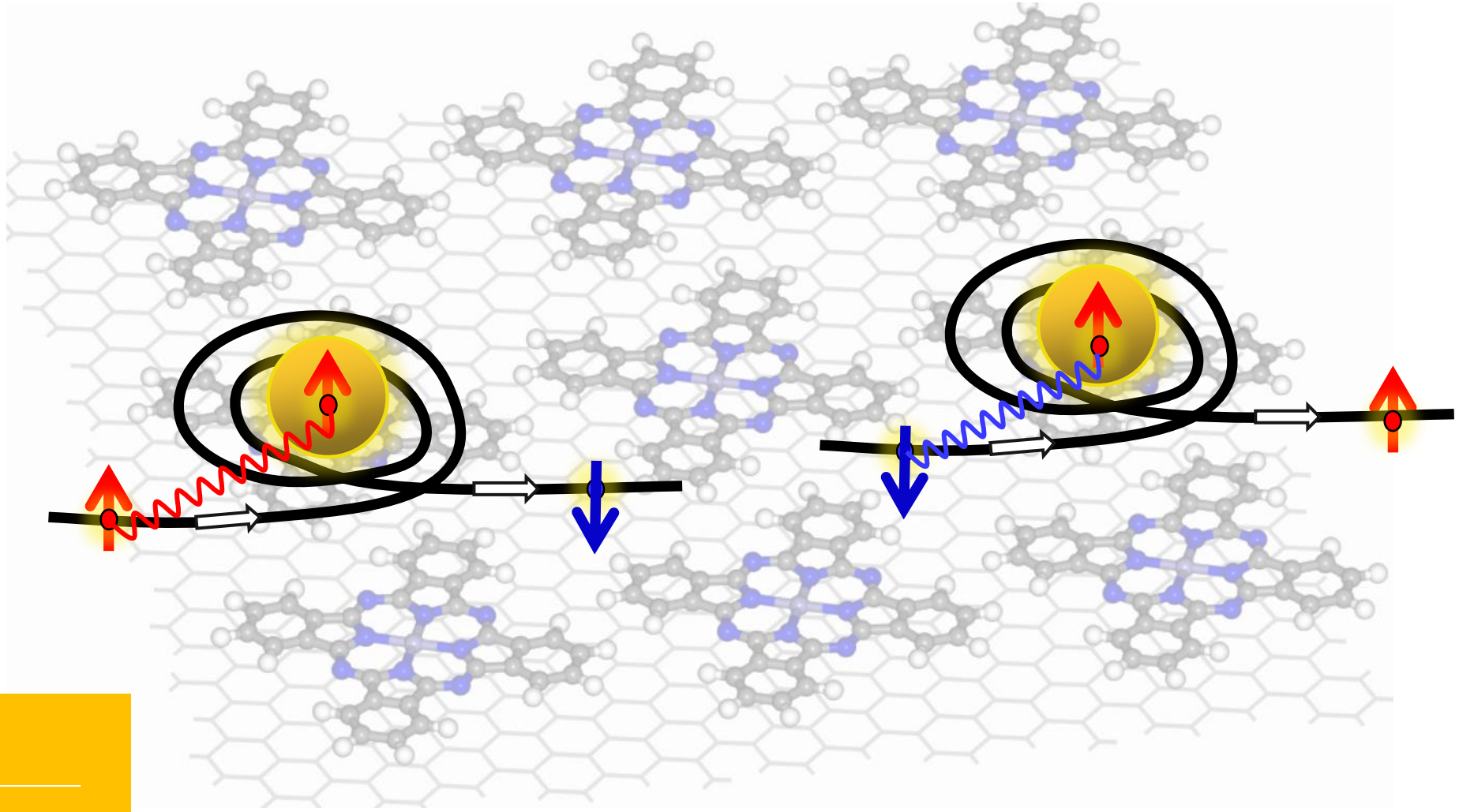

PART 01

Part 1 The Spin Resonant Scattering of Epitaxial Iron Phthalocyanine Molecules on Graphene on h-BN device

Resonant Scattering

Nonmagnetic resonant scattering

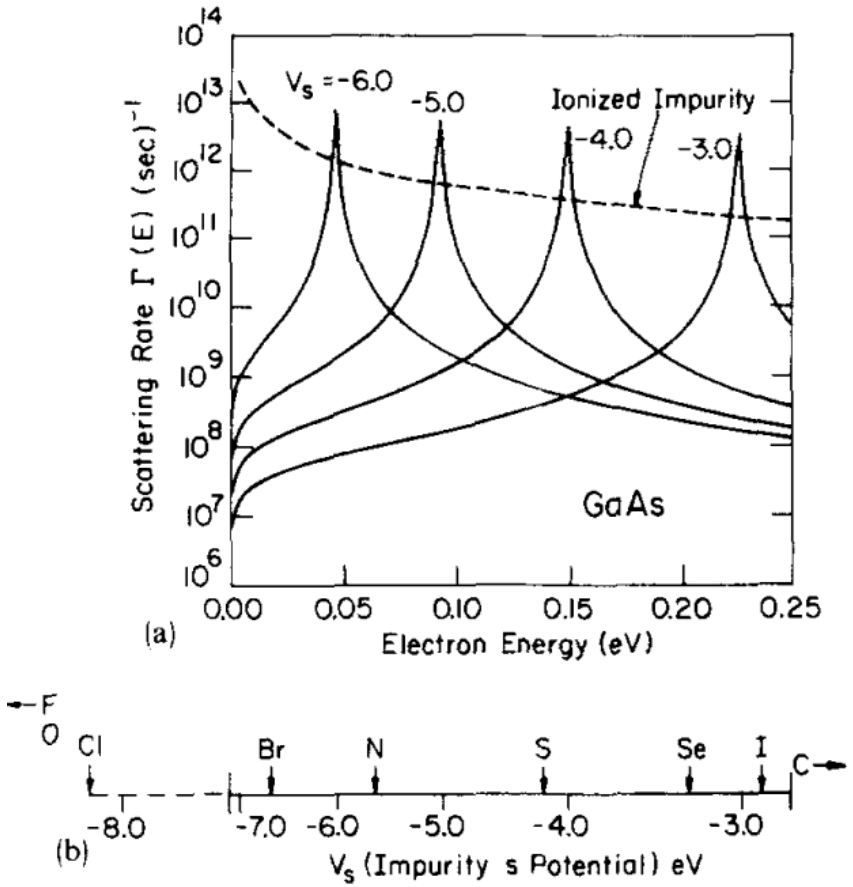

Doped Semiconductor GaAs

Tune the electron energy close to nonmagnetic impurity energy level and $J = 0$

The resonance occurs at the energy of sharp peak

Tune the spin electron energy close to magnetic impurity energy level and $J \neq 0$

The resonance occurs at the energy of two peaks which correspond to spin single and triple states with antiferromagnetic and ferromagnetic coupling

Spin resonant scattering

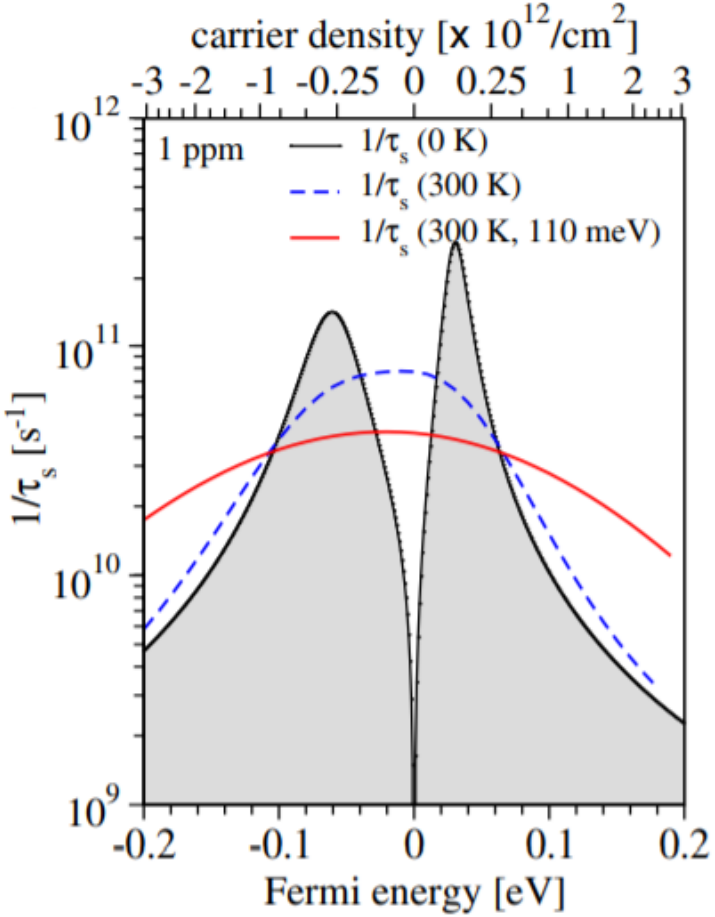

Magnetic impurity functionalized graphene

Appl. Phys. Lett. 41, 664 (1982)

PRL **112.11** 116602 (2014)

Molecular graphene device preparation

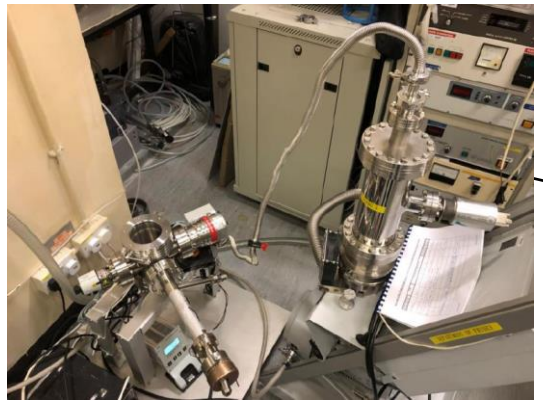

Thin film growing chamber

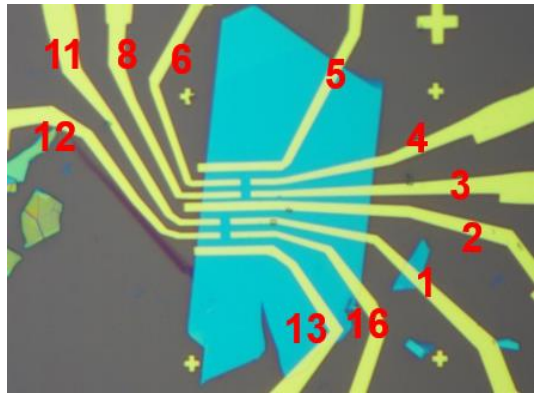

Graphene on h-BN device

Sketch Map

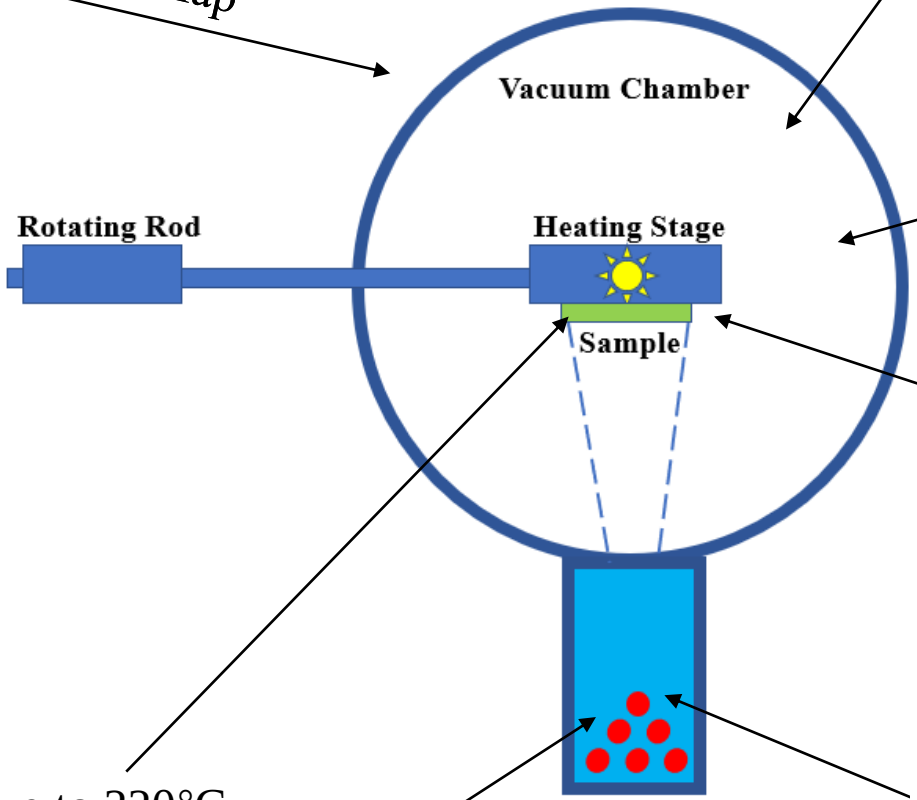

Base pressure 4.8×10^{-9}hPa

During deposition 1.7×10^{-7}hPa

Substrate was maintained at 135 °C to increase crystallization of FePc

Annealing the device with 10 hours up to 220°C

Sigma-Aldrich FePc was loaded into effusion cell and out-gassed for several hours before deposition.

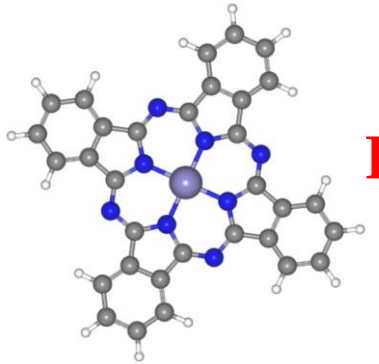

FePc

evaporator temperature of 380°C

Molecular graphene device characterization

Deposit on molybdenum plate

↓ Micro-Raman measurement

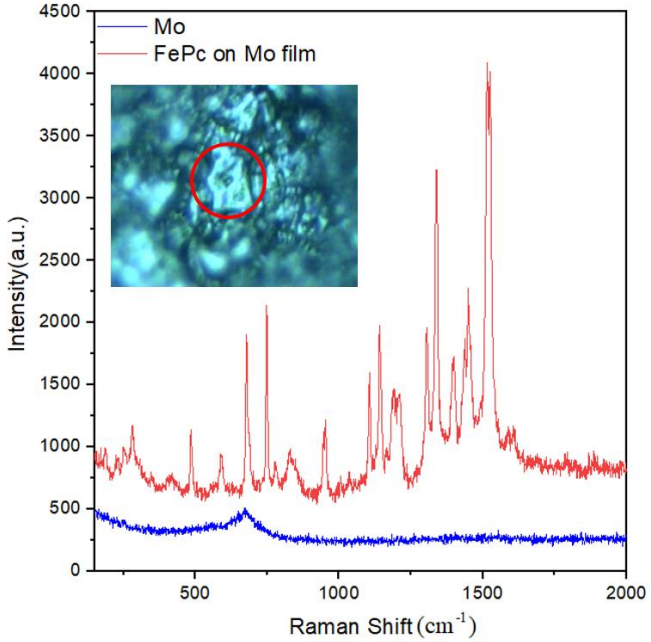

Deposit on HOPG

↓ STM measurement

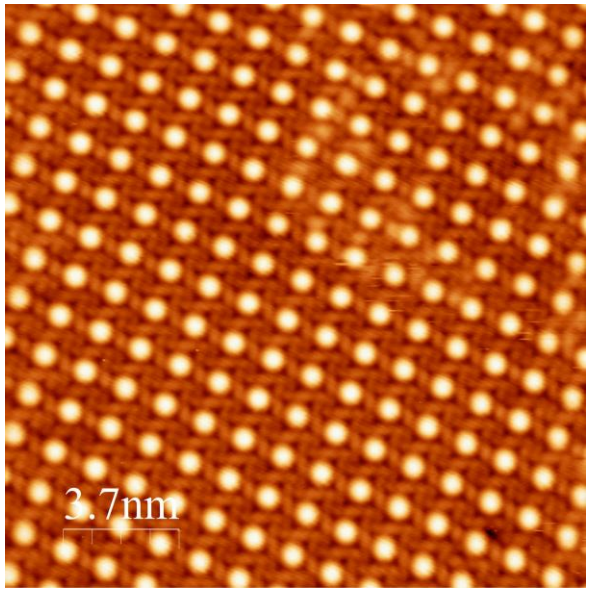

Square lattice

Lattice constant: a=b=1.54 ± 0.05 nm

FePc on graphene on h-BN device

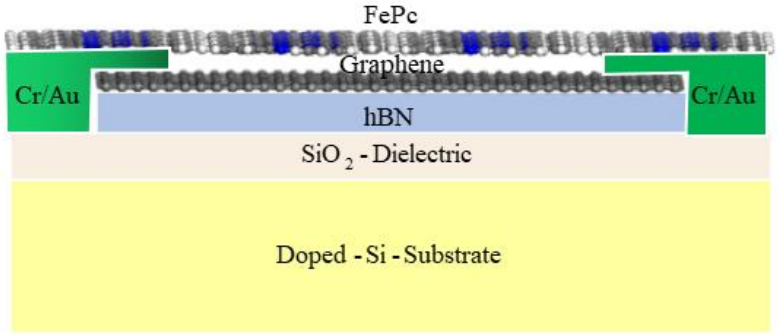

Carrier mobility

↓ Quantum transport measurement

G/BN: 1.39× $10^5 V^{-1}s^{-1}$

↓ FePc

G/BN with FePc: 1.4× $10^4 V^{-1}s^{-1}$

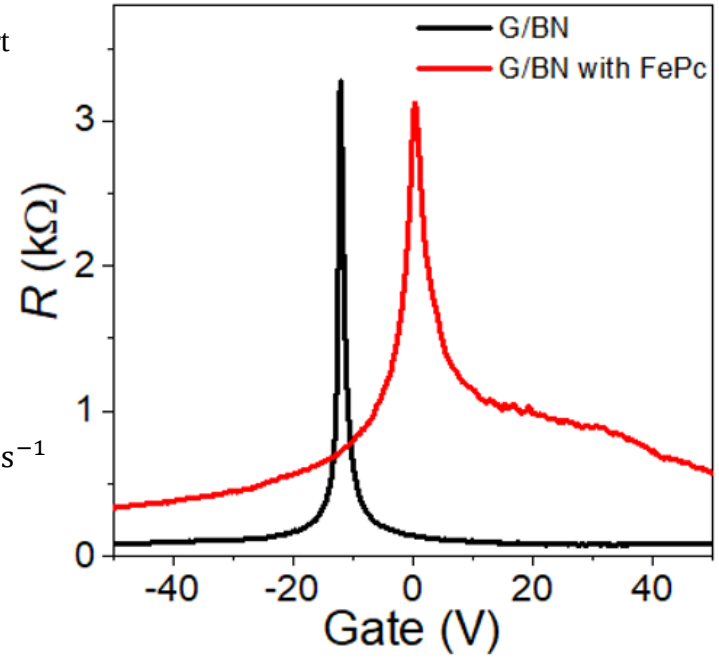

DFT calculations

The localized defect state in FePc graphene heterostructure from DFT calculation

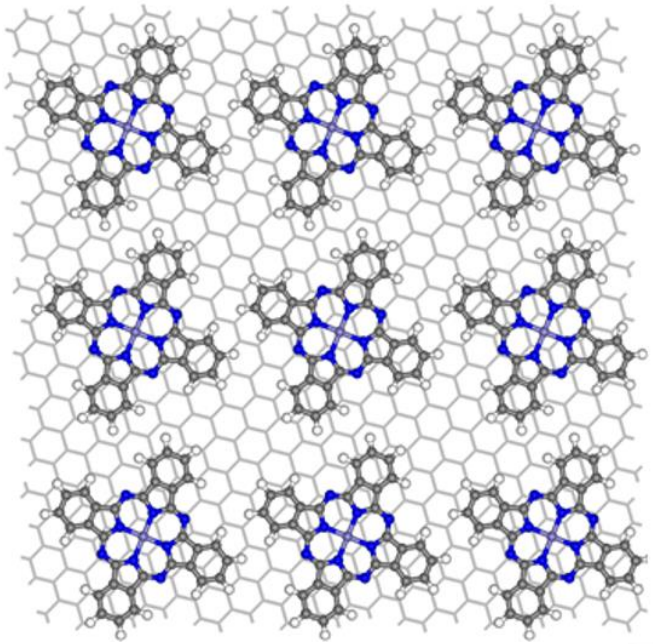

DFT optimized structure

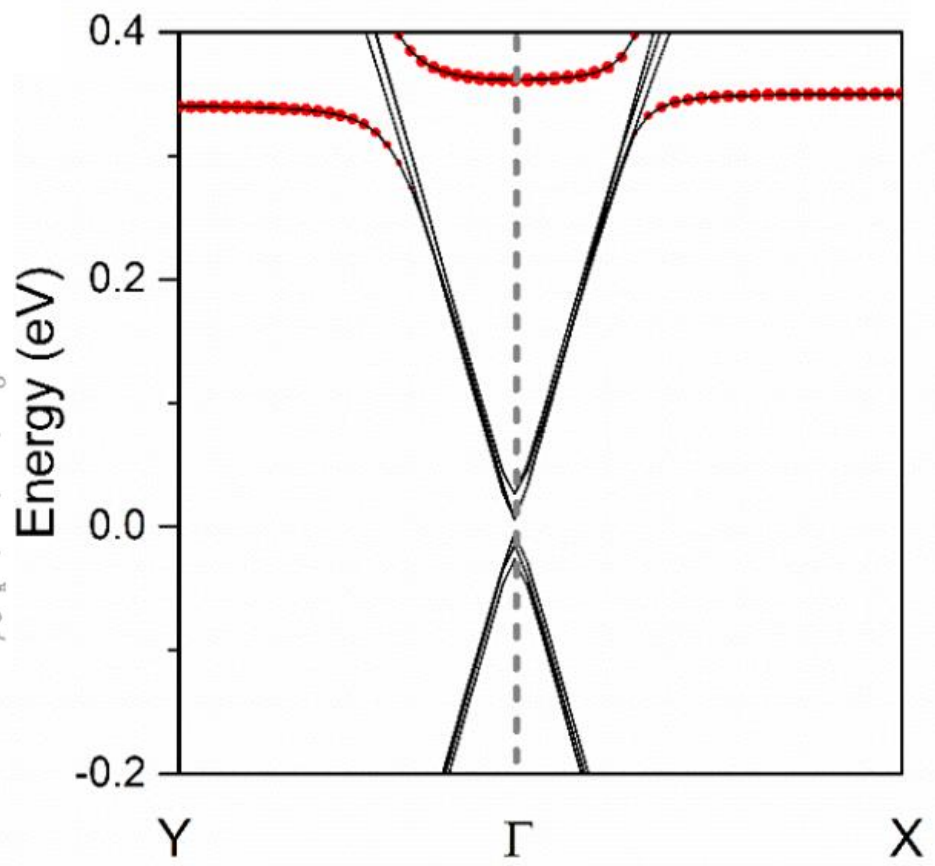

Band structure

Localized defect state contributed by iron 3d-orbital

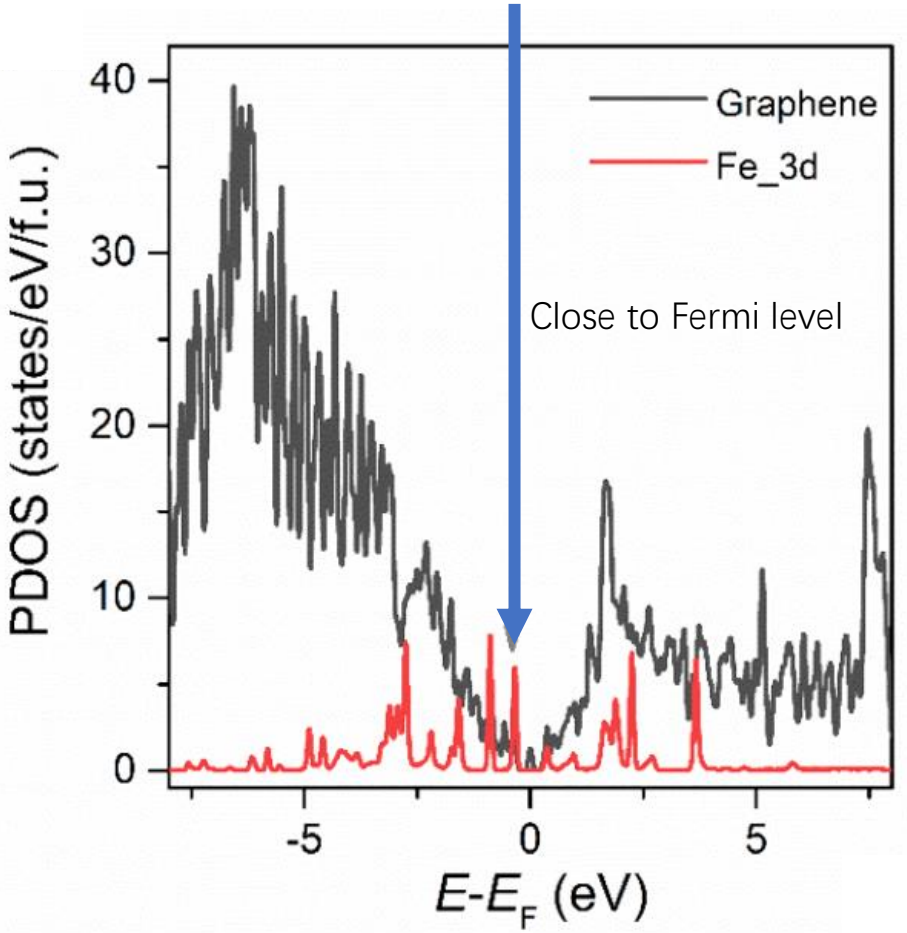

PDOS

Spin-Polarized diffusion electron

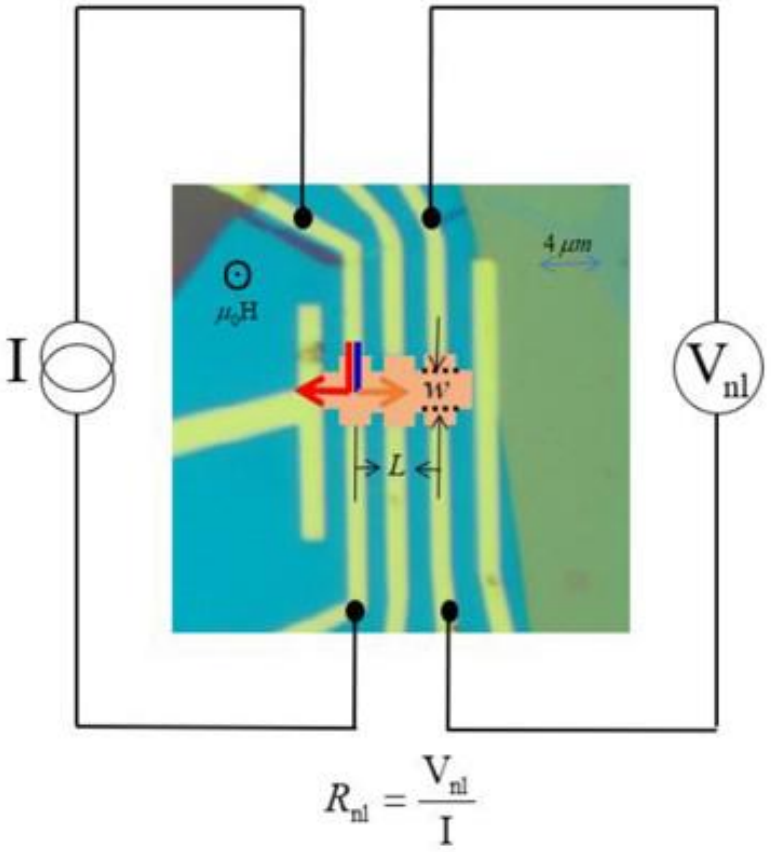

$$R_{nl} = \frac{V_{nl}}{I}$$

Spin injection

Spin resonant scattering

↓

Interplay

↔

Tune the graphene Fermi level near to the energy level of magnetic defect state

Magnetic defect state

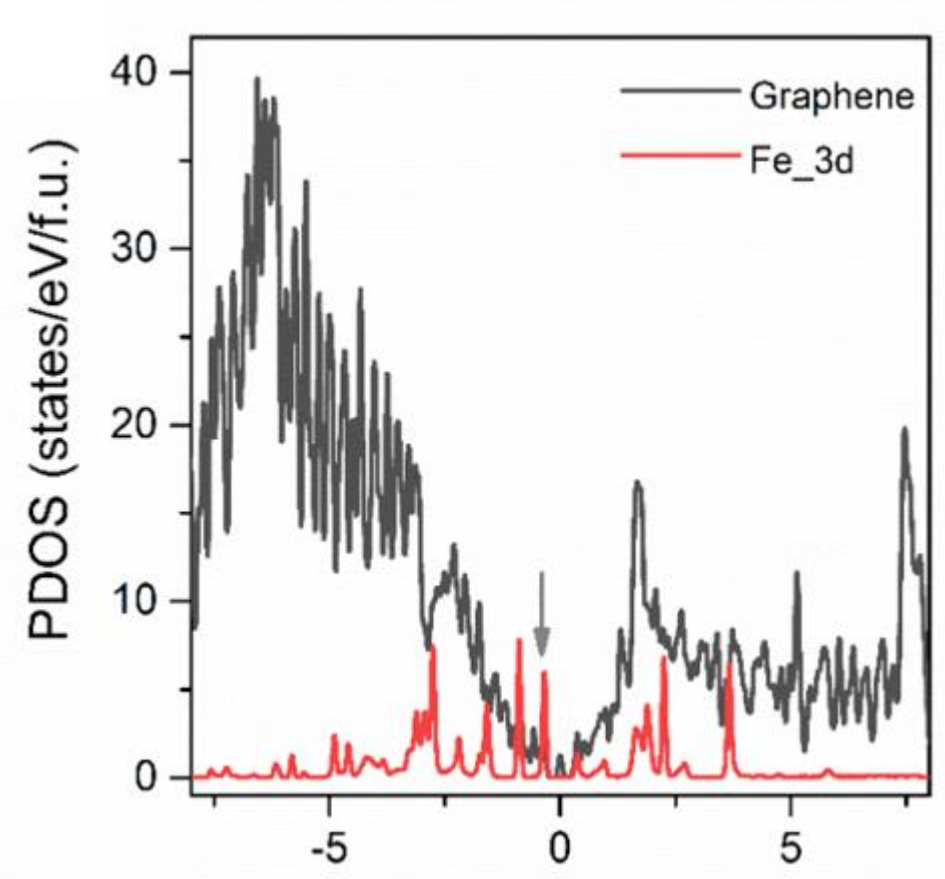

FePc

Interplay of spin-polarized diffusion electron and localized magnetic defect state
-Spin resonant scattering

Theoretical predication

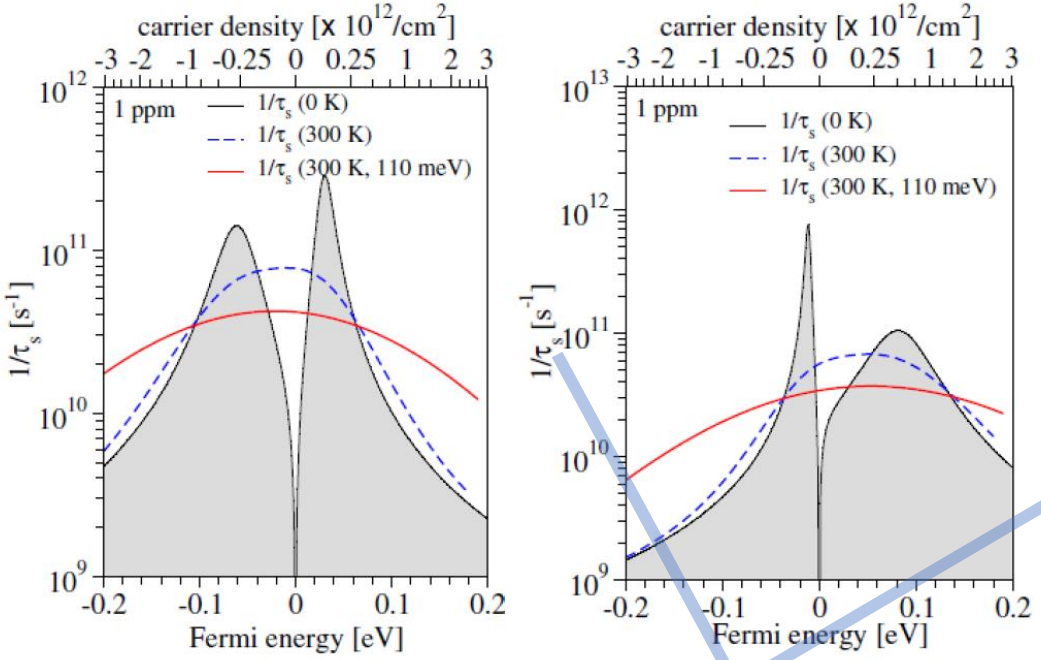

-|J|S. s **+|J|S. s**

The spin relaxation rate shows singlet and triplet split resonance peaks

In nonlocal measurement

$$R_{nl} = \frac{1}{4\rho_{xx}}\left(\frac{\partial\rho_{xy}}{\partial\mu}E_{Zeeman}\right)^2 \frac{w}{l_s}\exp\left(-\frac{L}{l_s}\right), l_s = \sqrt{D_s\tau_s}$$

PRL **112.11** 116602 (2014)

Experimental measurements

Gate-dependent nonlocal measurement of the FePc monolayer functionalized graphene on h-BN device

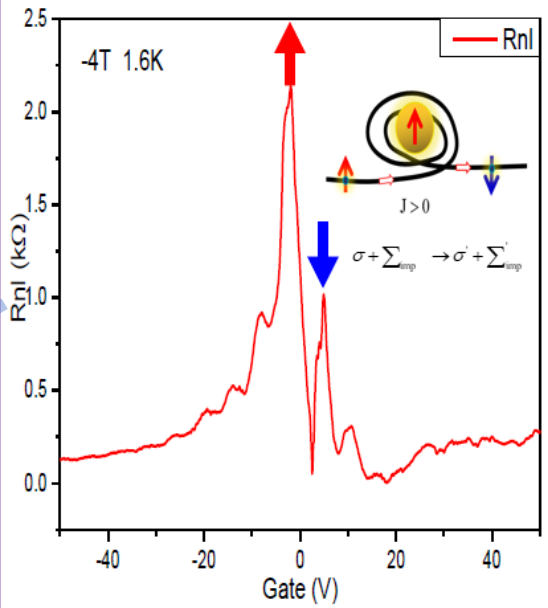

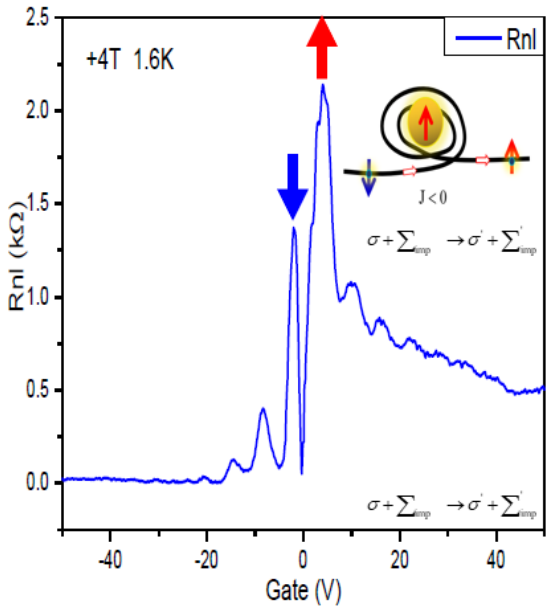

Nonlocal measurements show peaks of ferromagnetic coupling J′ >0 and antiferromagnetic coupling J′ <0

The spin single-state and triple-state transition under gate voltage control

Quasi-bounding states generated by magnetic defect states in graphene

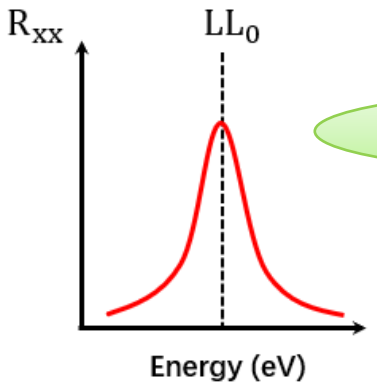

Theoretical predication

Cut

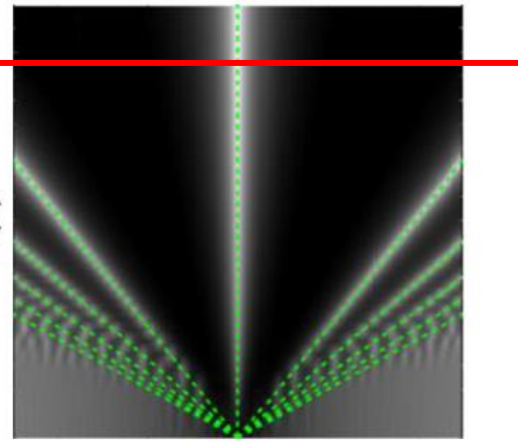

Fan diagram of pristine monolayer graphene

Half-integer quantum Hall effect

Experimental measurements

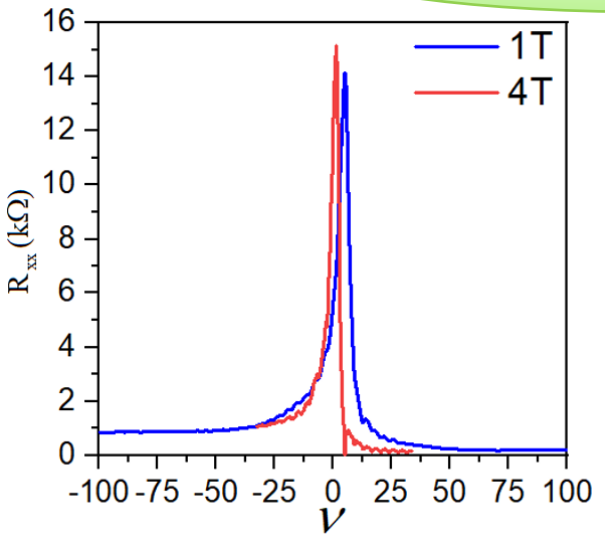

Gate-dependent magnetoresistance of pristine monolayer Graphene

$$\nu = \frac{C_g V_g h}{eB}$$

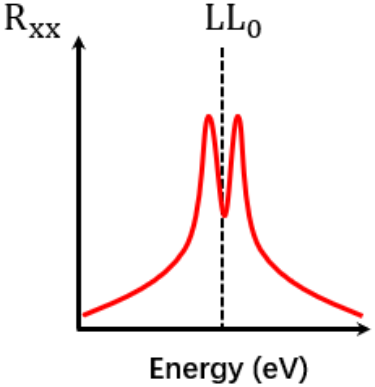

Cut

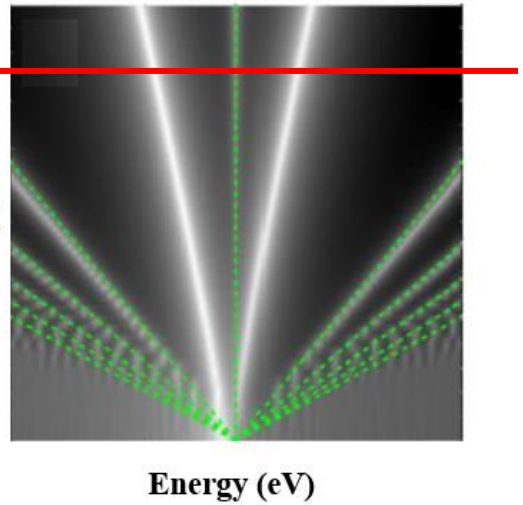

Fan diagram with magnetic impurity on graphene surface

Two Quasi-bounding states separated by LL_0

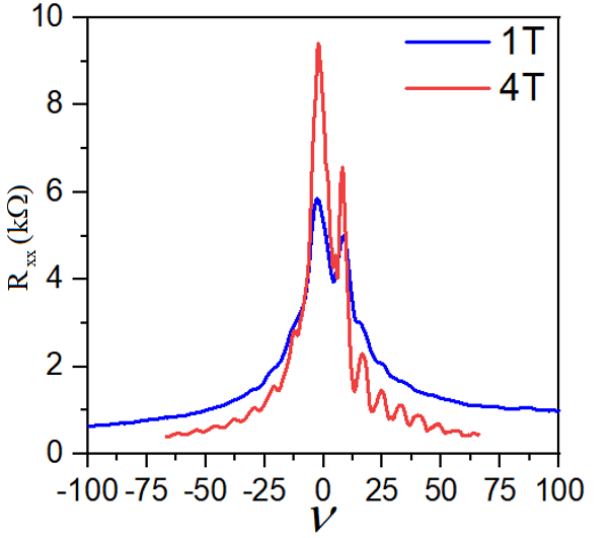

Gate-dependent magnetoresistance of FePc deposited on monolayer Graphene

Quasi-bounding states separated by LL_0

PRB **99.3** 035412 (2019)

Conclusions

The results of interplay with the graphene spin diffusion electrons and ferromagnetic FePc induced periodic magnetic defect state.

(1) The spin resonant scattering associated with spin single-state and triple-state transition under gate control shown in nonlocal measurement.

(2) The quasi-bonding state induced by spin resonant scattering shown in graphene magnetoresistance measurement.

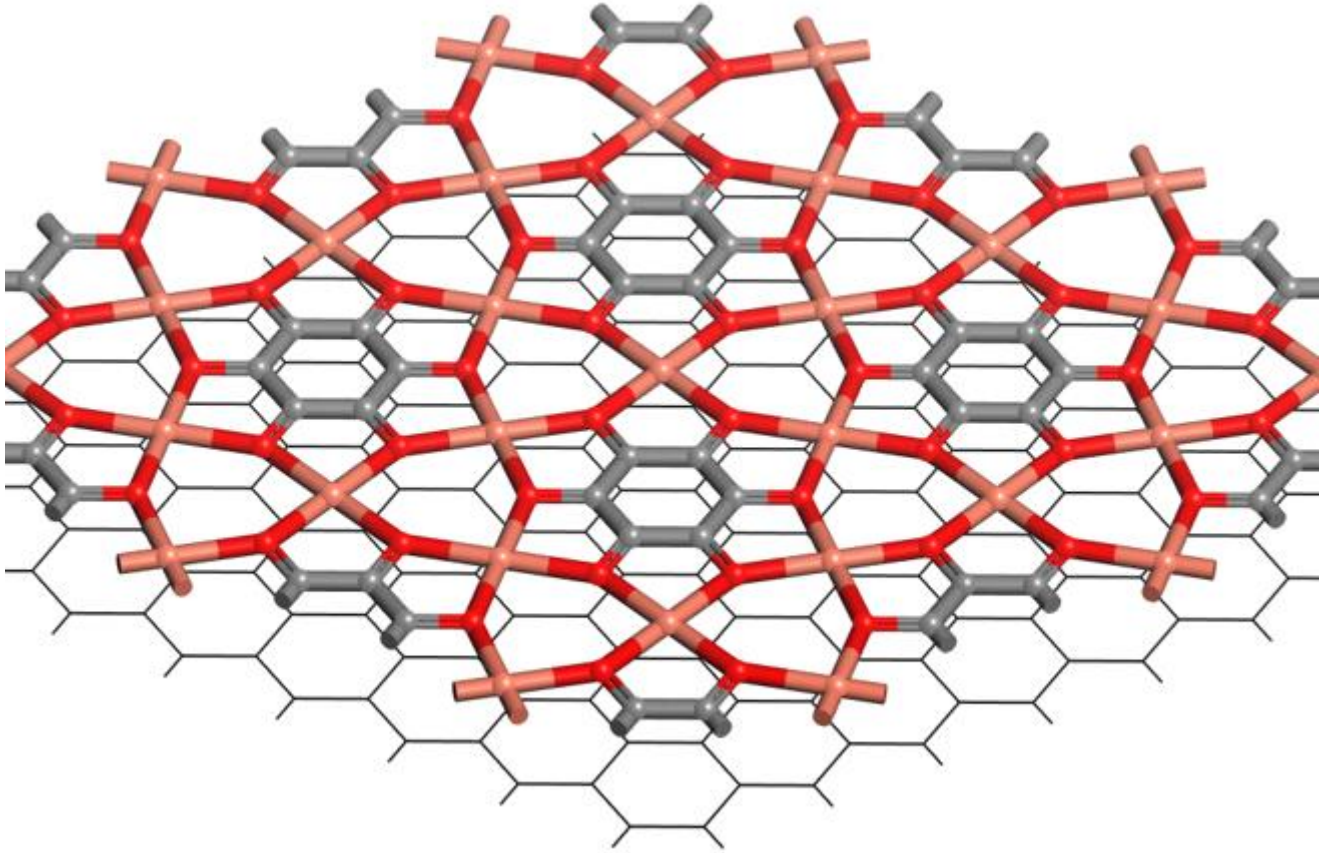

PART 02

Part 2 $\mathbf{Cu_2(C_6O_6)}$ Metal-Organic Monolayer Grown on Silicon Carbide Epitaxial Graphene

Scanning Tunneling Microscopy (STM)

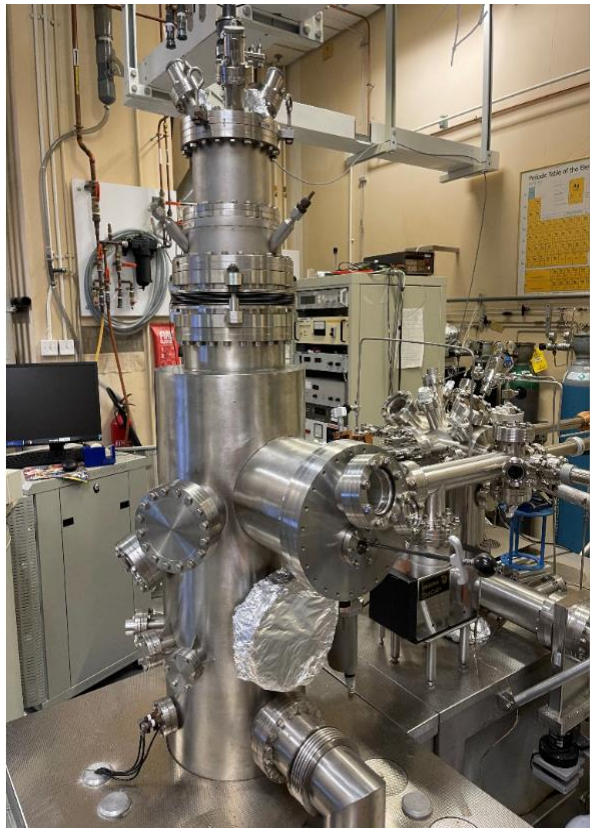

An overview of STM equipment (Omicron nanotechnology).

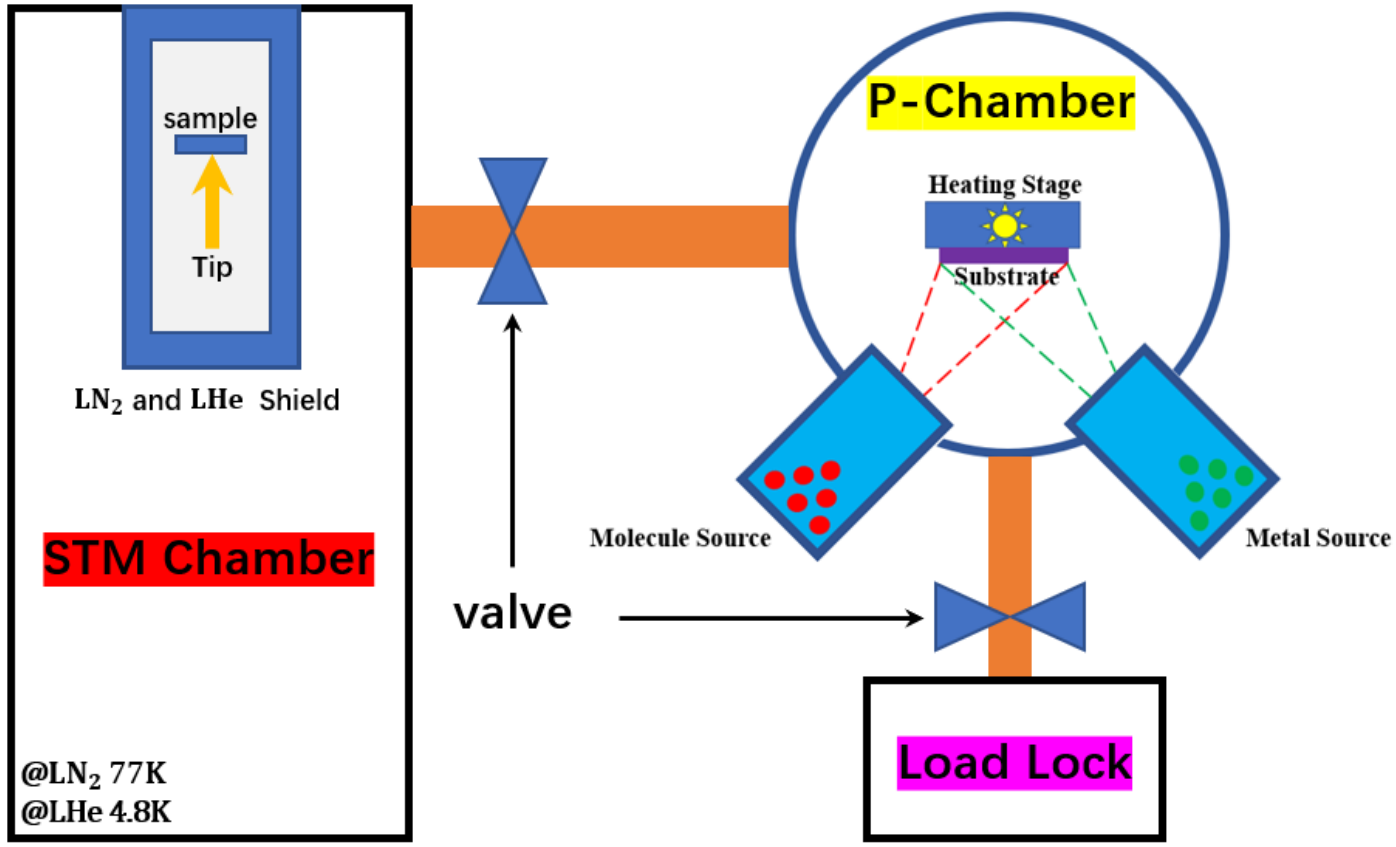

A schematic diagram of this system: preparation chamber and analysis chamber

Experiment of graphene sample preparation

Graphene sample preparation

The epitaxial growth of graphene is achieved by thermal graphitization

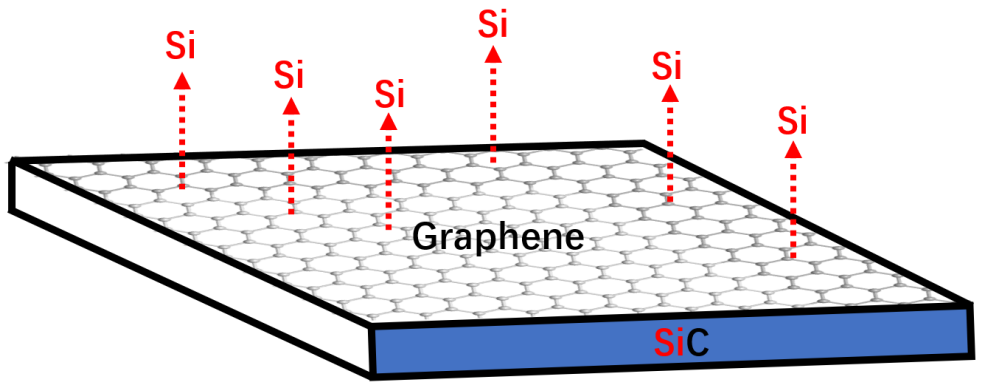

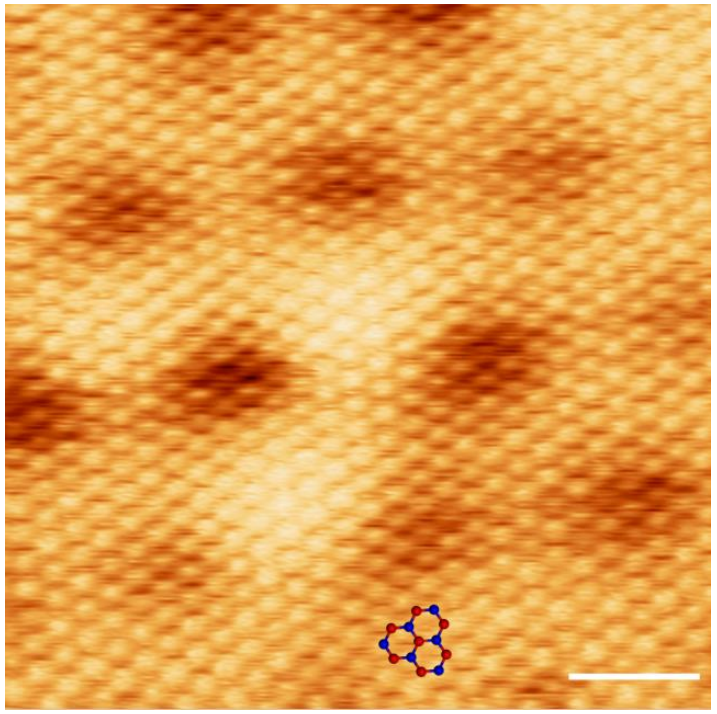

Bilayer graphene

Scale bar: 1 nm

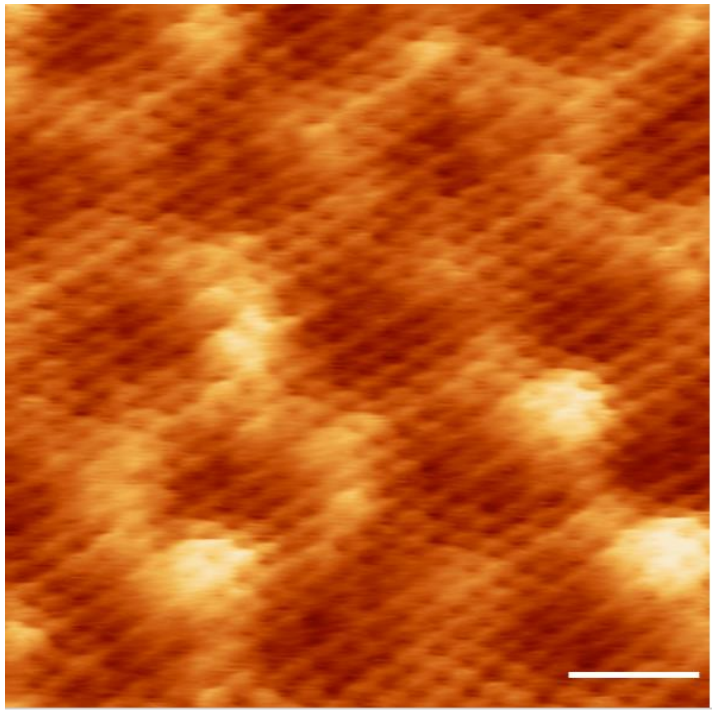

Monolayer graphene

Scale bar: 1 nm

Lattice constant: 2.46 Å

Experiment

Step 1: Depositing BHO on graphene

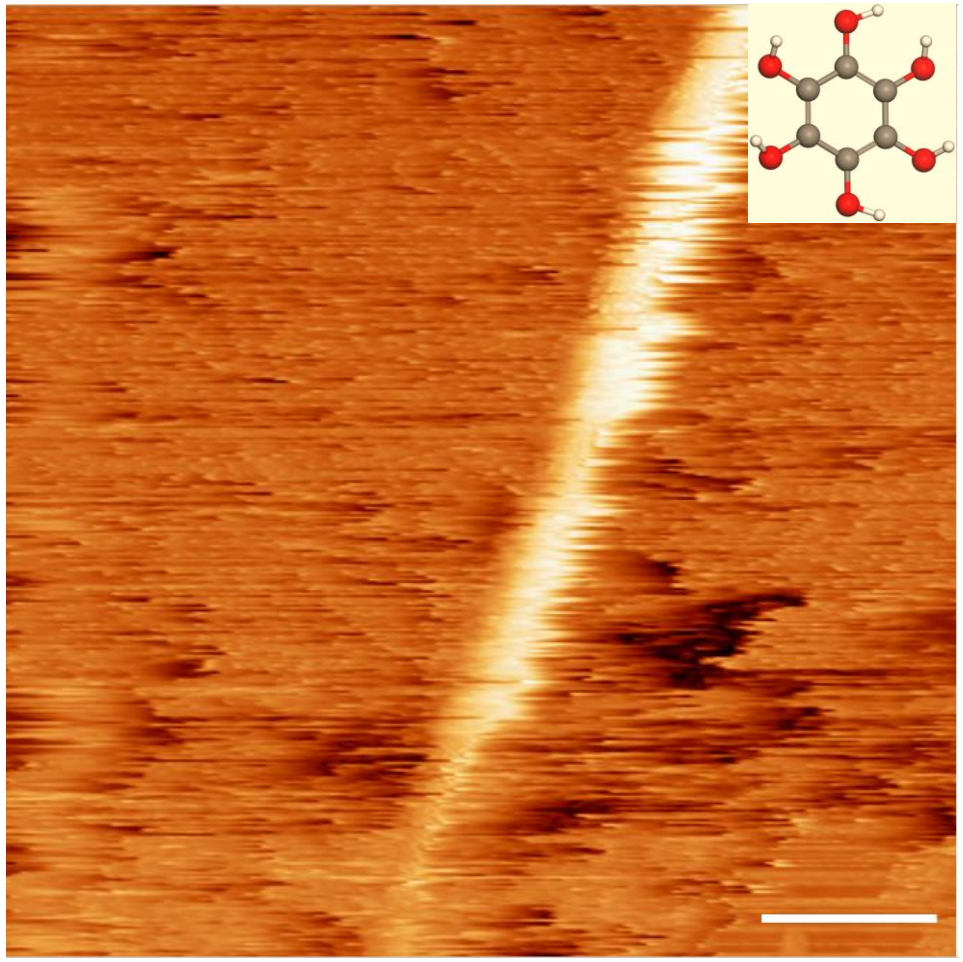

freely moving molecules on the surface

Scale bar: 10 nm

Step 2: Depositing Cu on graphene+BHO

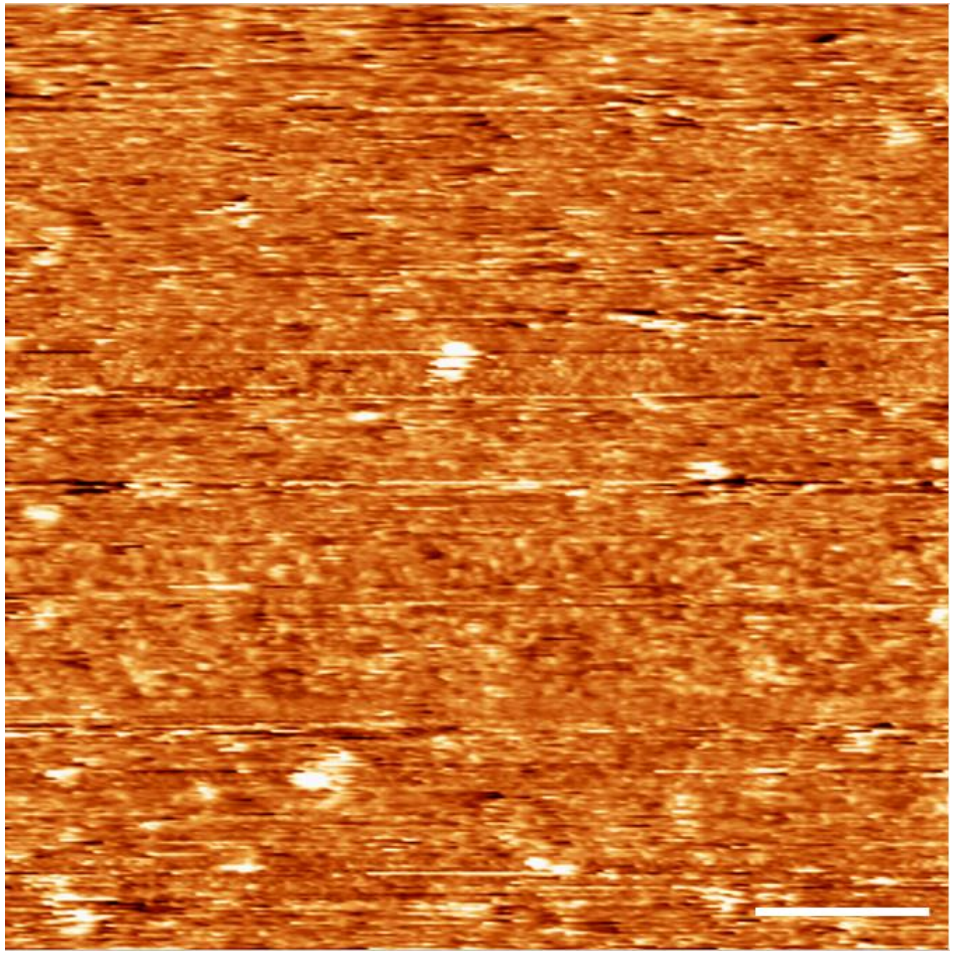

cannot resolve any stable structures

Scale bar: 10 nm

Experiment

Step 3: Annealing the sample to 75 C°

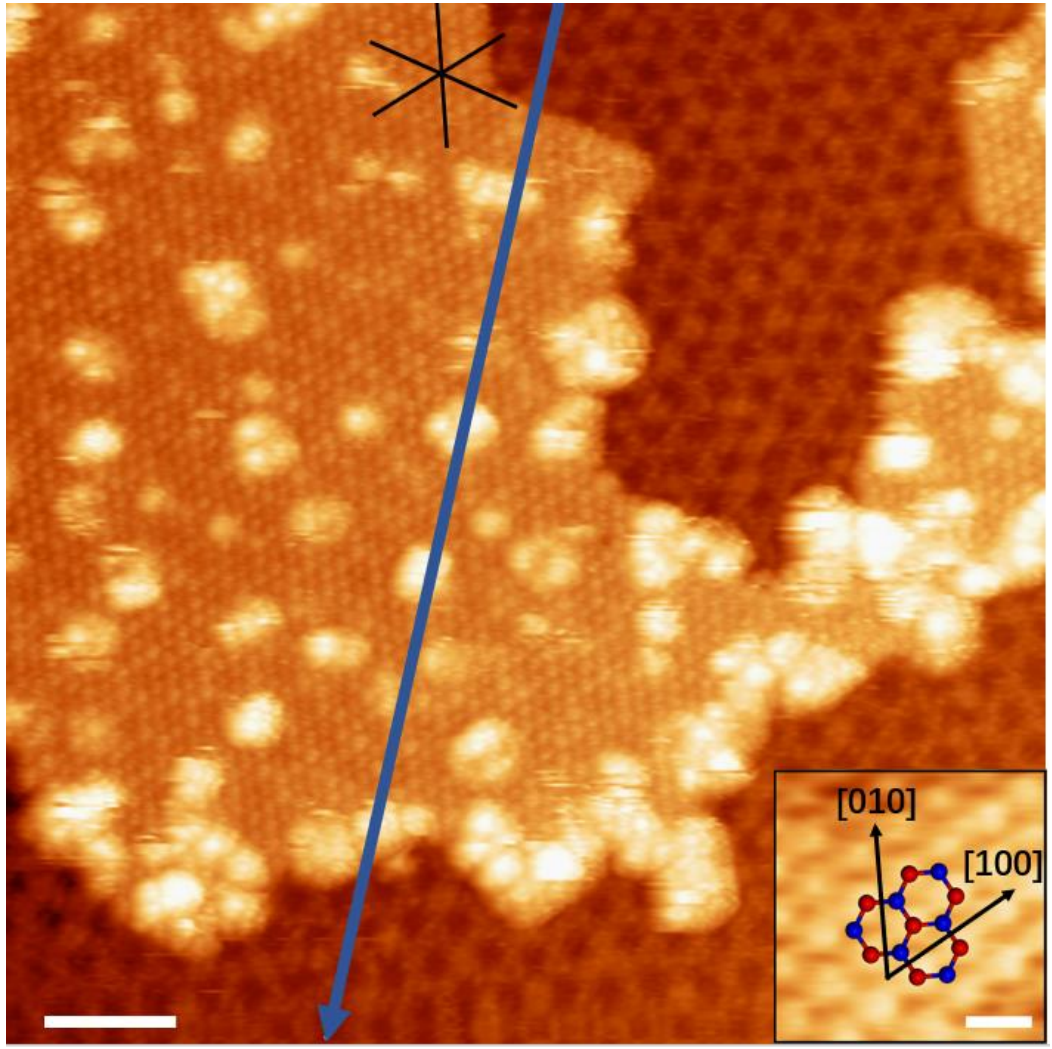

Scale bar: 5 nm

Scale bar: 0.3 nm

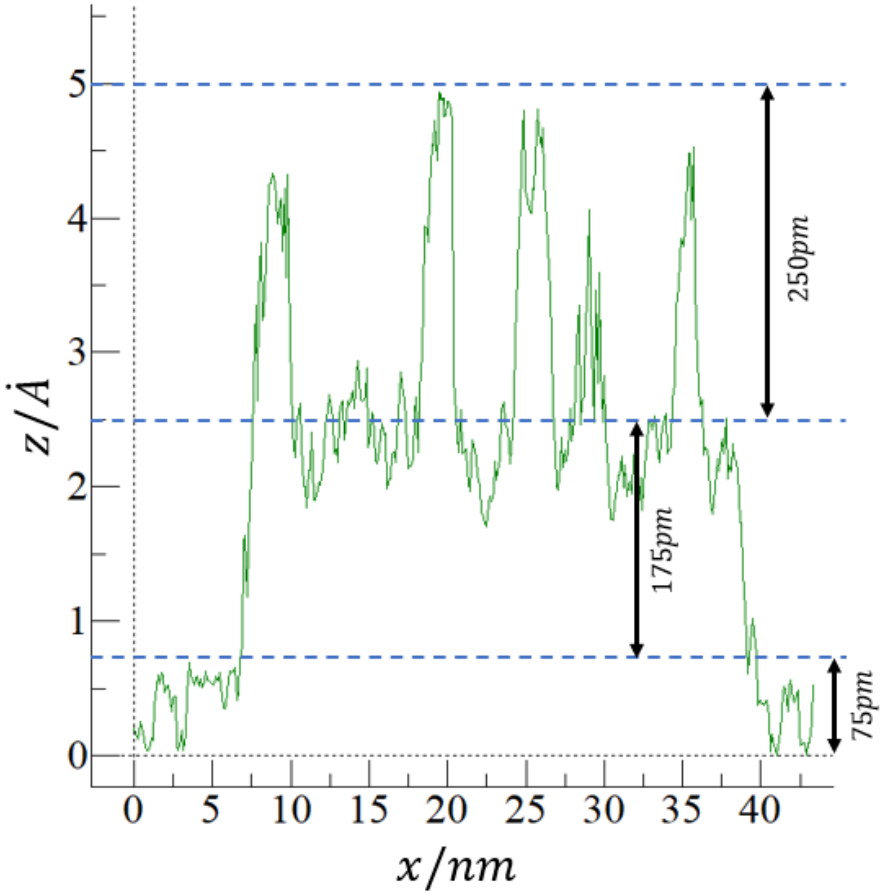

Triangular coordination network

Lattice constant: 7.39 Å

Monolayer

Experiment

Cu atom

bi-petal-shaped BHO molecule

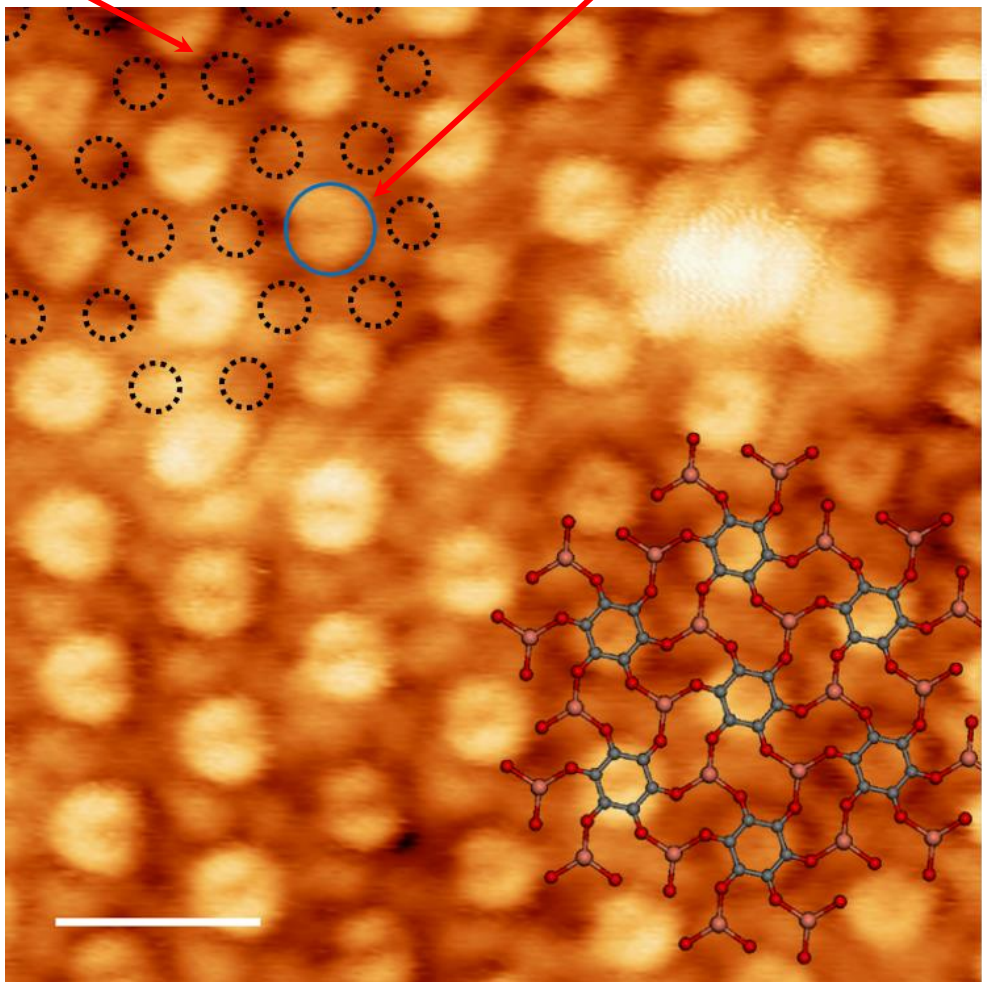

Scale bar: 1 nm

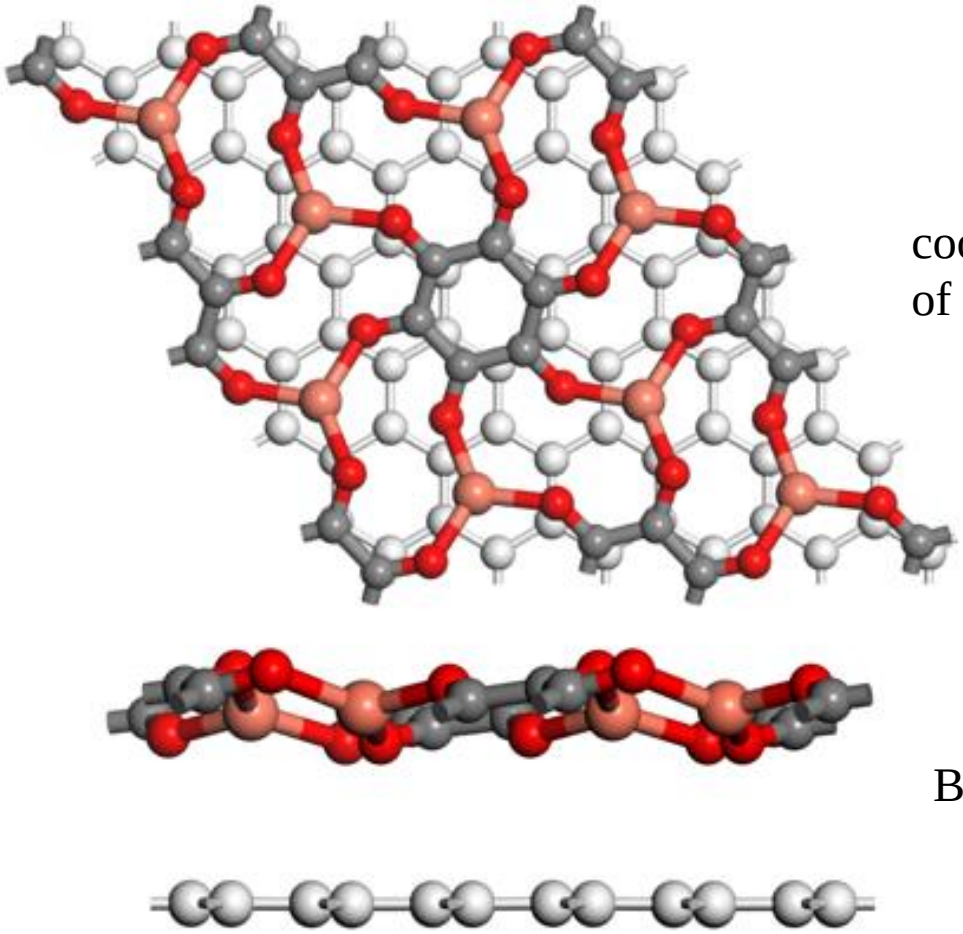

coordination network of $Cu_2(C_6O_6)$

Buckled on graphene

DFT calculated $Cu_2(C_6O_6)$/graphene structural model

Density-functional theory calculations

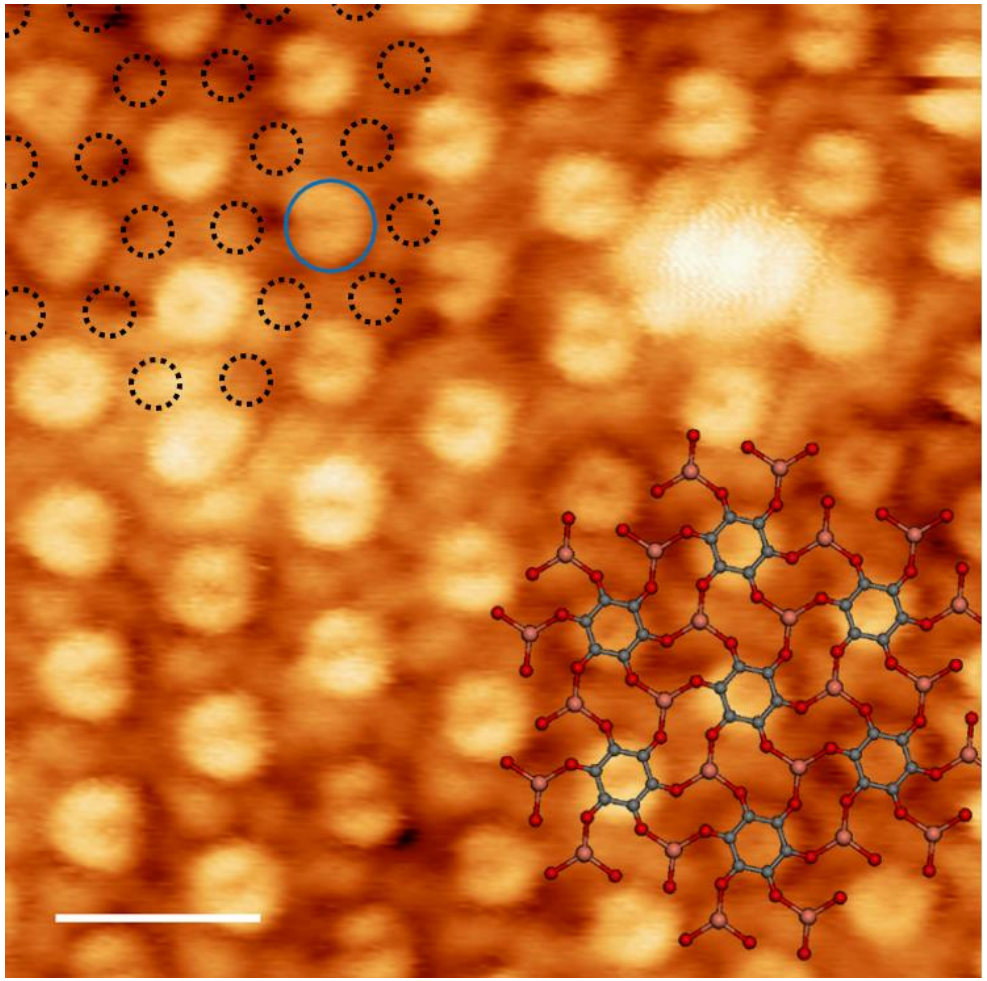

Scale bar: 1 nm

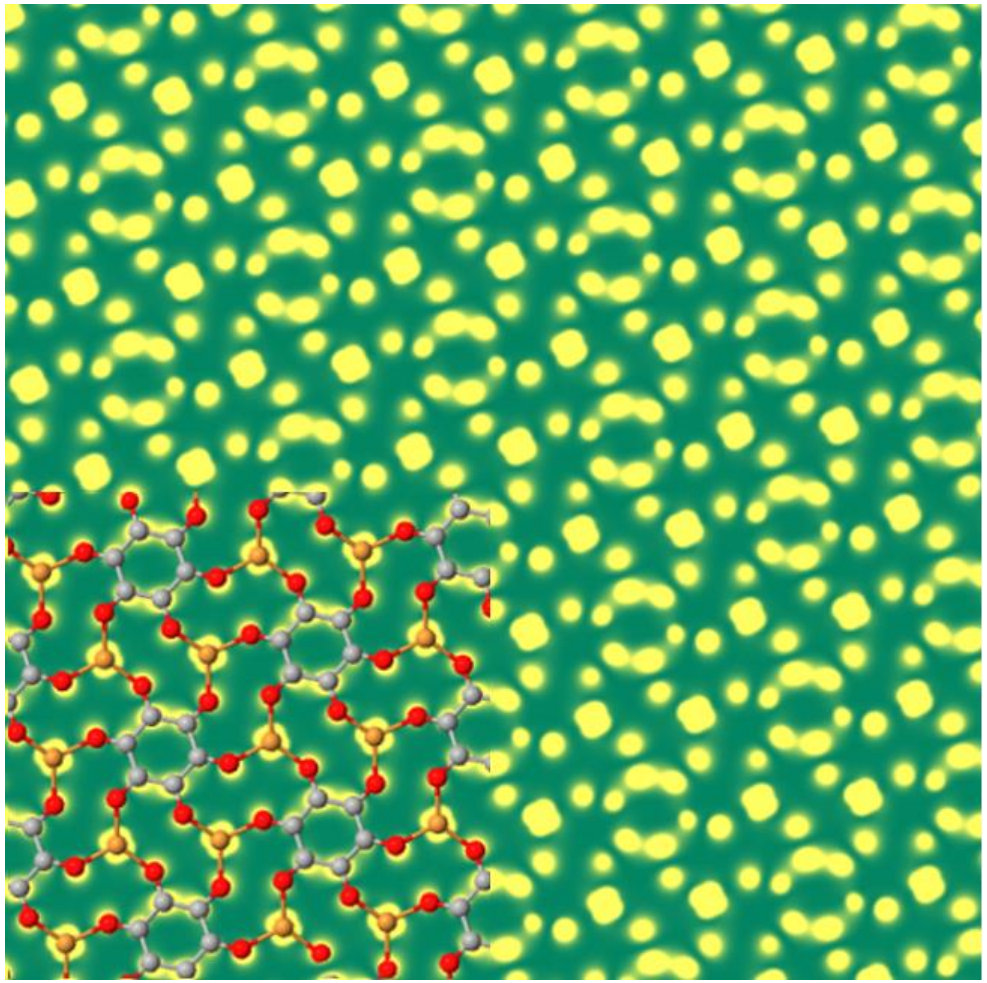

DFT-simulated constant current STM image of $Cu_2(C_6O_6)$/graphene

BHO

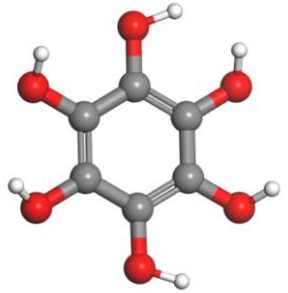

Six-fold symmetry

?

Bi-petal-shaped BHO molecule

Molecular orbital state is influenced by the electric field induced by the STM tip

E= 0.8 V/Å

Experiment

Scheme of $Cu_2(C_6O_6)$ coordination network forming process

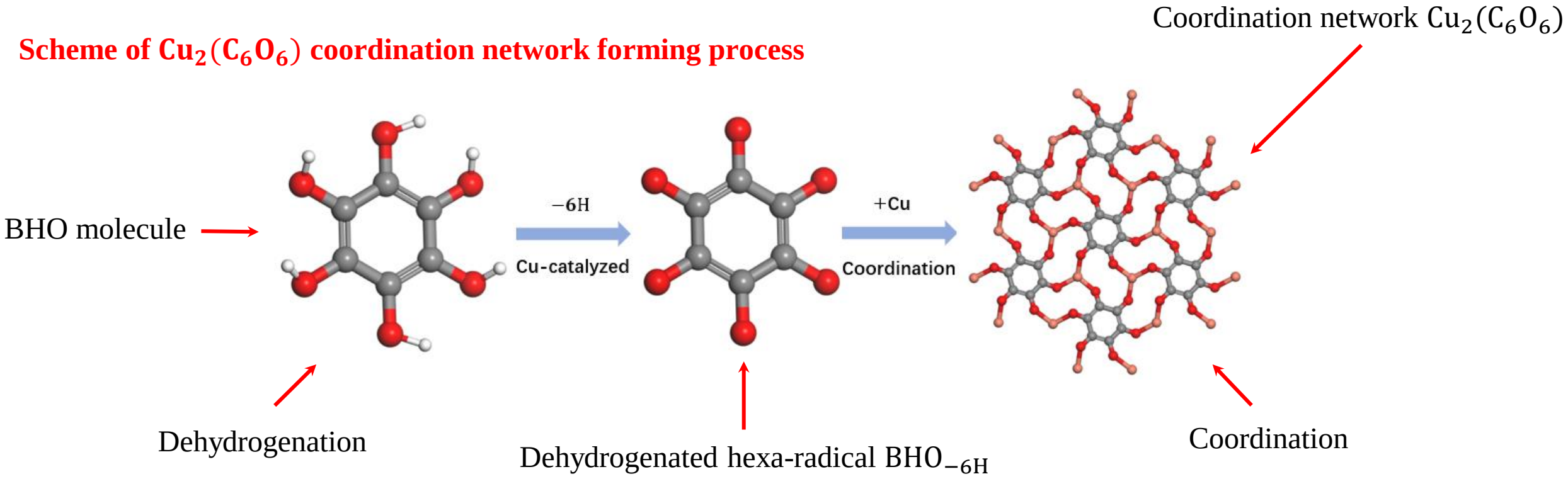

(1) Surface Cu atoms on graphene surface possess the advantages of both high diffuse mobility and efficient catalytic ability of dehydrogenation.
(2) Single Cu atom can be easily detached from the Cu clusters in the annealing process and participate as a metal linker for coordination formation.

Density-functional theory calculations

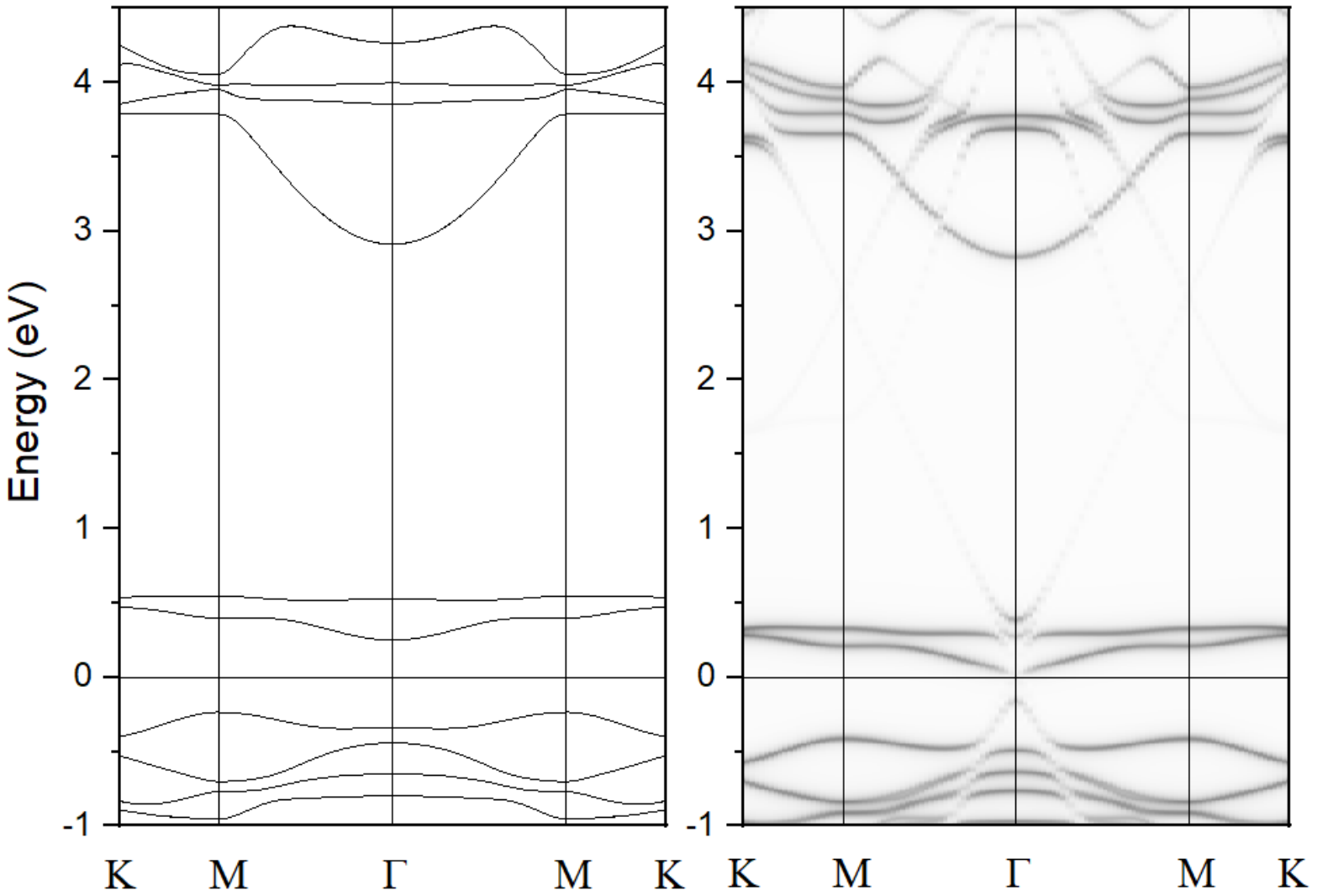

Free-standing $Cu_2(C_6O_6)$

$Cu_2(C_6O_6)$/Graphene

Free-standing Gap = 0.485 eV

Conduction and valance band downshift 0.19 eV and 0.17 eV

Charge transfer

Band deformation

} Small

Weak interaction between $Cu_2(C_6O_6)$ and graphene

Conclusions

- Monolayer of two-dimensional $Cu_2(C_6O_6)$ can be synthesized on graphene.
- The density-functional theory (DFT) calculation indicates it is a narrow band gap semiconductor with band gap of 0.485 eV.
- The interaction between the coordination network and graphene is weak and the intrinsic electronic structure of $Cu_2(C_6O_6)$ coordination network is preserved.

Introduction

Introduction two

Orbital design of 2D-MOFs with complex orbital symmetry

Experimental realized 2D-MOF structures with simple lattice symmetry

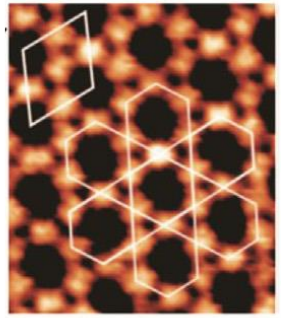

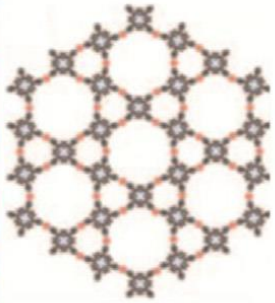

JACS. 131 (2009) 5376–5377.

Au-(pyridyl)2

2D-MOFs

Kagome lattices

Hexagonal lattices

Co-(CN)3

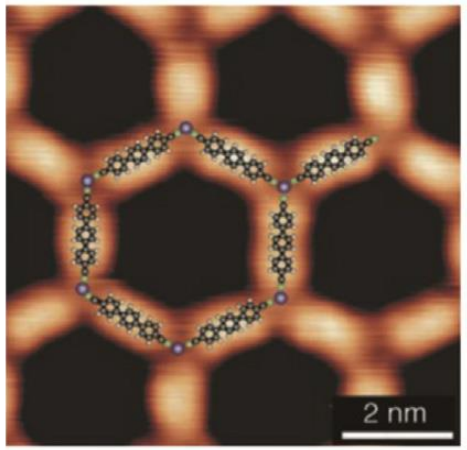

Angew. Chem. 119 (2007) 724–727.

Fe-(pyridyl)3

Triangular lattices

Square lattices

Rectangular lattices

carboxylate and pyridyl with Fe

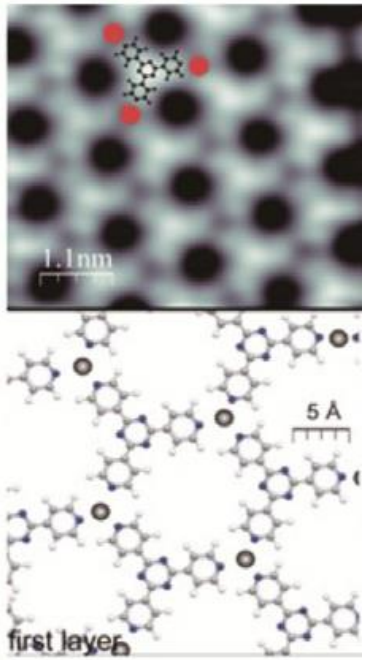

PRL 109 (2012) 267207.

Co–(CN)4

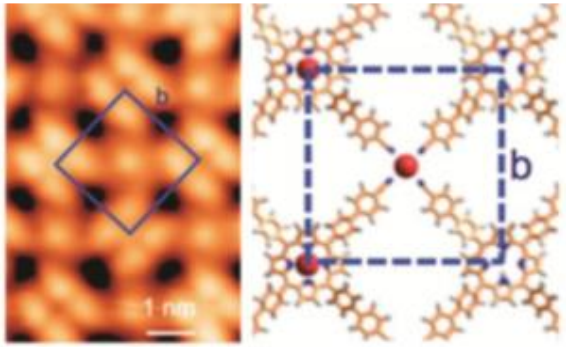

JACS 137 (2015) 2420–2423.

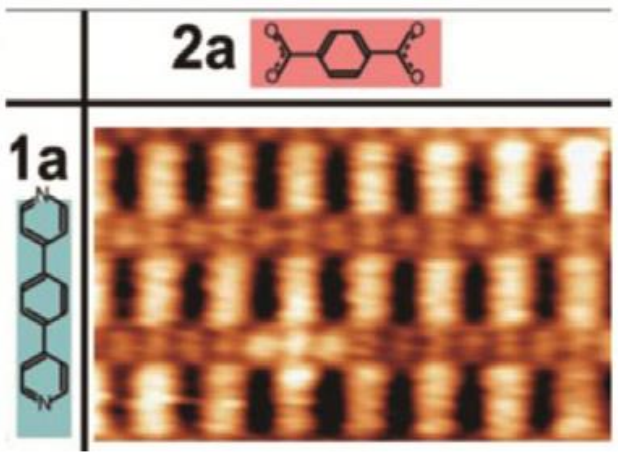

PNAS 104 (2007) 17927–17930.

Electronic structure of 2D MOFs with complex orbital symmetry

Honeycomb lattice

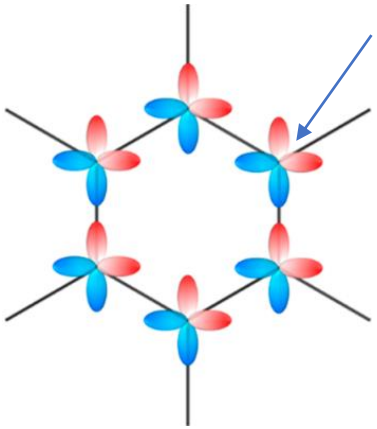

p_x, p_y-orbital

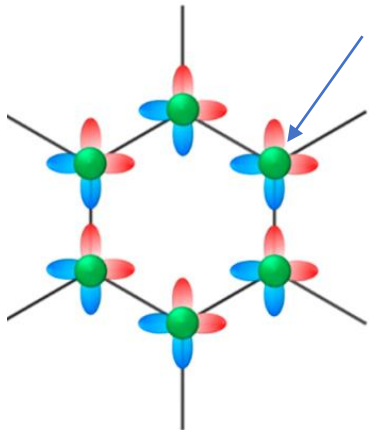

s, p_x, p_y-orbital

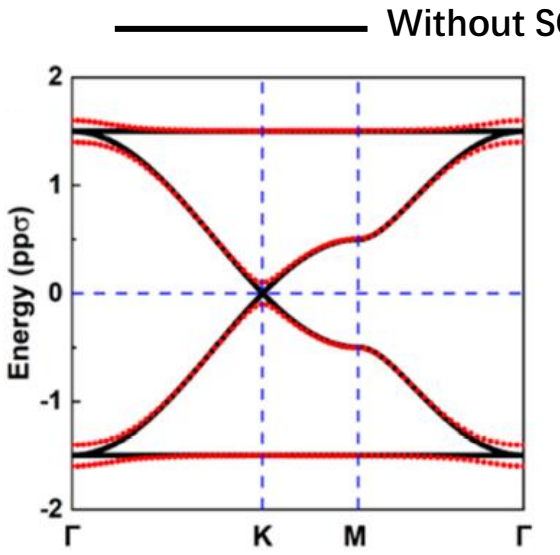

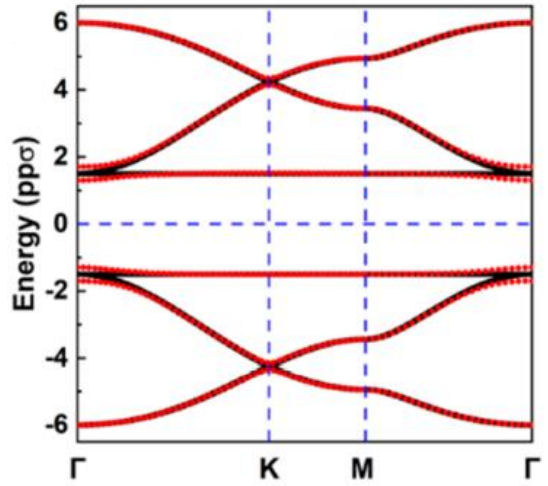

Honeycomb Kagome lattice

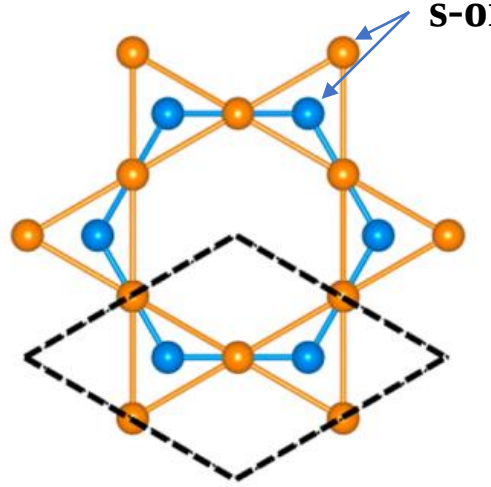

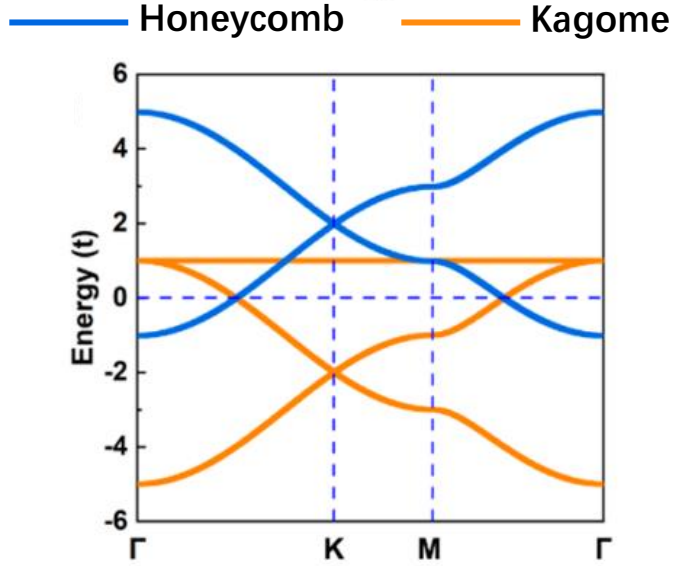

Acc. Chem. Res. 54 416426 (2021)

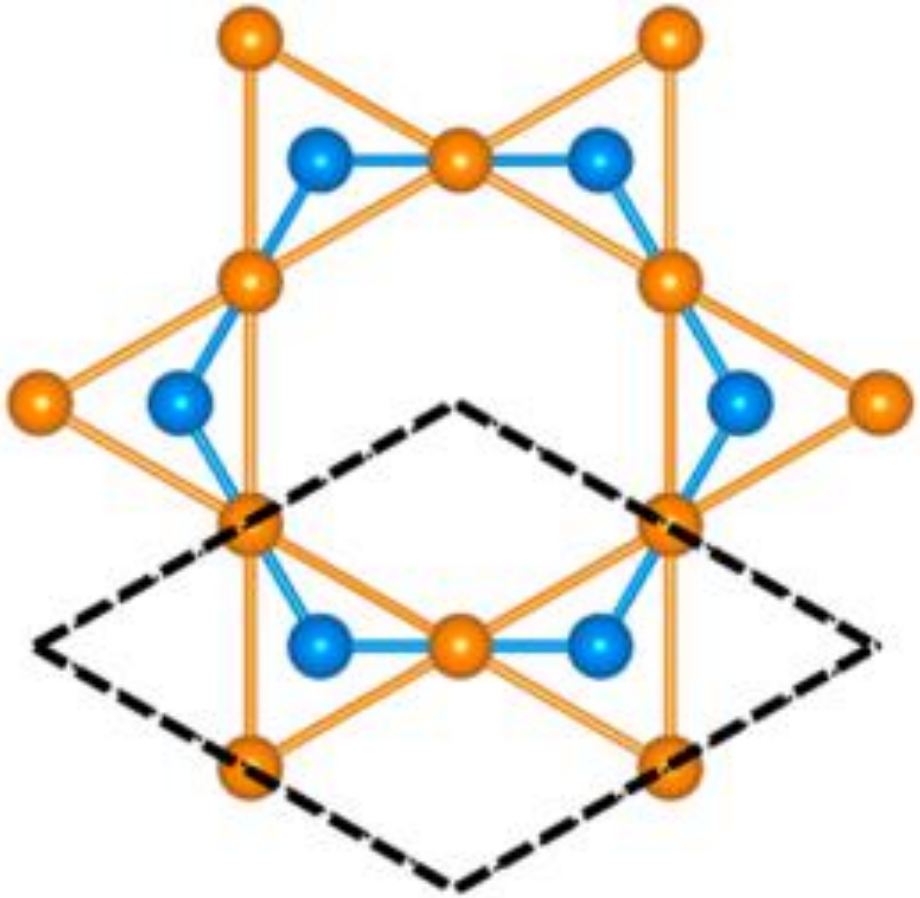

PART 03

Part 3 Two-Dimensional Metal-Organic Fe-porphyrin Coordination framework Exhibiting Mixed Spin States

Experiment

1. Depositing DPyP on Au(111) surface held at RT: the molecules are in closed-packed islands.
2. Depositing Fe onto the sample and annealing the sample to 250°C: 2D hexagonal lattice were observed.

1. UHV-LT-STM;
2. 4.8 K;
3. Au(111) substrate;

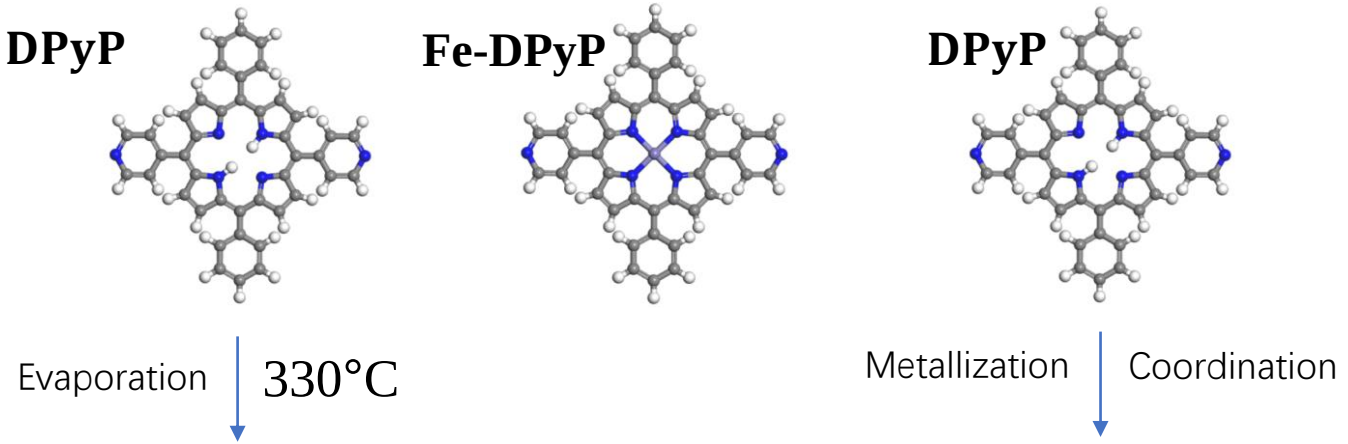

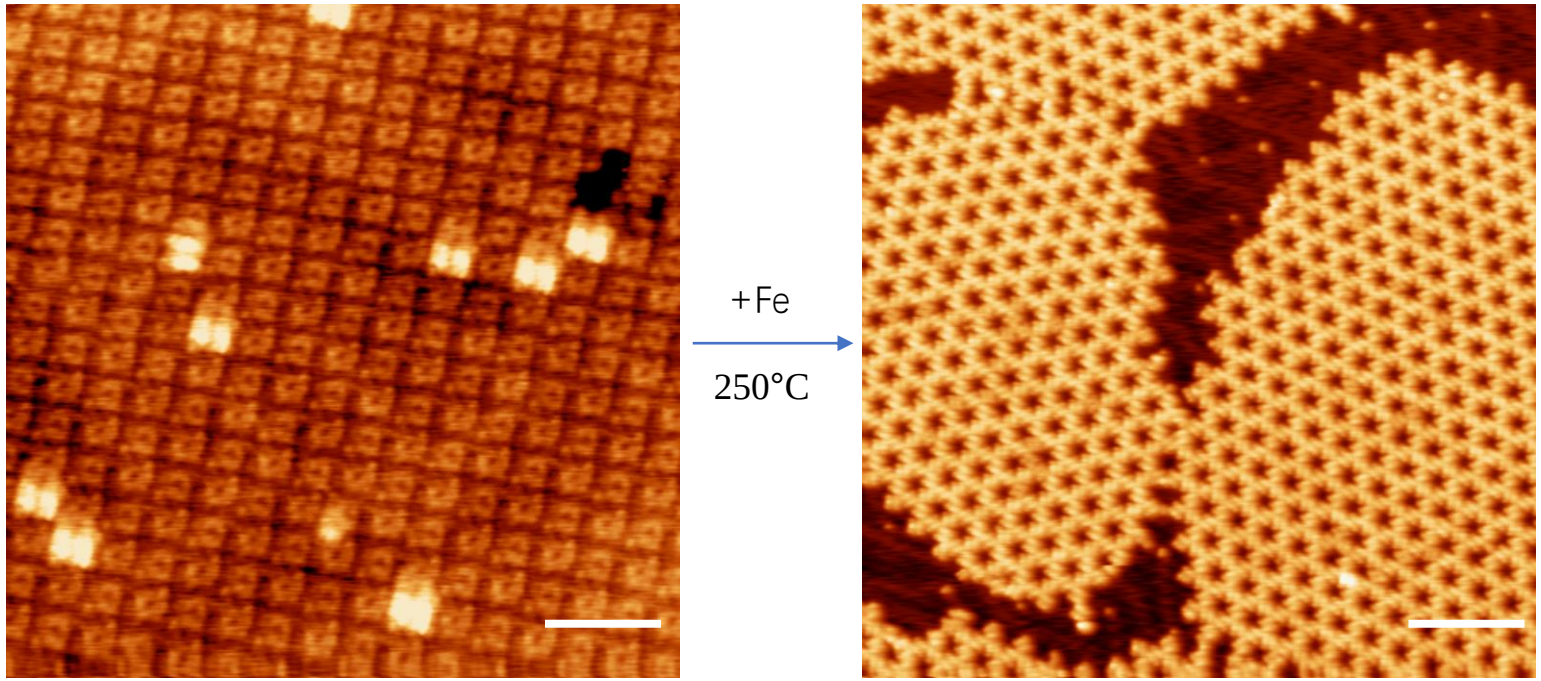

Scale bar: 4 nm

Scale bar: 10 nm

Experiment

Monolayer of $Fe_2(Fe-DPP)_3$ network self-assembled on Au(111).

Lattice constant:
3.46 ± 0.05 nm

Hexagonal structure can extend to large than 92 nm across

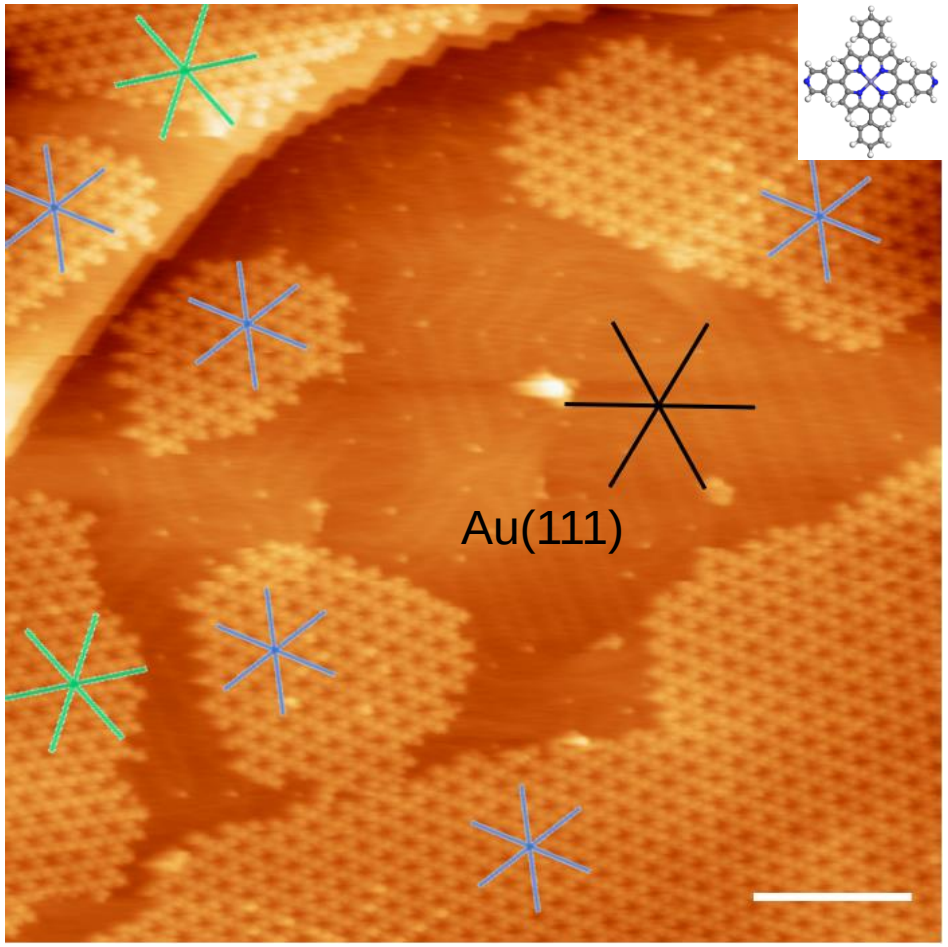

Scale bar: 10 nm

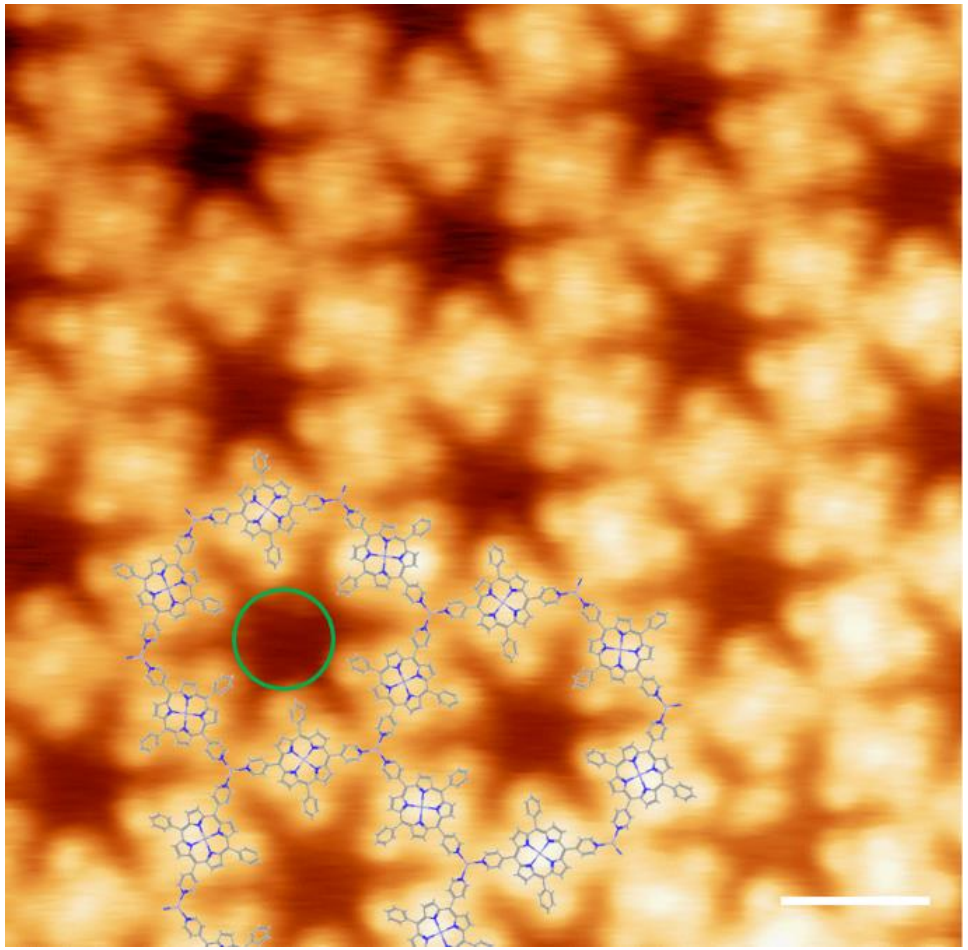

Scale bar: 2 nm

There exists two different lattice orientations with angles of ±13° mirrored with respect to the [01−1] direction of the Au(111) substrate.

Density-functional theory calculations

DFT optimized free-standing $Fe_2(Fe-DPP)_3$ structure

Top view

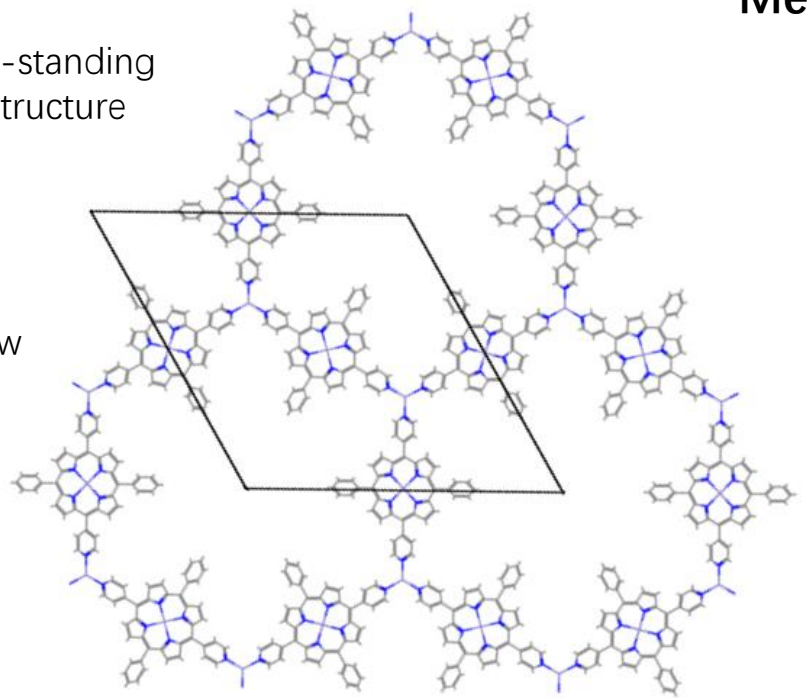

Metallated iron: Fe_M

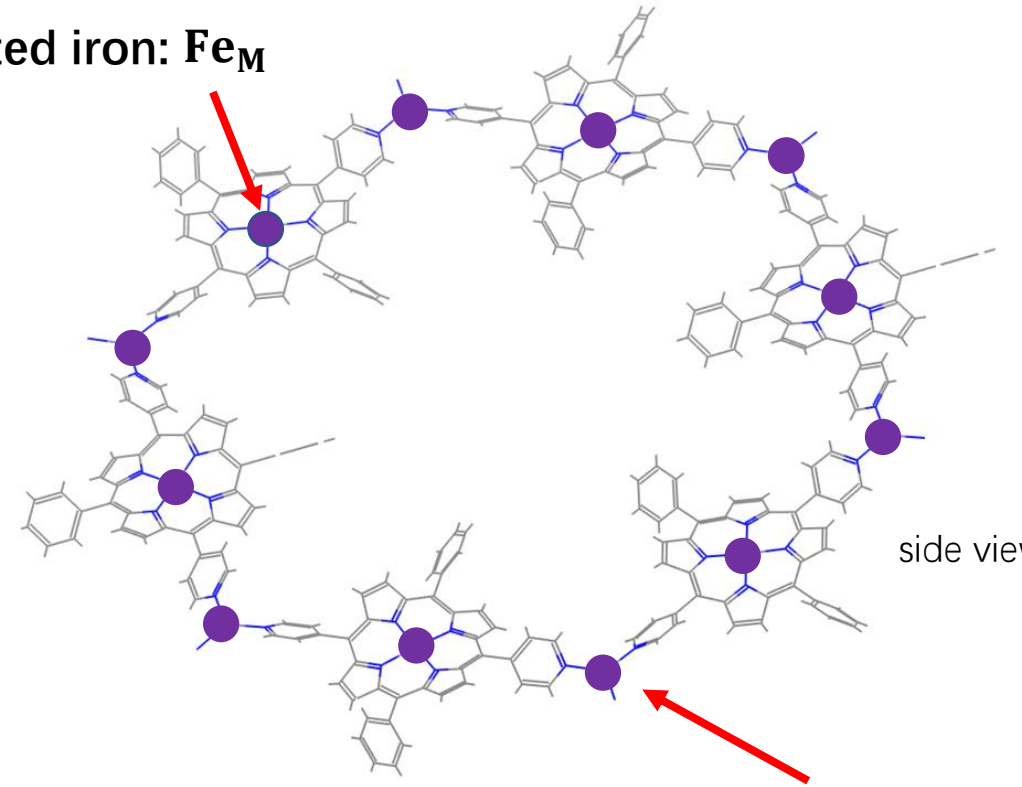

side view

Coordinated iron: Fe_C

	Bond length	Magnetic moment
Fe_C	2.033 Å	3.000 μ_B
Fe_M	1.979 Å	2.000 μ_B
N		-0.018 μ_B

Coordinated Fe: Fe_C S=3/2

Metallated Fe: Fe_M S=1

Density-functional theory calculations

Valence states of two types of Fe

Bader charge analysis

The neutrality of coordination network per unit cell is achieved ($\sum \Delta q_{tot} = 0$)

	q_{Fe}	$\sum q_c$	$\sum q_N$	$\sum q_H$	$\sum q_{tot}$	d_{Fe-N}(Å)
Fe_C	+0.92	+10.55	-21.23	+5.50	+0.01	2.034
	+0.93					
Fe_M	+1.12					
	+1.12					1.979
	+1.12					

Deviations from the integer value of +2 e

Delocalized distribution of excess positive charge

Valence state of Fe_M: +2

Valence state of Fe_C: +2

$3Fe_M$ red dash circle

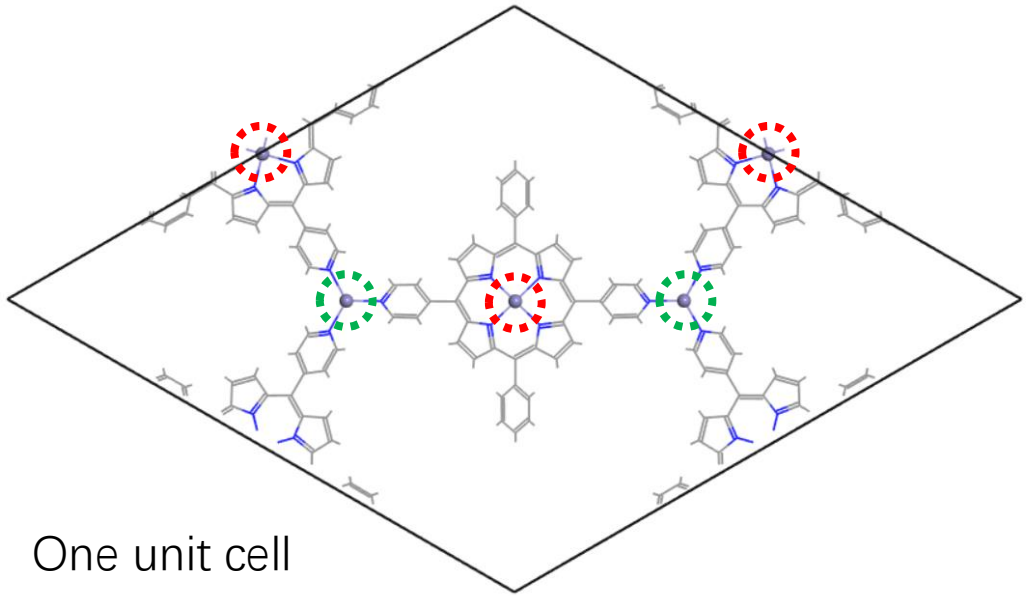

One unit cell

$2Fe_C$ green dash circle

Density-functional theory calculations

Spin states on Fe_C atom

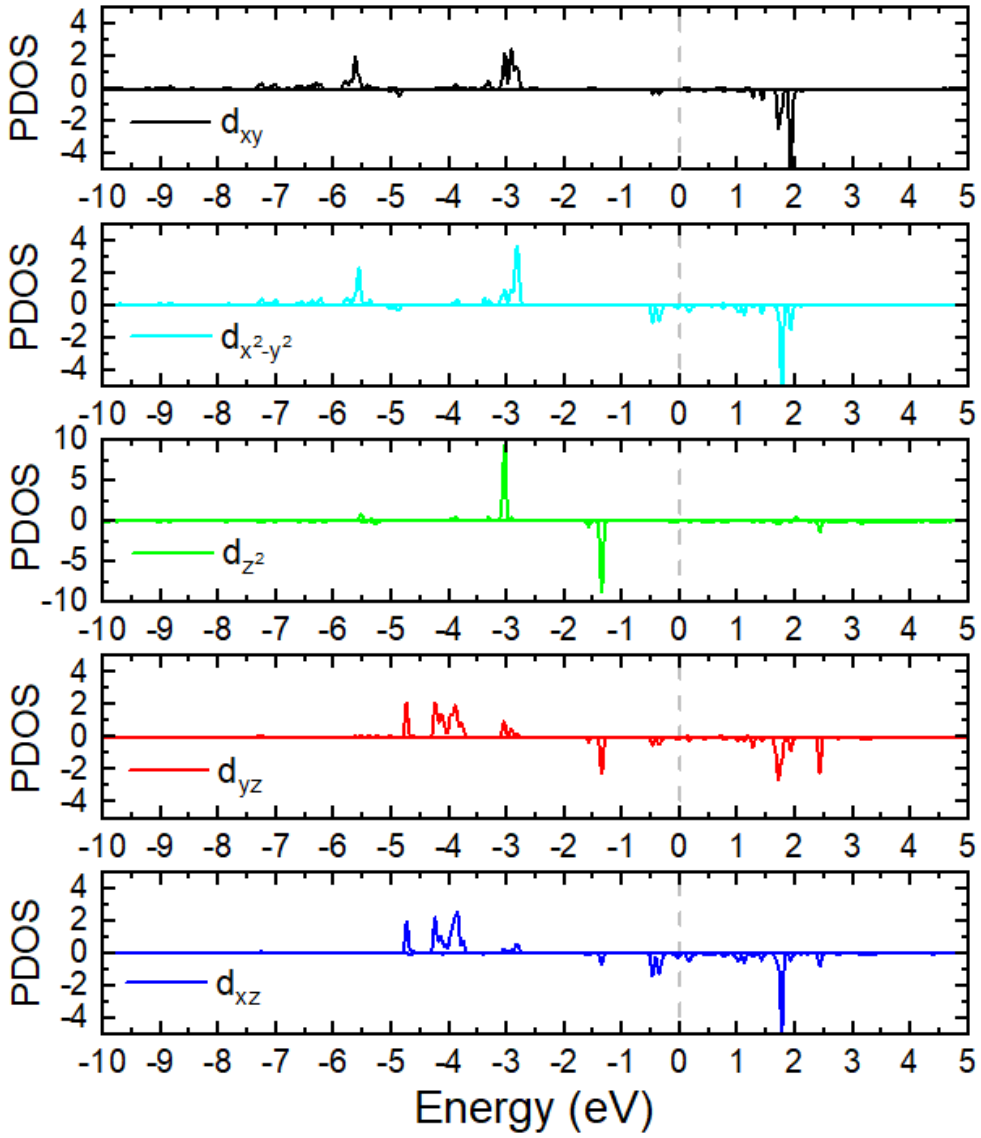

Occupied integration

$$O^{ob} = 5\frac{O^D}{T^D}$$

Total integration of PDOS

The number of occupied d-orbitals

Crystal field theory
Trigonal

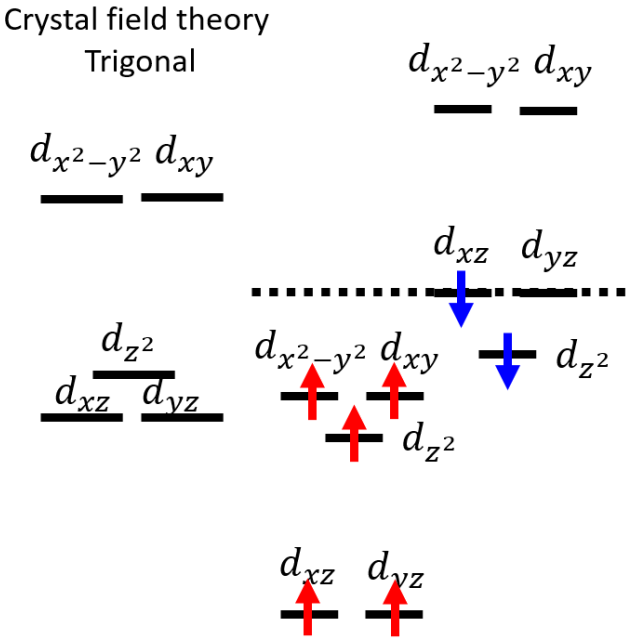

Spin up O^{ob}=4.90

Spin down O^{ob}=1.71

4.9-1.71=3.19

8-4.9-1.71=1.39

Spin state of Fe_C: S =3/2

Valence state of Fe_C: +2

Density-functional theory calculations

Spin states on Fe_M atom

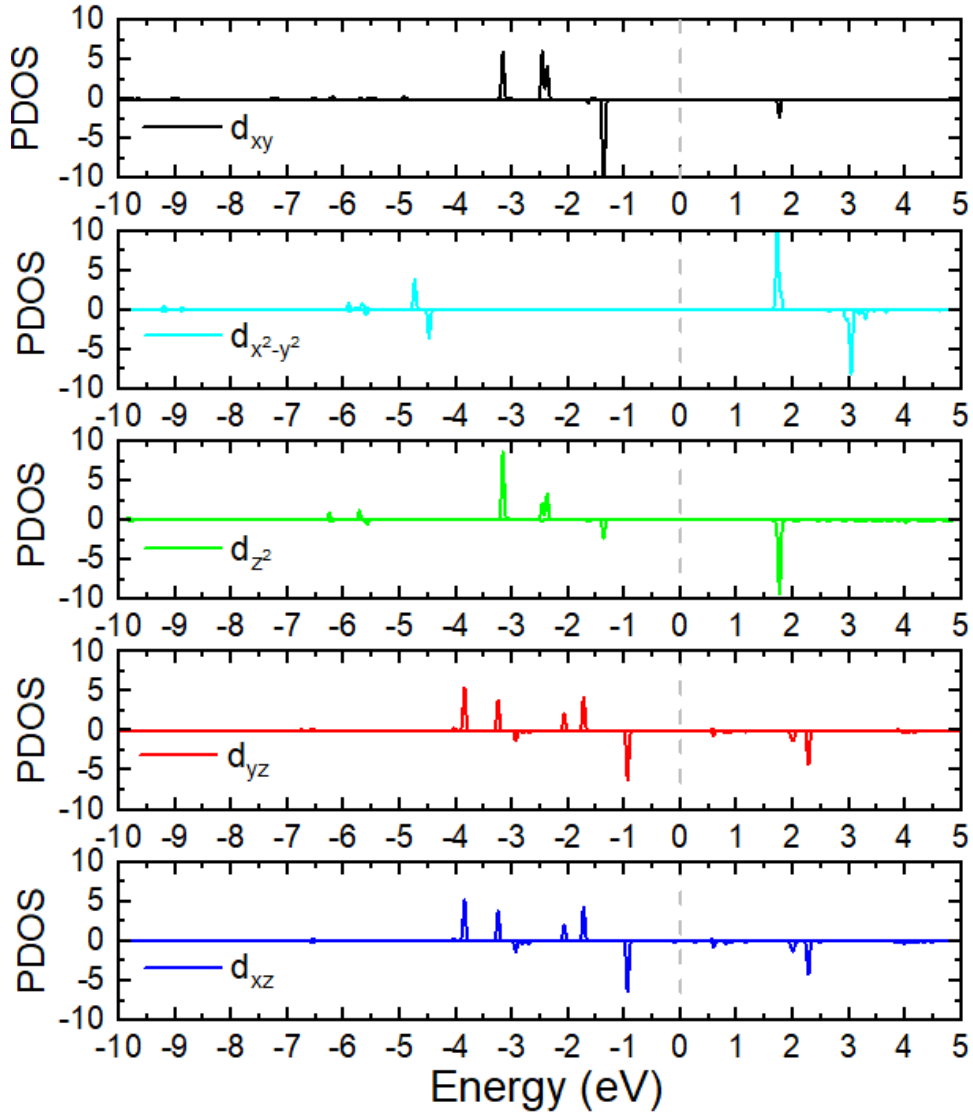

Occupied integration

$$O^{ob} = 5\frac{O^D}{T^D}$$

Total integration of PDOS

The number of occupied d-orbitals

Crystal field theory

Square

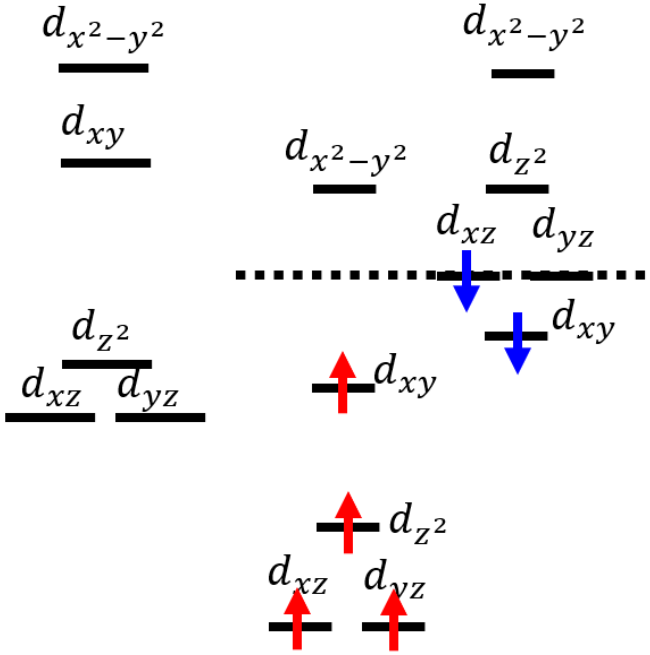

Spin up O^{ob}=4.26

Spin down O^{ob}=2.31

4.26-2.31=1.95

8-4.26-2.31=1.43

Spin state of Fe_M: $S = 1$

Valence state of Fe_M: +2

Density-functional theory calculations

Magnetic configuration

Consider four magnetic configurations (labeled as FM, FIM1, FIM2, FIM3) in primitive cell 1X1 unit cell

$$E_R = \left(E_{1\times1} - E_{1\times1}^{FM}\right)$$

Spin linear polarized calculation (GGA+U)

The red and blue circles denote the majority and minority of spins, respectively

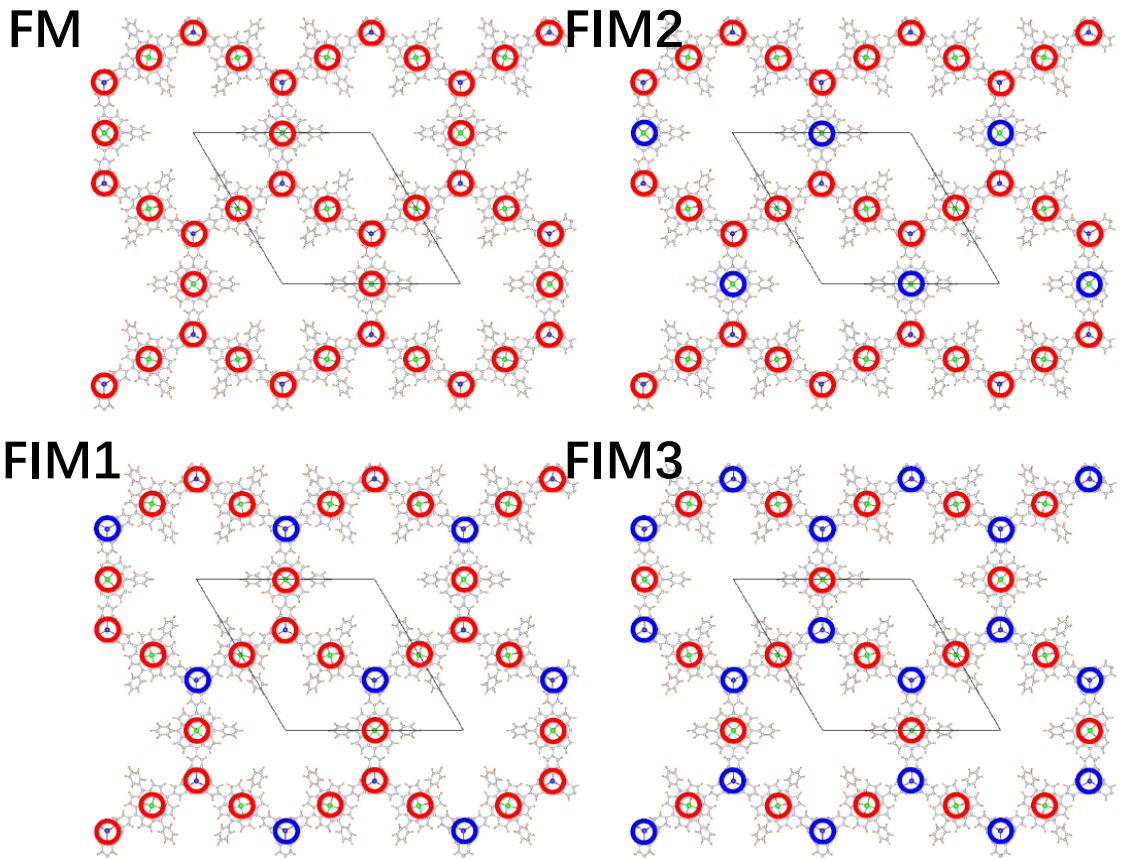

		FM	FIM1	FIM2	FIM3	J (meV)
GGA	E_R (meV)	0.00	3.1	15.6	39.8	0.69
	M (μ_B)	10.03	4.06	7.36	-1.93	
U=1.0	E_R (meV)	0.00	11.6	33.5	101.4	2.58
	M (μ_B)	10.21	4.23	7.44	-1.16	
U=2.0	E_R (meV)	0.00	18.6	45.4	110.0	4.13
	M (μ_B)	10.26	4.36	7.56	-1.00	
U=3.0	E_R (meV)	0.00	19.4	57.1	119.7	4.31
	M (μ_B)	10.28	4.42	7.53	-0.97	

Magnetic anisotropy

Spin orbital coupling calculation $E_R^{SOC} = (E - E_{in-plane}^{FM})$

			ΔE_R^{SOC} (meV)
U=3.0	FM	In-plane	0.0
		Out-of-plane	4.8
	FIM1	In-plane	18.0
		Out-of-plane	23.0
	FIM2	In-plane	42.1
		Out-of-plane	51.4
	FIM3	In-plane	121.4
		Out-of-plane	125.5

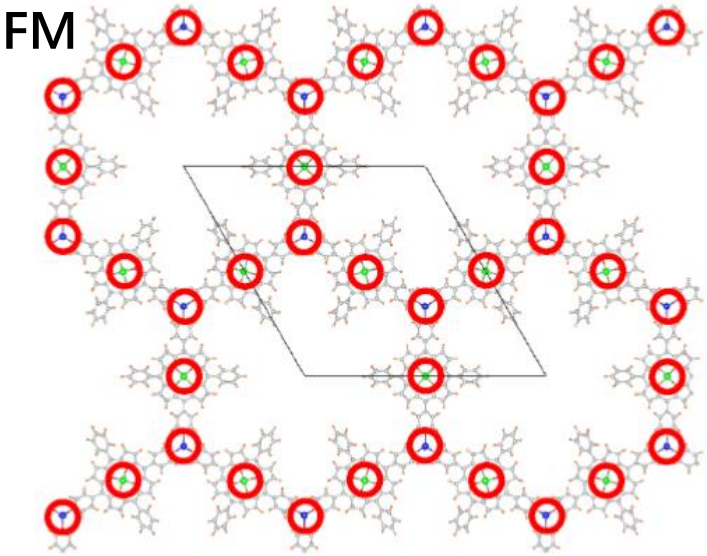

Magnetic quantisation axis is $(s_x\ 0\ 0)$
In-plane

Energy difference is 0.5meV

Magnetic quantisation axis is $(0\ s_y\ 0)$
In-plane

∧ Out-of-plane is higher than in-plane 4.8meV

Magnetic quantisation axis is $(0\ 0\ s_z)$
Out-of-plane

Experiment

Spin excitation

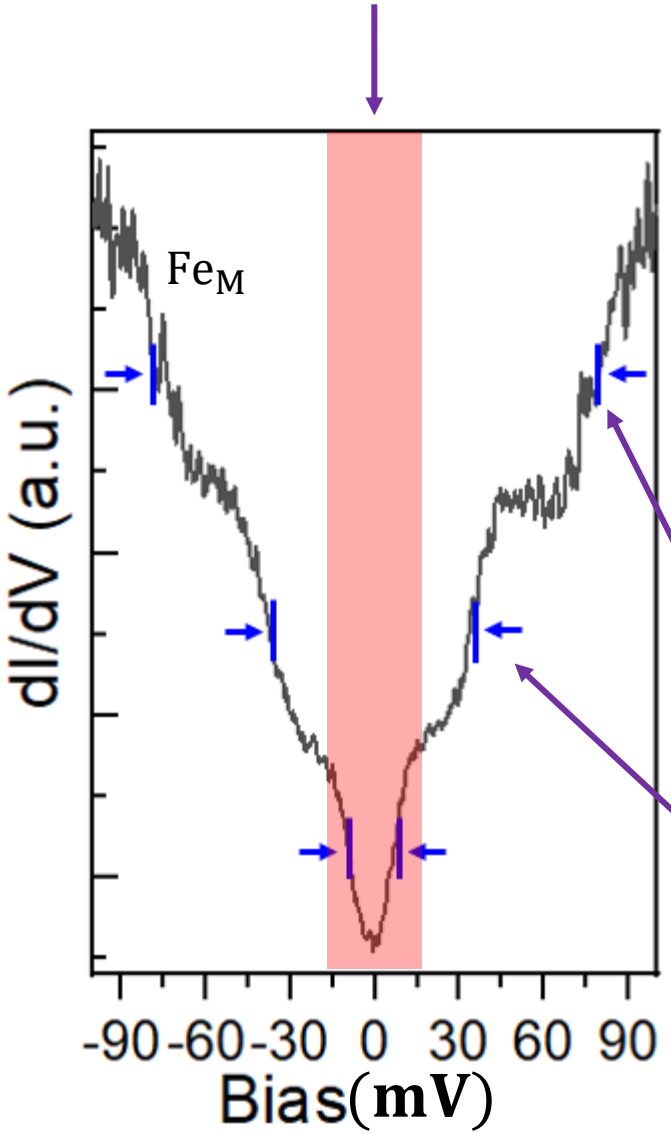

Fe-DPyP

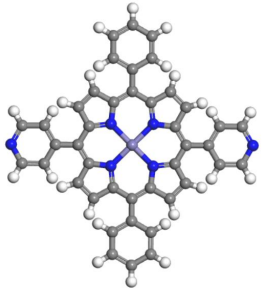

E < 16meV: Spin excitation dominated

E > 16meV: Molecular vibration dominated

Spin excitation: $\pm 8.41meV$

Molecular vibration: $\pm 36meV$

Fe-tapping mode

Molecular vibration: $\pm 79.6meV$

C-C/C-H stretching and bending modes

Principle of spin-flip excitation

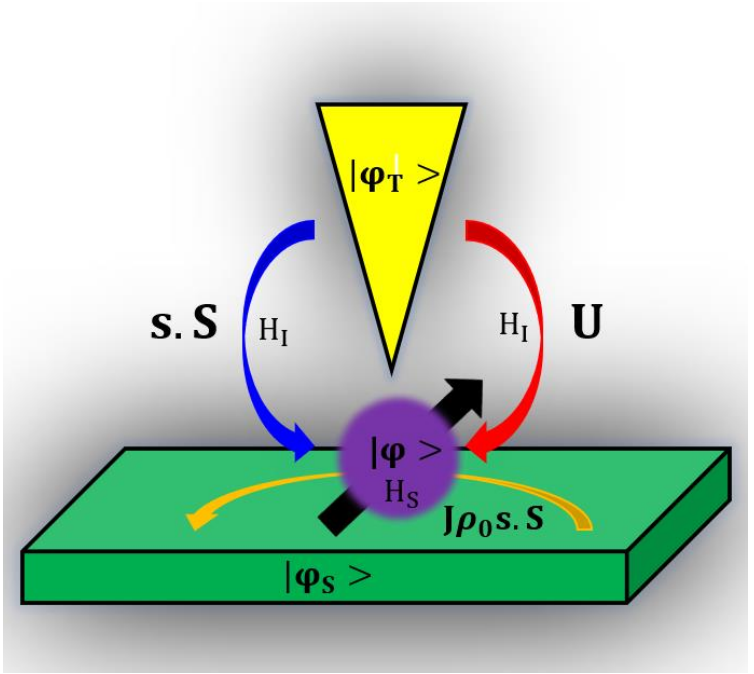

$$H_S = DS_z^2 + E(S_x^2 - S_y^2) \qquad H_I = J_i\rho(\frac{1}{2}\hat{\sigma}.\hat{S}^i + U_i\hat{I}_i)$$

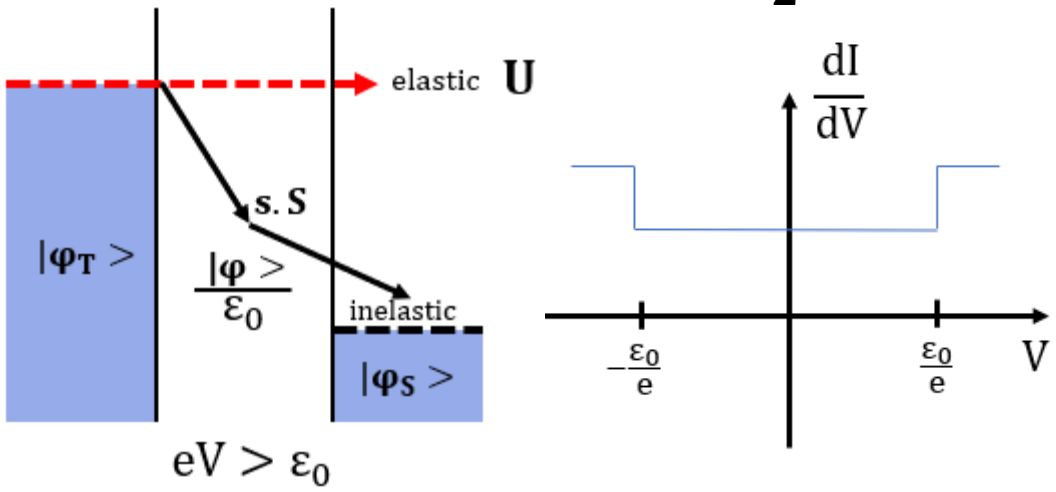

Experiment

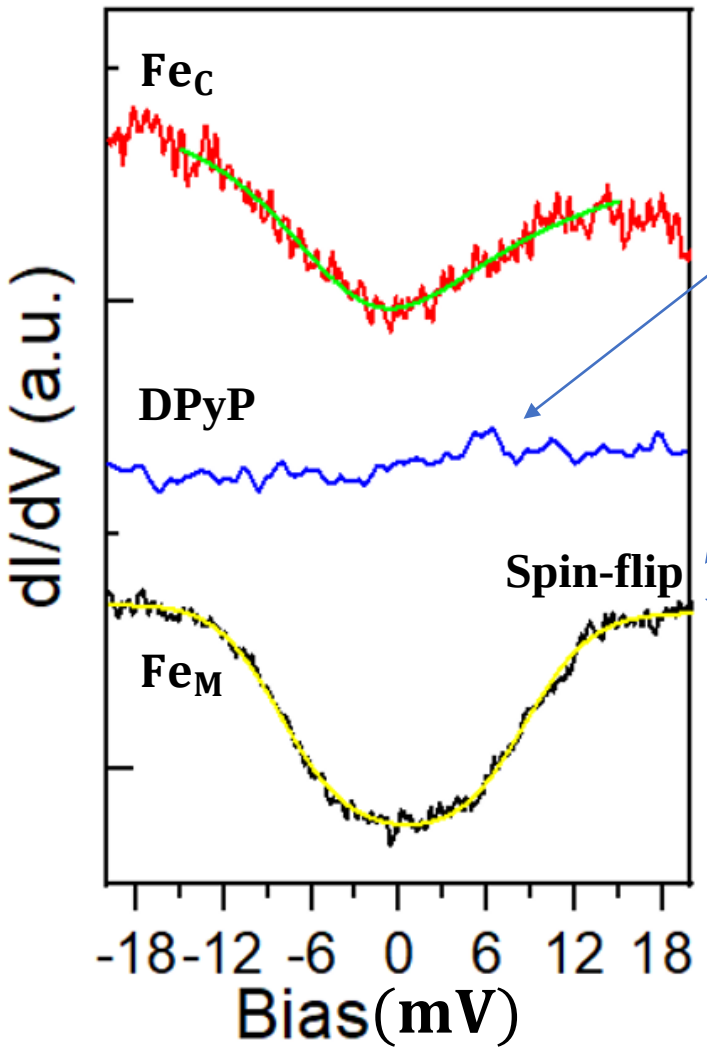

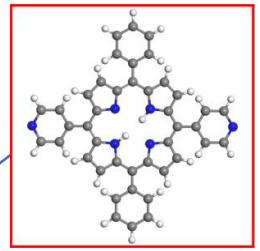

DPyP

For zero-field splitting (ZFS)

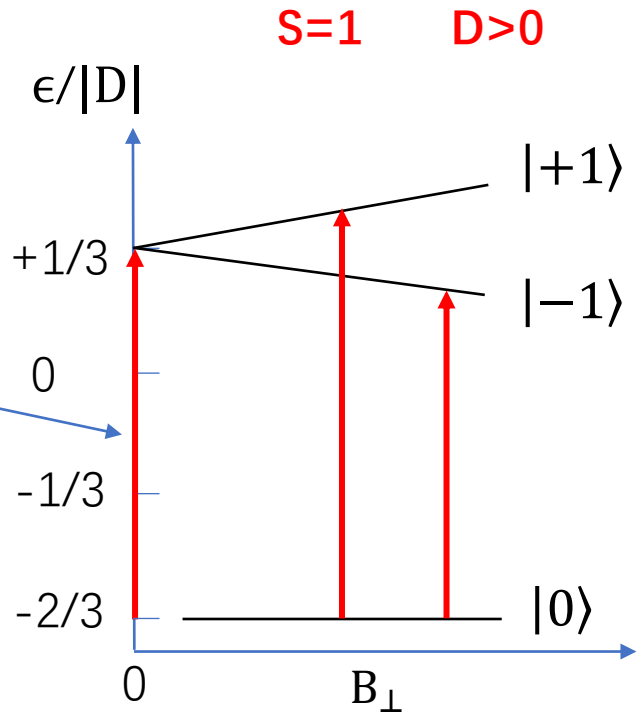

Fitting results: **D=8.41meV, E=0**

D>0, easy-plane type magnetic anisotropy

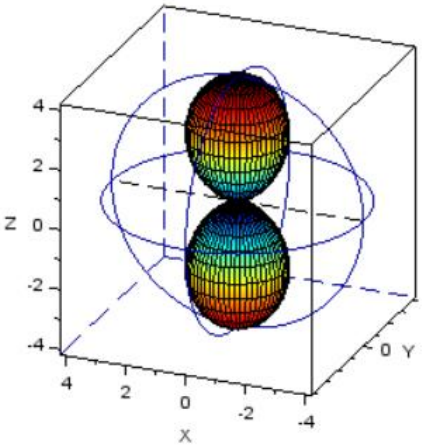

Experiment

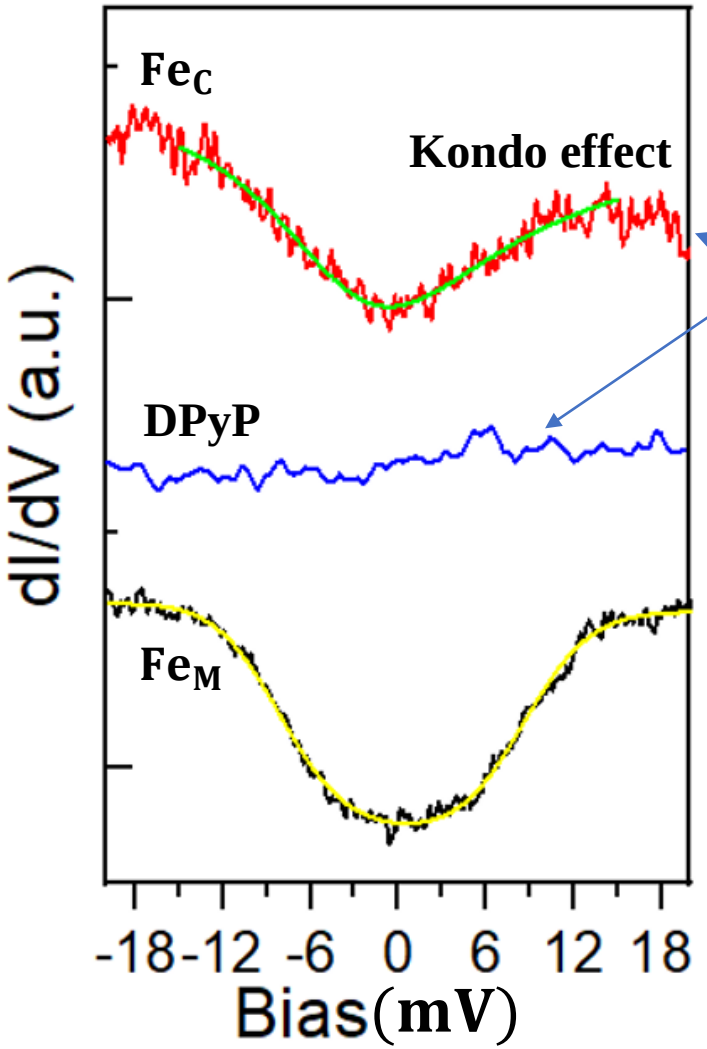

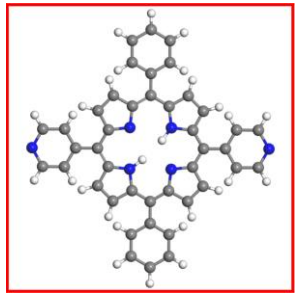

DPyP

Fano function

$$\frac{dI}{dV} = A\frac{[q + (x - \epsilon_0)/\Gamma]^2}{1 + [(x - \epsilon_0)/\Gamma]^2} + B$$

$$\Gamma = k_B T_K = 9.69\ \text{mV}$$

$$T_K = 112\ \text{K}$$

Principle of Kondo effect

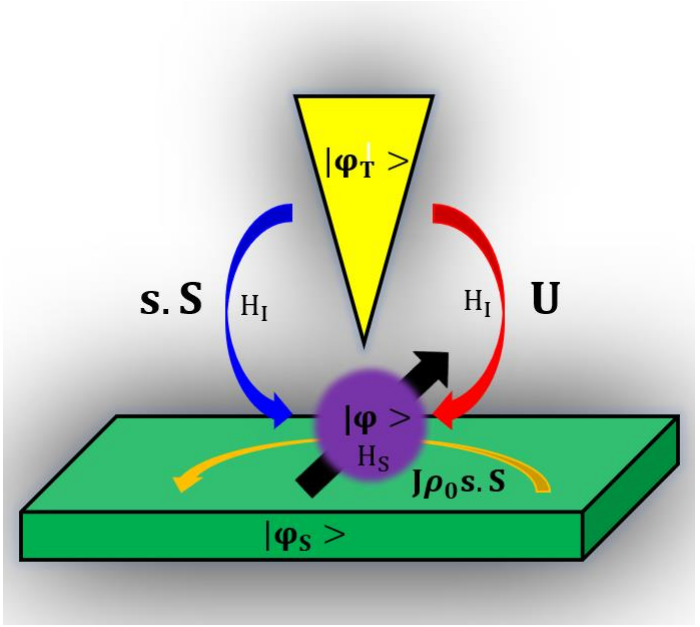

Completely screened by substrate electrons

Dominated

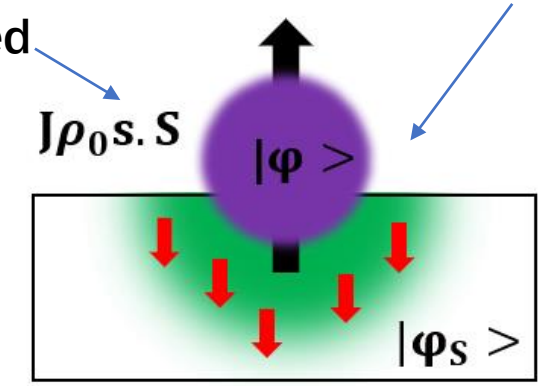

Many-body non-magnetic singlet state

Experiment and DFT calculations

Local density of states

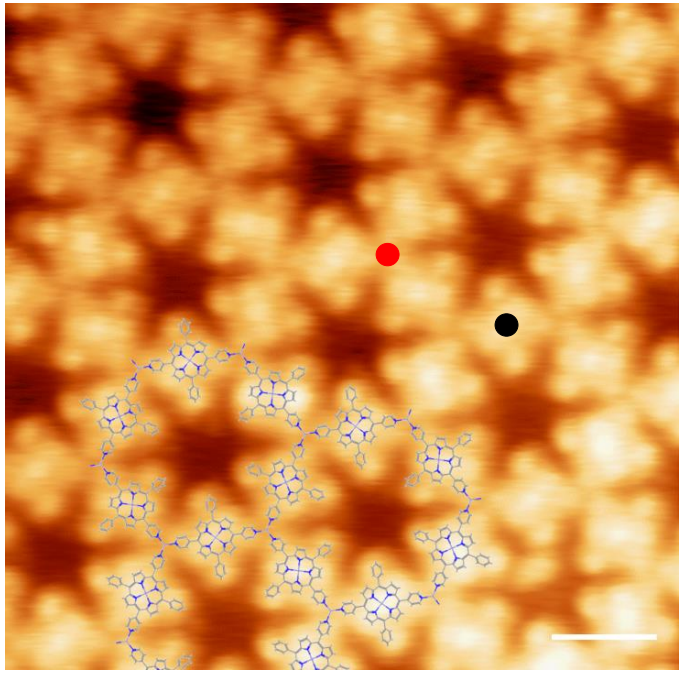

Scale bar: 2 nm

PBE+U=3.0, +SOC,

in-plane ferromagnetic

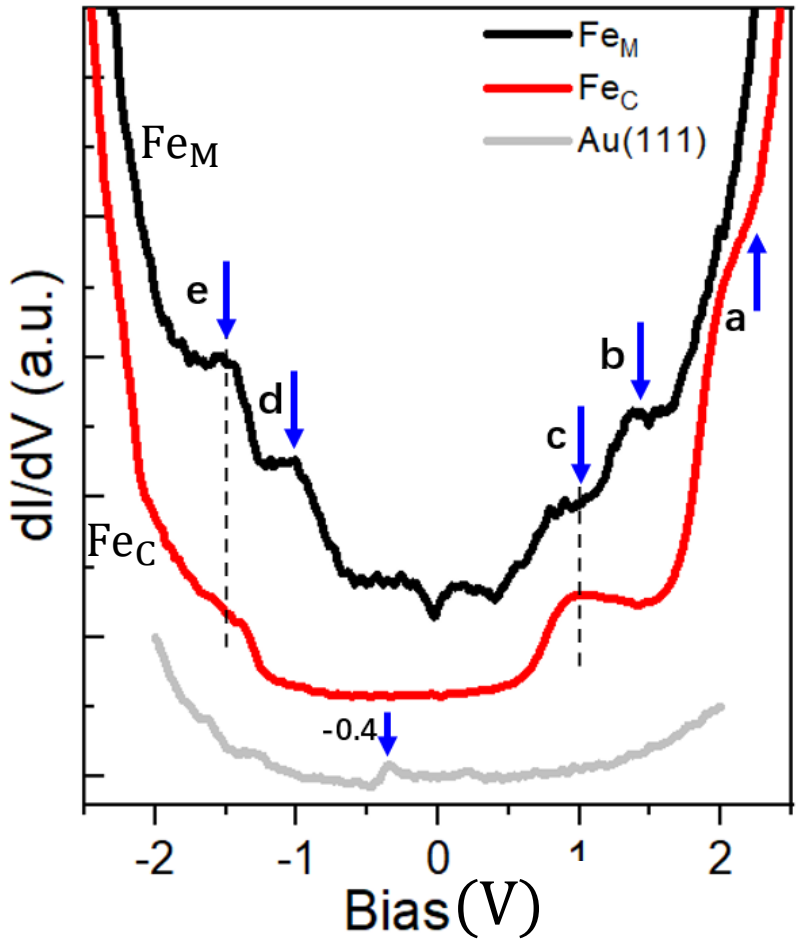

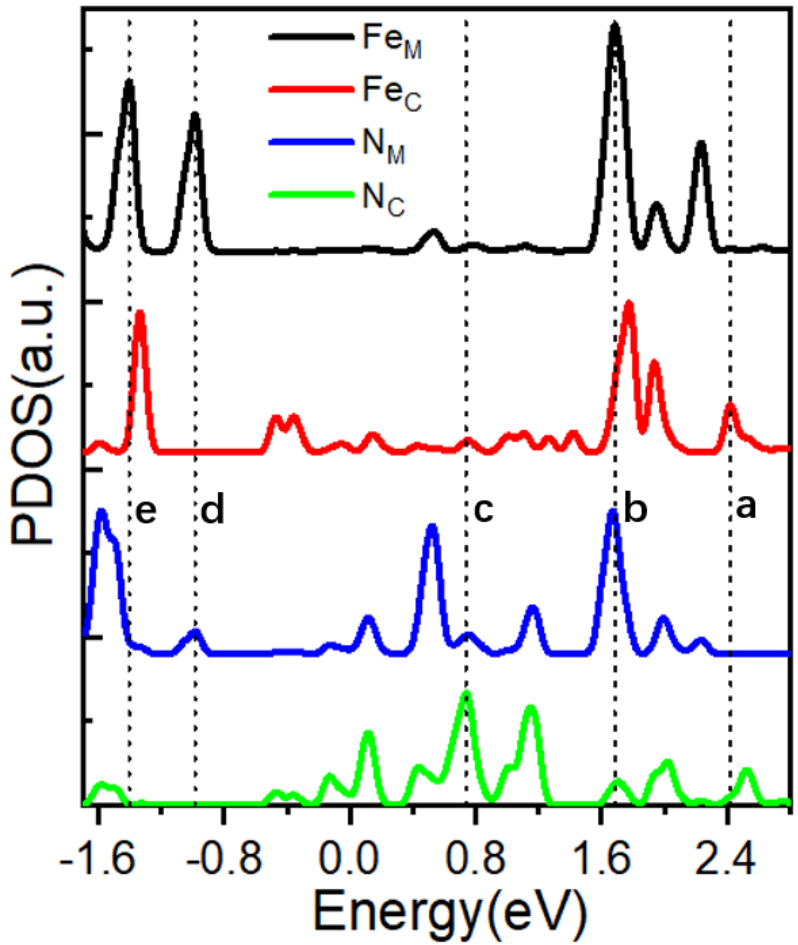

Experiment and DFT calculations

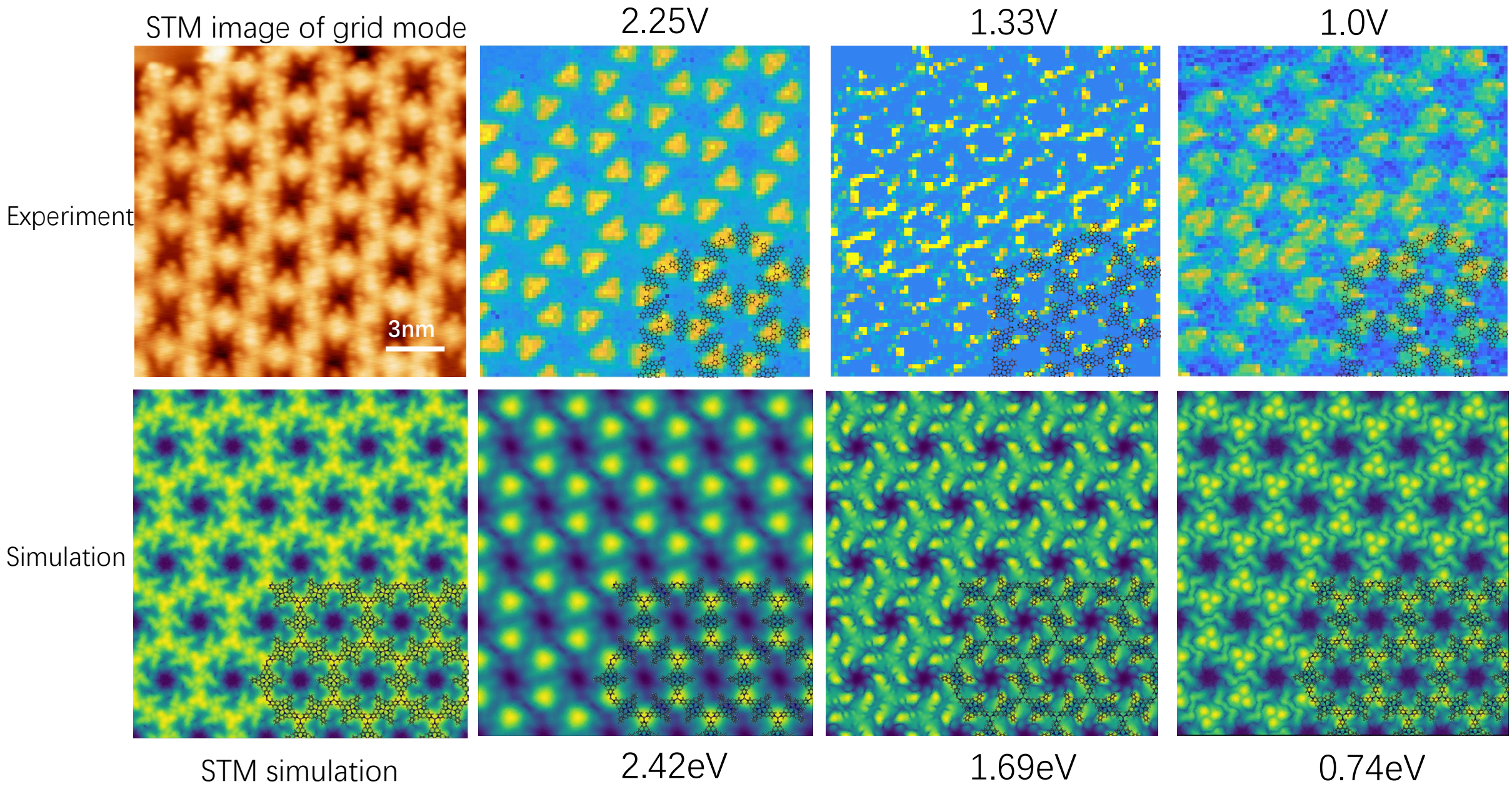

Experiment and DFT calculations

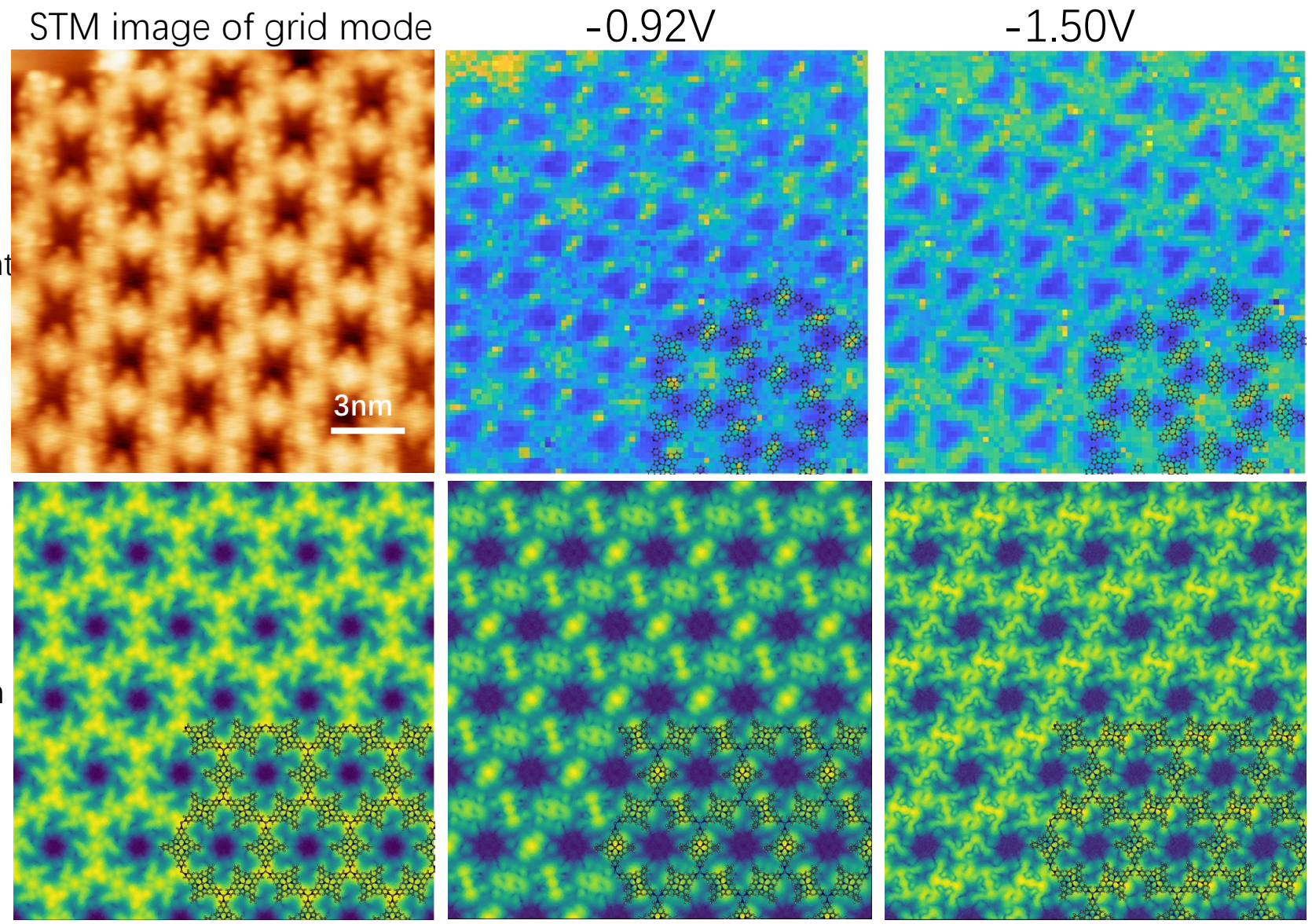

Conclusions

- Monolayer of two-dimensional honeycomb Kagome lattice synthesized on Au(111) substrate.
- The experimental measurements indicate that the coordination network has two types of spin states of iron.
- The DFT calculations show spin states of Fe_M is S=1 and Fe_C S= 3/2 and the magnetic ground state is in-plane ferromagnetic.

(1) The Kondo effect suggests that Au(111) substrate quenches the magnetic order.

(2) To preserve the magnetic order, directly synthesizing this coordination network on inert substrate like graphene is highly desired.

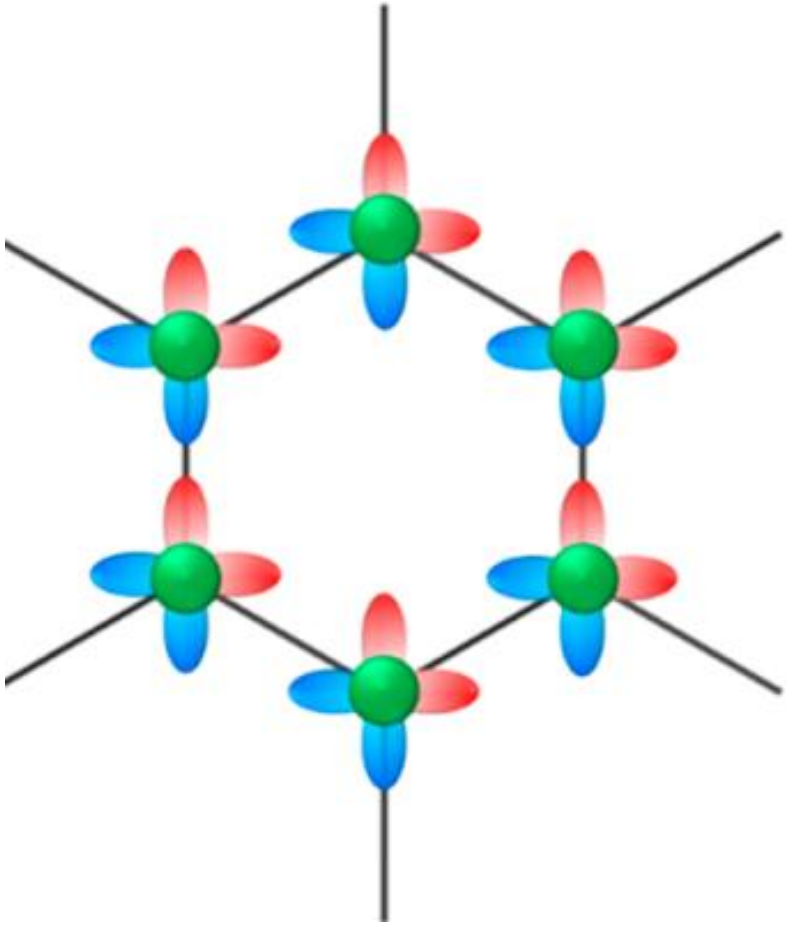

PART 04

Part 4 Two-Dimensional Metal Organic Network with p-Orbital Honeycomb Kagome Lattice

Experiment

Step 1: Depositing DPyP on Au(111) surface held at RT: the molecules are closed pack in rectangular, string-like shape molecular islands.

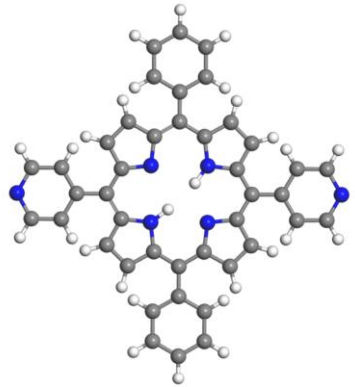

DPyP

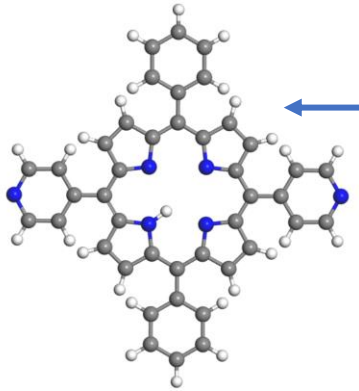

$DPyP_{-H}$

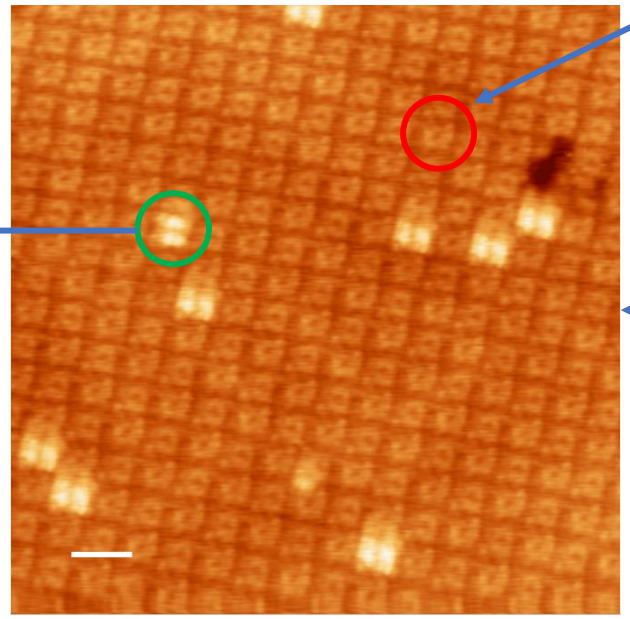

Scale bar: 2 nm

Zoom in

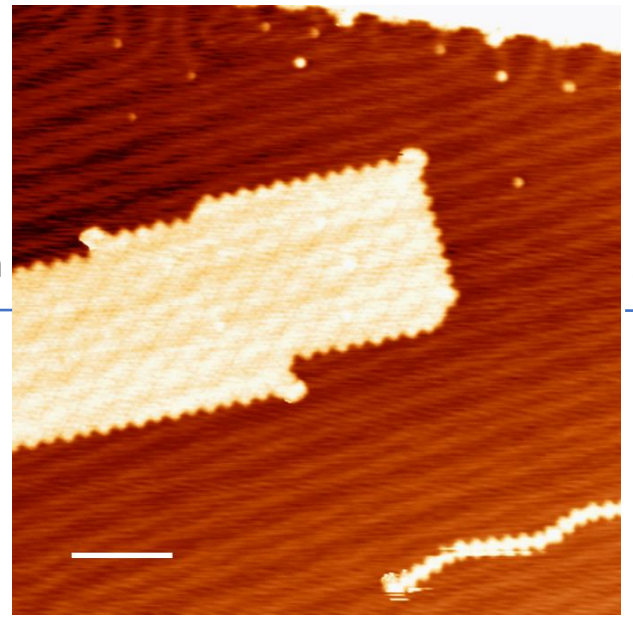

Scale bar: 10 nm

Zoom in

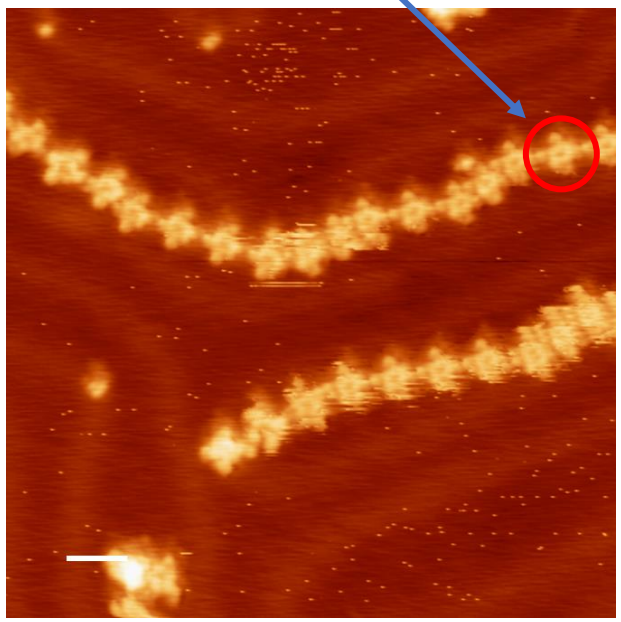

Scale bar: 2 nm

Experiment

Step 2: Depositing HAT on Au(111)+DPyP surface held at RT: Large size hexagonal closed pack islands appear on the surface.

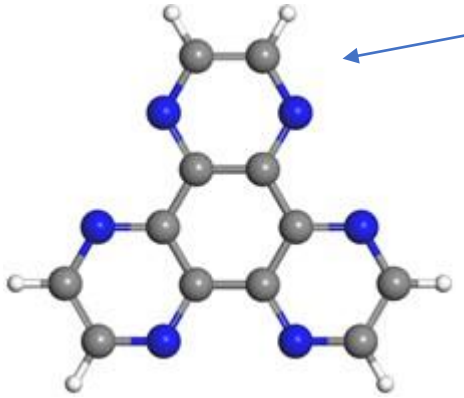

HAT

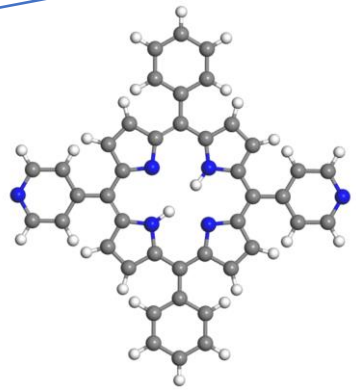

DPyP

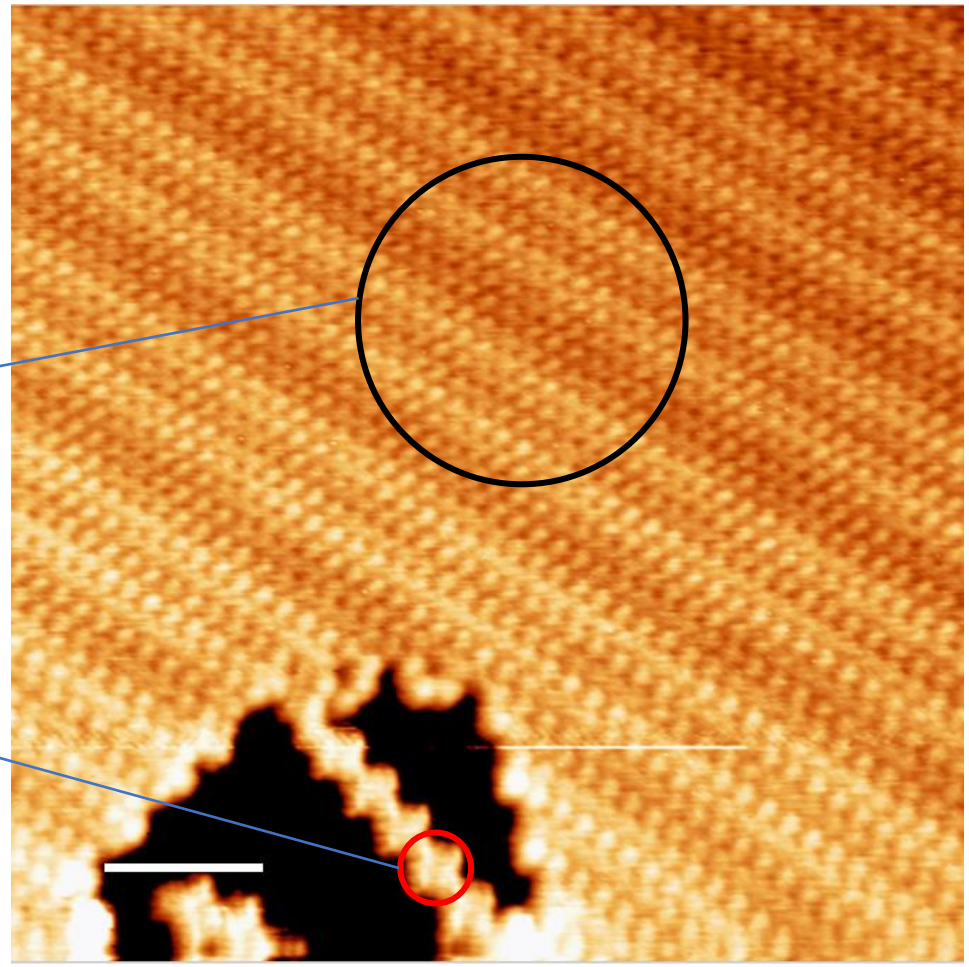

Scale bar: 5 nm

Experiment

Step 3: Depositing Fe onto the Au(111)+DPyP+HAT and annealing the sample to 170°C: 2D Porous networks are observed.

Step 1+step 2+step 3

Two molecular component MOF consisting of DPyP and HAT coordinated with Fe

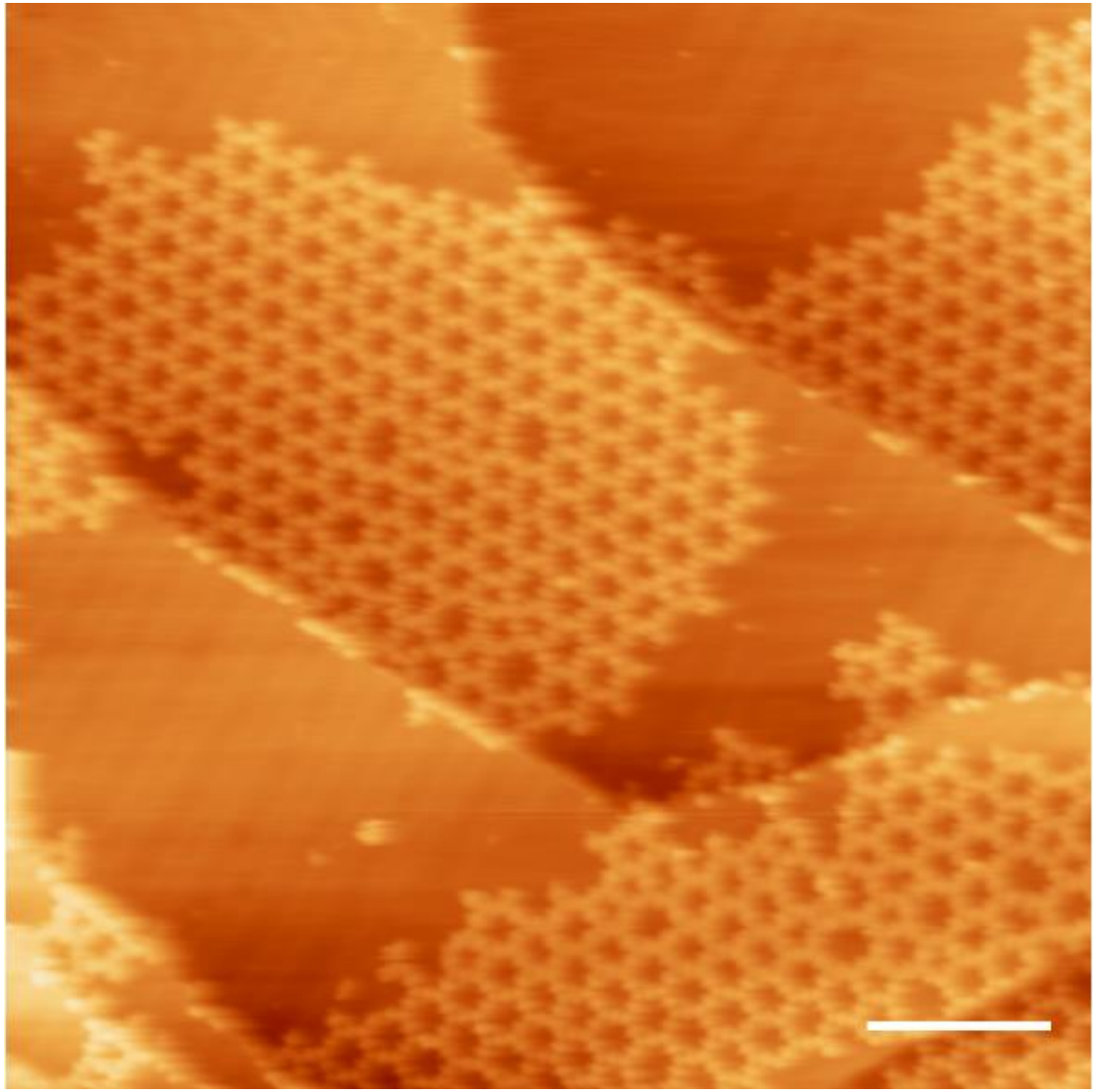

Scale bar: 20 nm

Experiment

6-member ring hexagonal structure

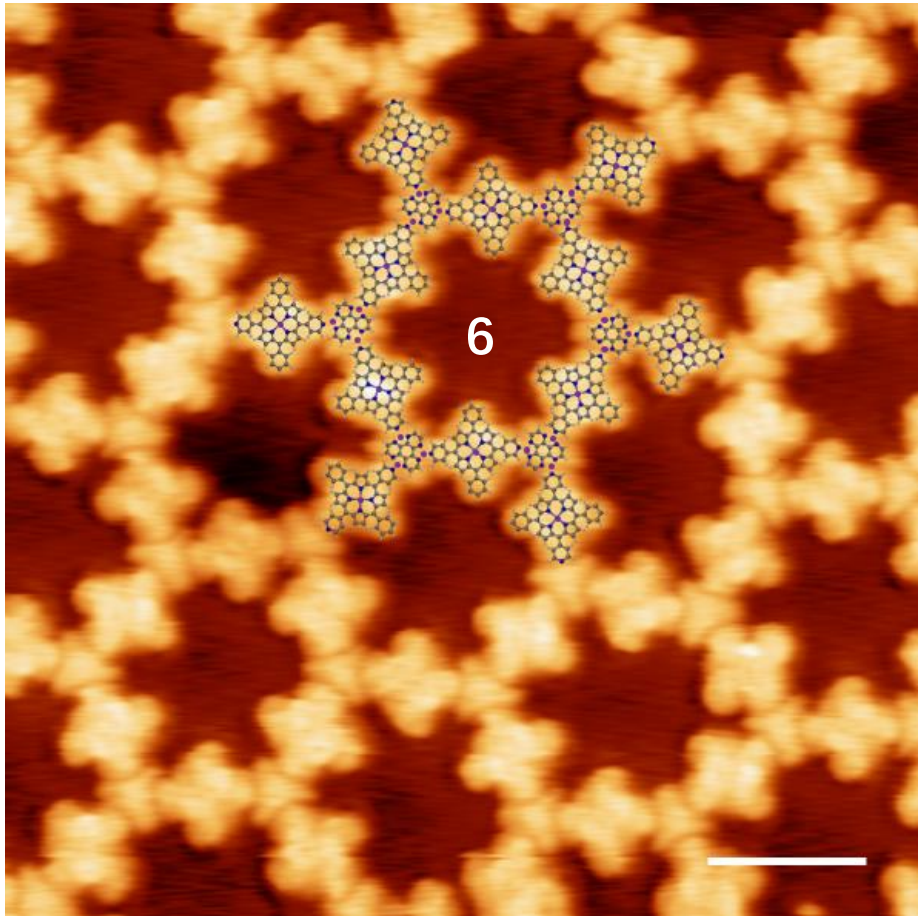

Lattice constant: 4.61 ± 0.2nm

Scale bar: 3 nm

5-, 7-, and 8-member ring structures

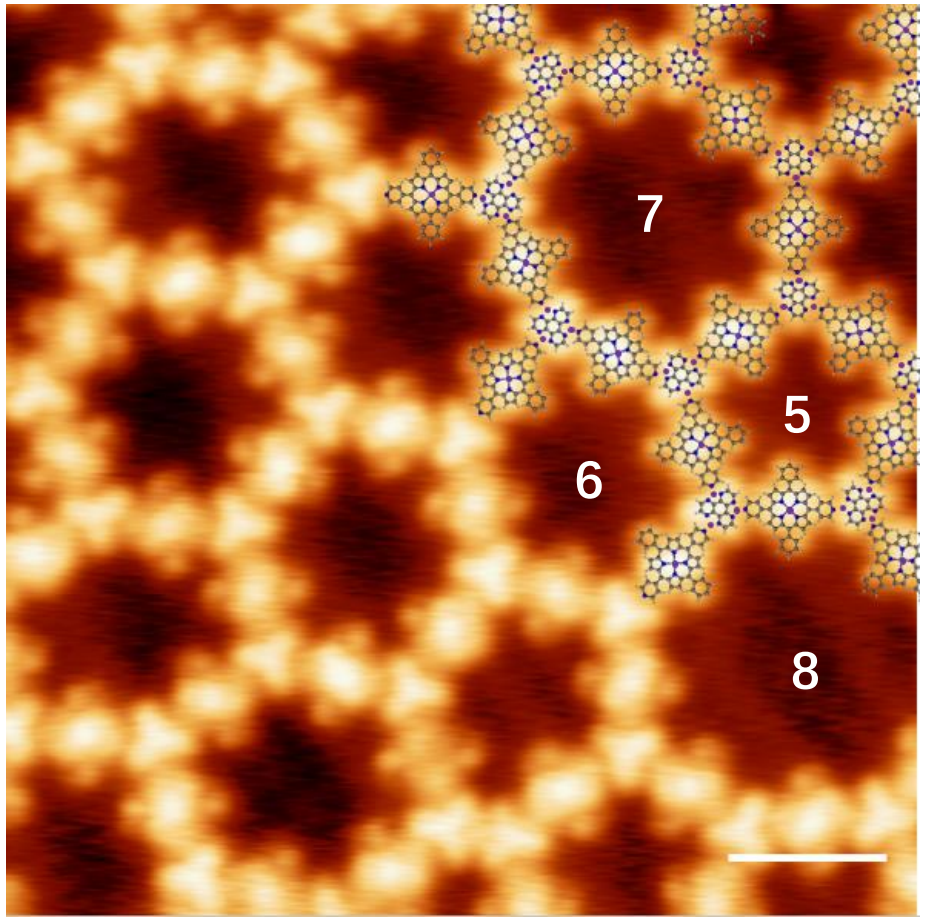

Scale bar: 3 nm

DFT calculations

Top View

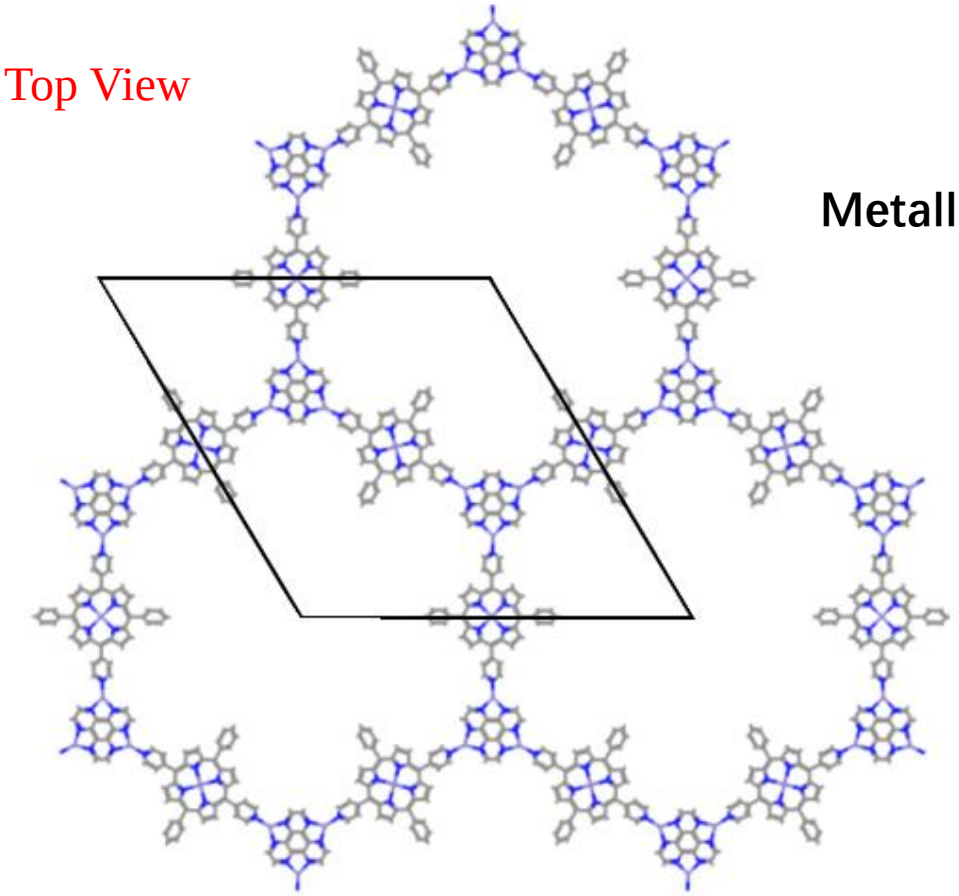

Side View

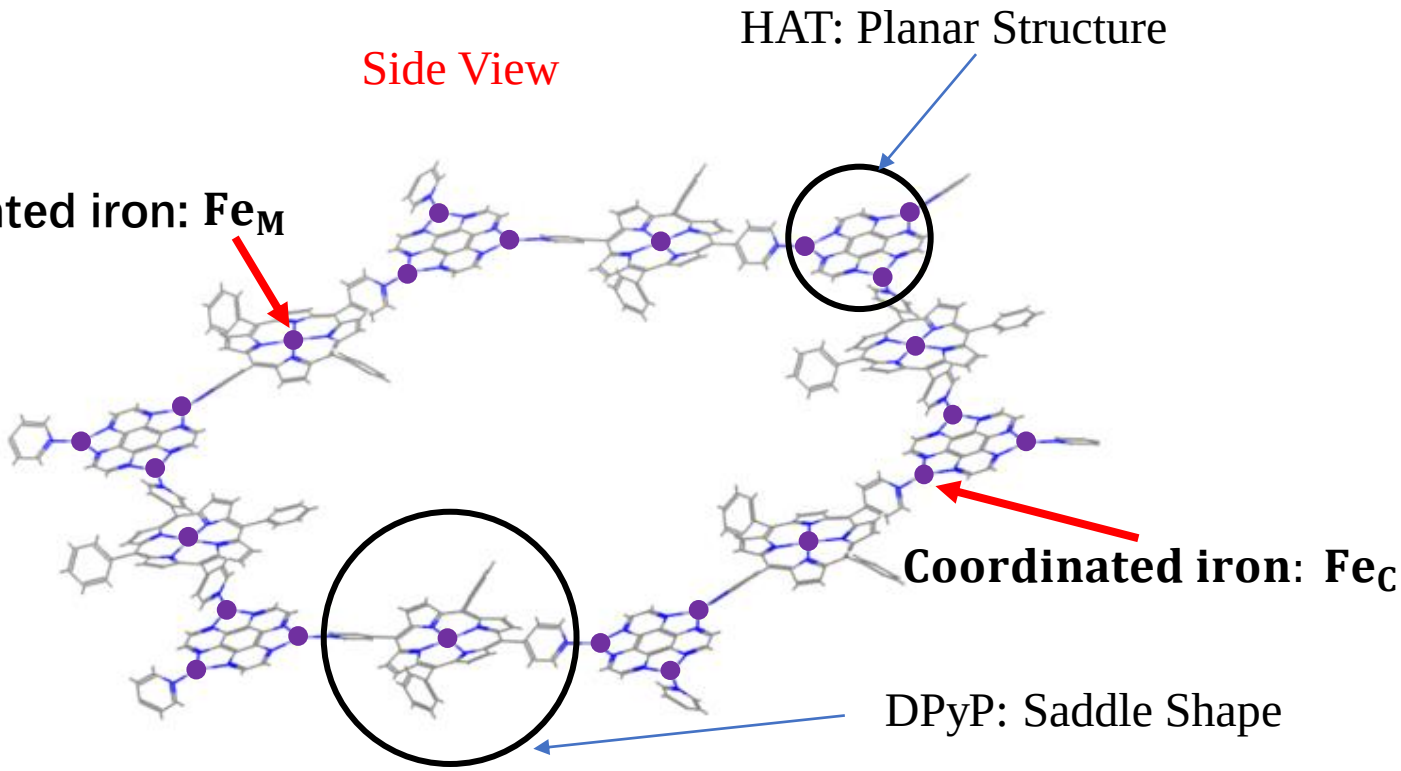

Magnetic moment on Fe-DPyP: $3.61\mu_B$ → S=2

Lattice constant

Experiment: 4.61 ± 0.2nm

Calculation: 4.7nm

S=2 —conformation change (Au(111) surface)→ S=1

Switch

Fe-N bond length

Experiment

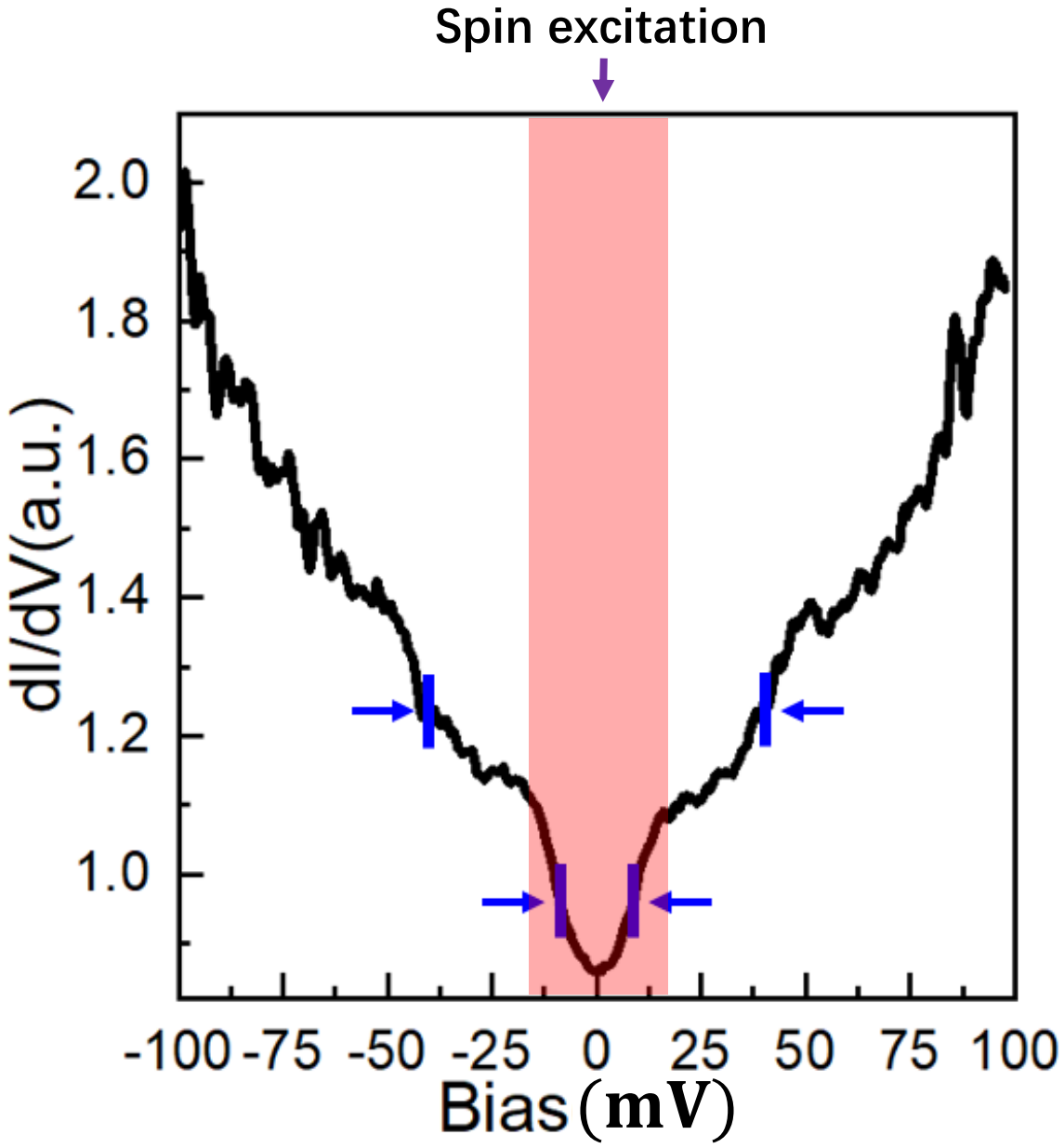

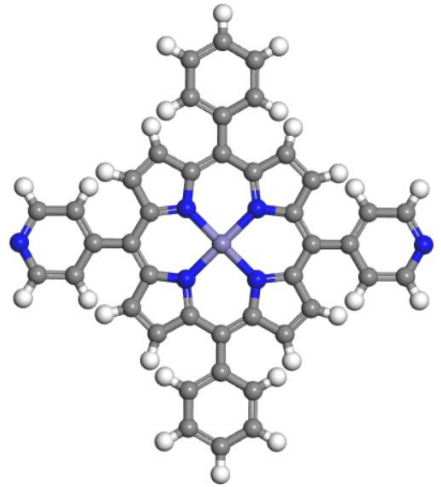

Fe-DPyP

Spin excitation : $\pm 8.4 meV$

Molecular vibration : $\pm 38.4 meV$

The local magnetic moments in Fe break the time-reversal symmetry and lift the spin degeneracy of coordination network

Experiment

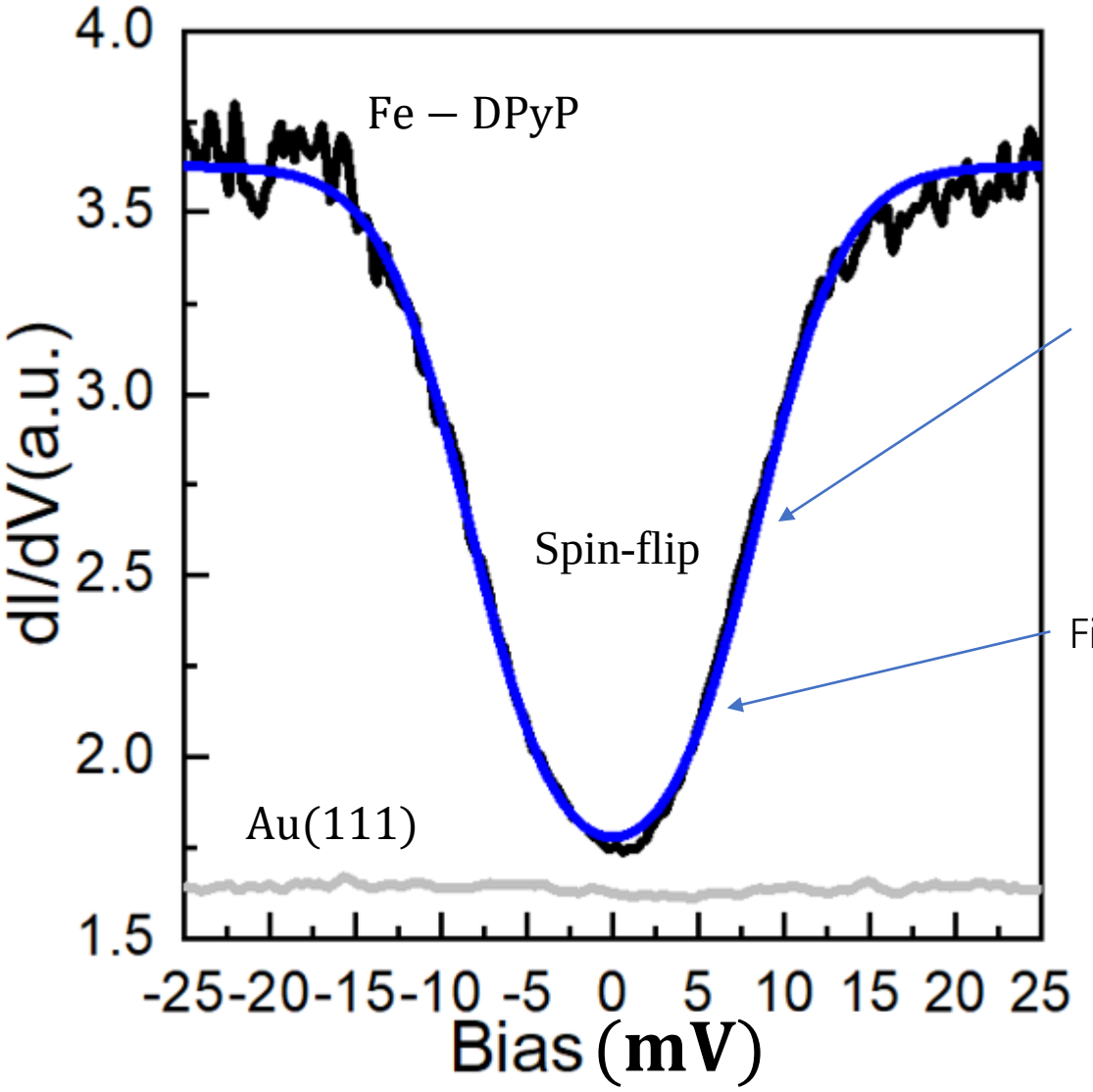

For zero-field splitting (ZFS)

Fitting results: **D=8.41meV, E=0**

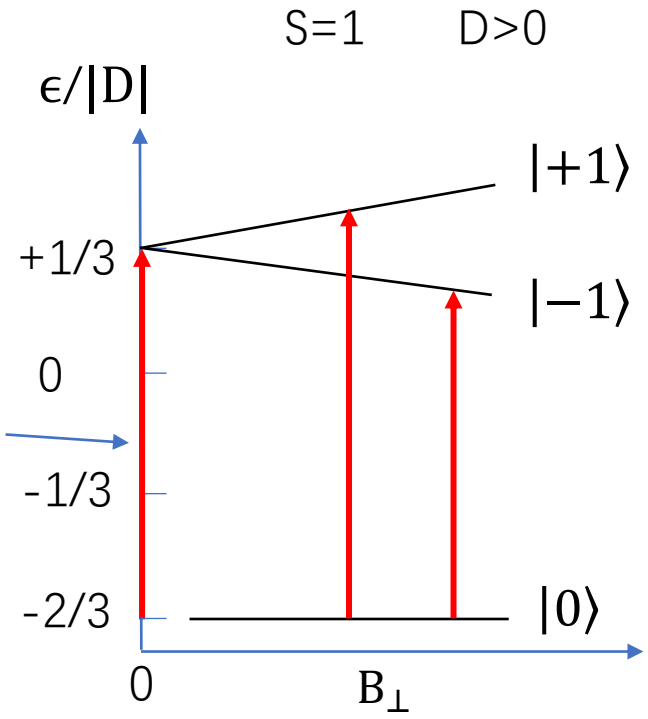

D>0, easy-plane type magnetic anisotropy

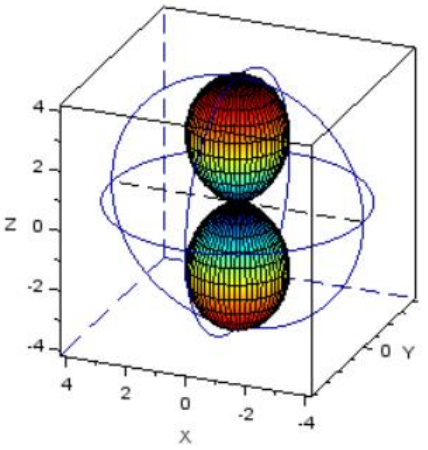

DFT calculation

Hybridization between Fe orbitals and molecular orbitals

Dirac cone bands

Flat-bands

Atomic pz orbitals of C and N atoms in molecules

Spin-up band sets

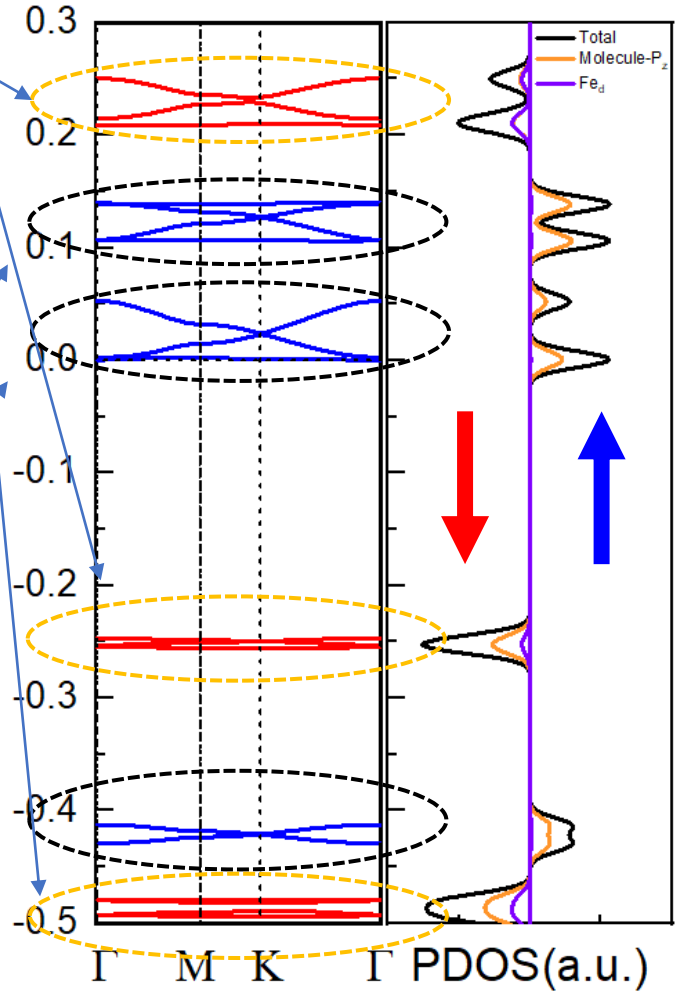

Spin-polarized Band Partial Density of States

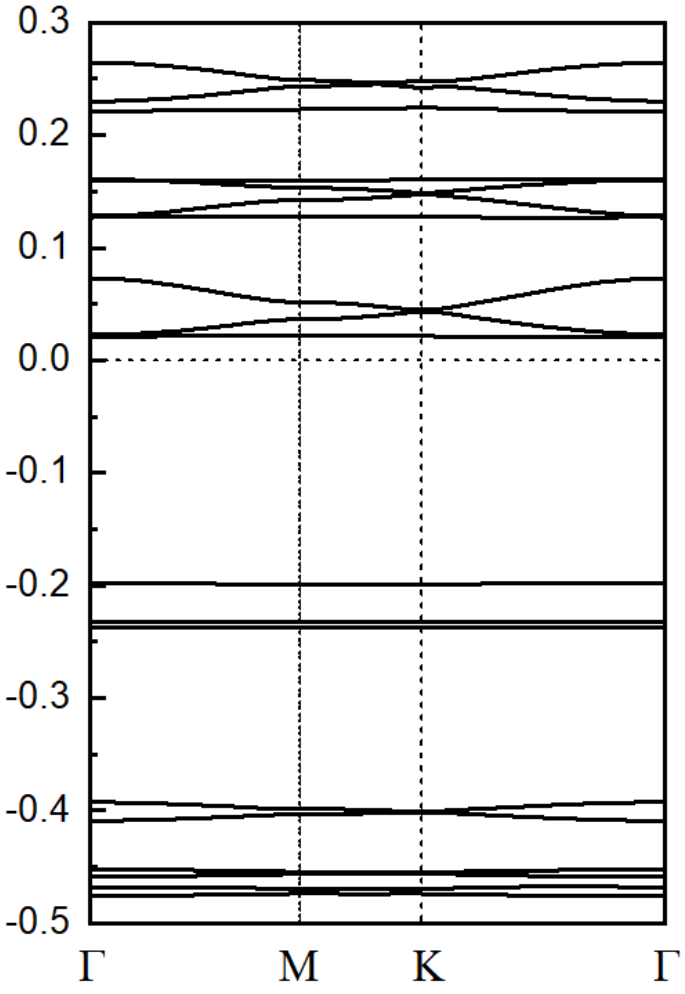

SOC Band

SOC rarely changes the band structure

C and N atoms are very light

Tight-Binding Modeling

Treat the DPyP and HAT molecules as super-atoms

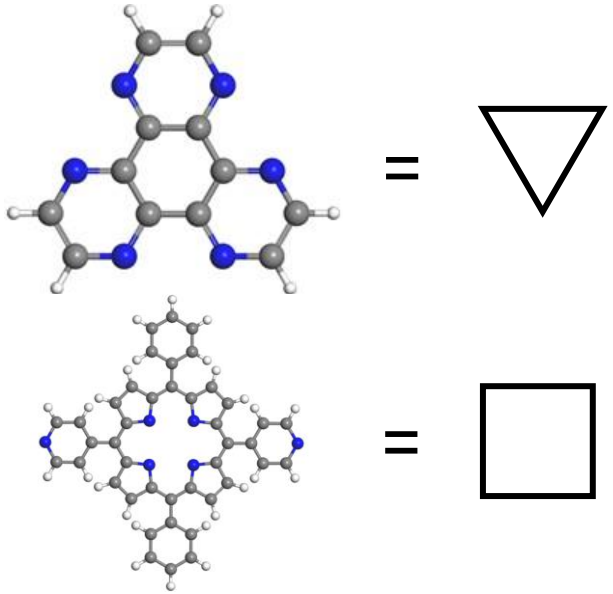

The salient features of the DFT calculated band structure can be highlighted and explained with TB modeling

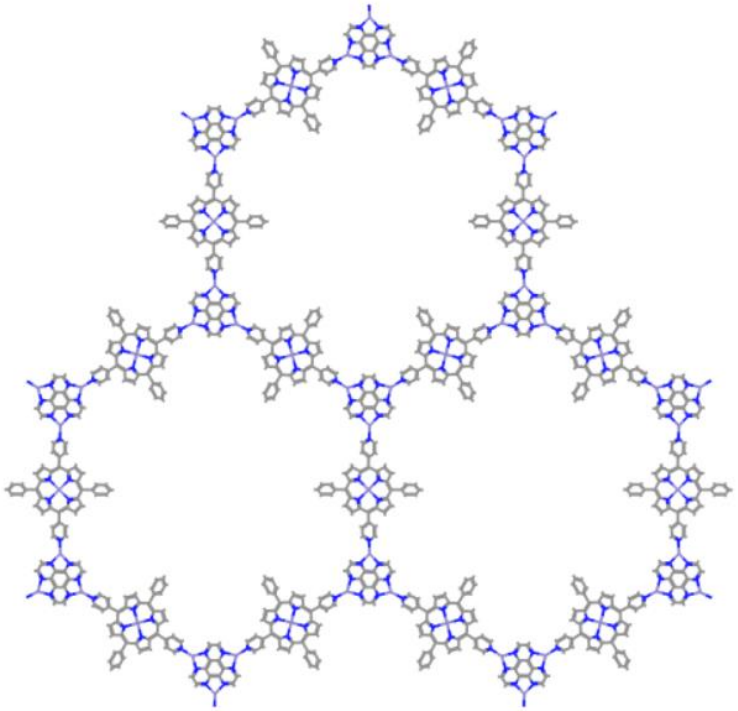

super-atoms at lattice sites

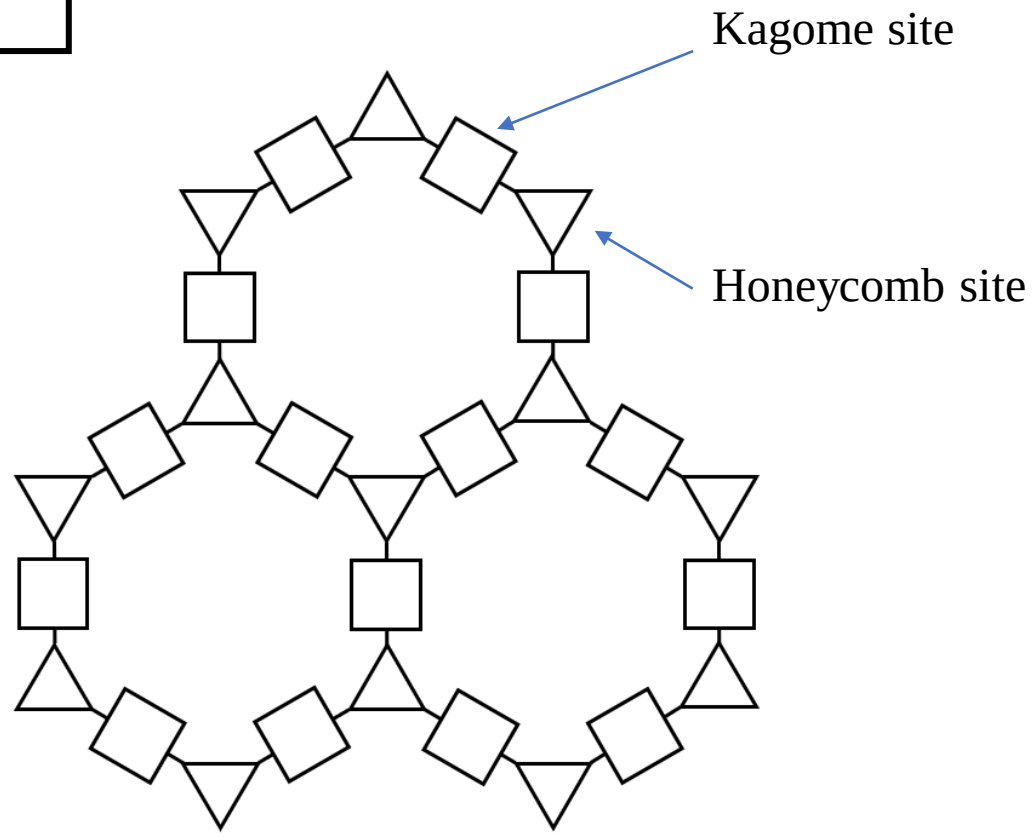

Honeycomb Kagome lattice

Tight-Binding Modeling

Simplify the HAT molecules as super-atoms

18 orbitals TB

Analyze the symmetry of the super-atom orbitals

The lowest orbitals show the symmetry of s, px/py, orbital symmetry in HAT

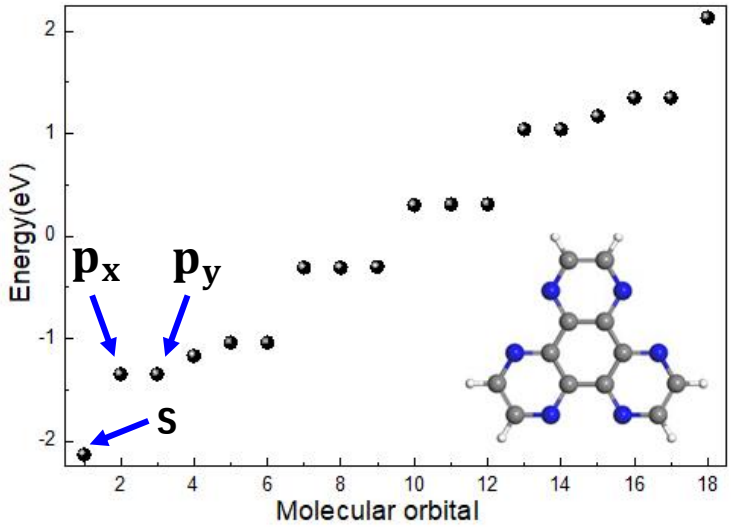

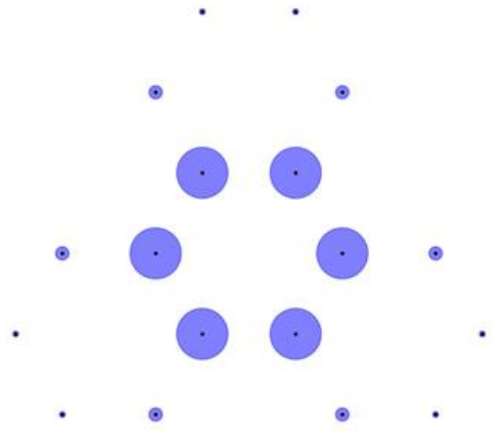

s orbital symmetry

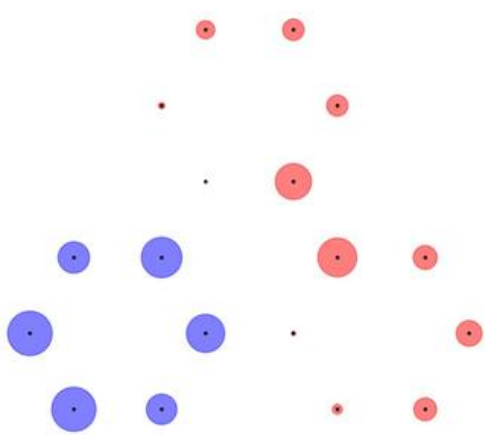

p_x orbital symmetry

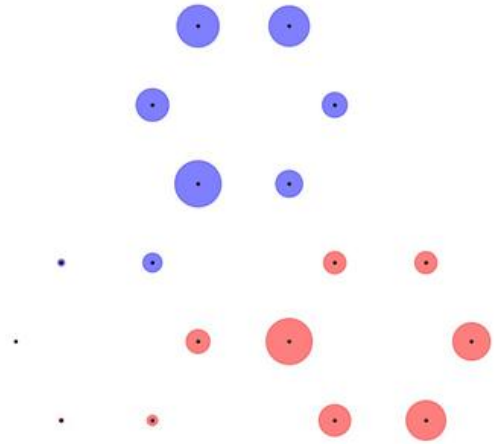

p_y orbital symmetry

Tight-Binding Modeling

Honeycomb kagome lattice

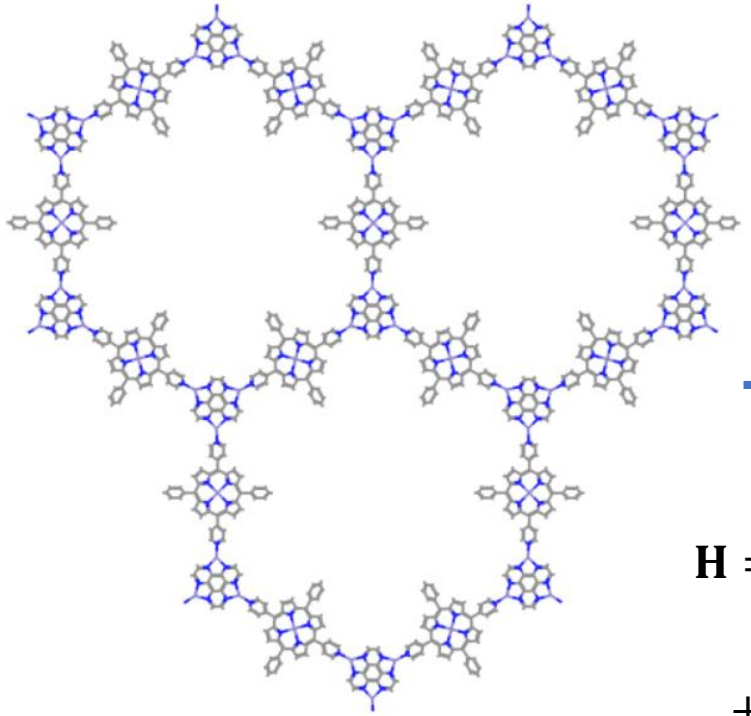

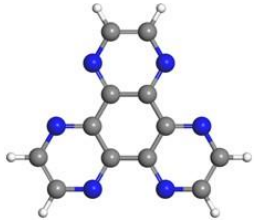

→ s orbital

→ p_x/p_y orbital

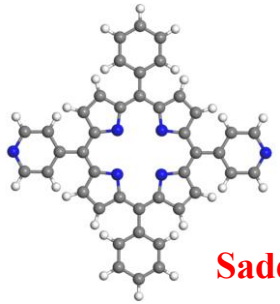

→ s orbital

Saddle shape with low spatial symmetry

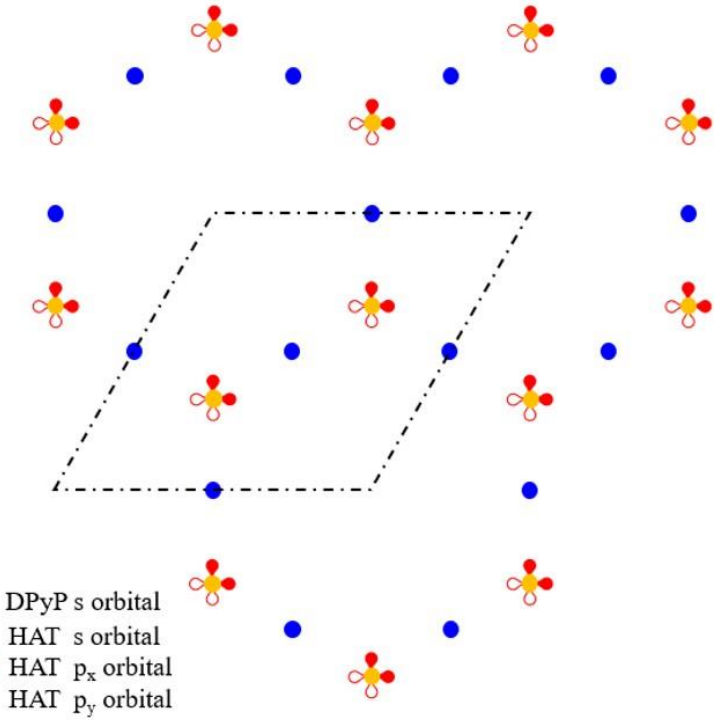

$$\mathbf{H} = \mathbf{t_{sp\sigma}} \sum_{\mathbf{p\in\{px,py\},<HAT,DPyP>}} \mathbf{|HAT,p\rangle\langle DPyP,s|}$$

$$+\mathbf{t_{ss\sigma}} \sum_{\mathbf{p\in\{px,py\},<HAT,DPyP>}} \mathbf{|HAT,s\rangle\langle DPyP,s|}$$

DFT calculation and Tight-Binding Modeling

TB parameters

$\mathbf{Onsite_{DPyP\_s} = 0.035\ eV}$

$\mathbf{Onsite_{HAT\_s} = -0.41\ eV}$

$\mathbf{Onsite_{HAT\_p} = 0.1\ eV}$

$\mathbf{t_{sp\sigma} = -0.035\ eV}$

$\mathbf{t_{ss\sigma} = -0.04\ eV}$

Hamiltonian

$$H = t_{sp\sigma} \sum_{p\in\{px,py\},<HAT,DPyP>} |HAT,p\rangle\langle DPyP,s| + t_{ss\sigma} \sum_{p\in\{px,py\},<HAT,DPyP>} |HAT,s\rangle\langle DPyP,s|$$

Tight-Binding calculated Band structure

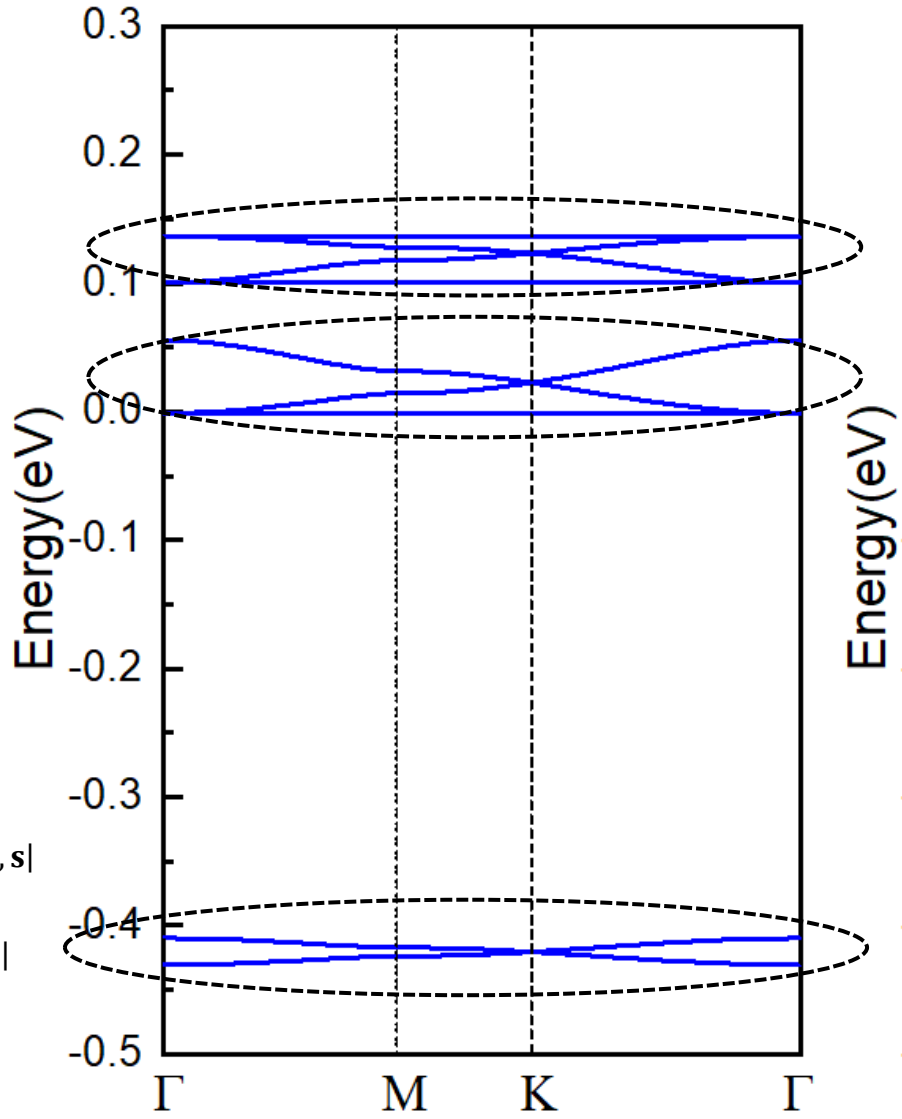

DFT calculated Band structure

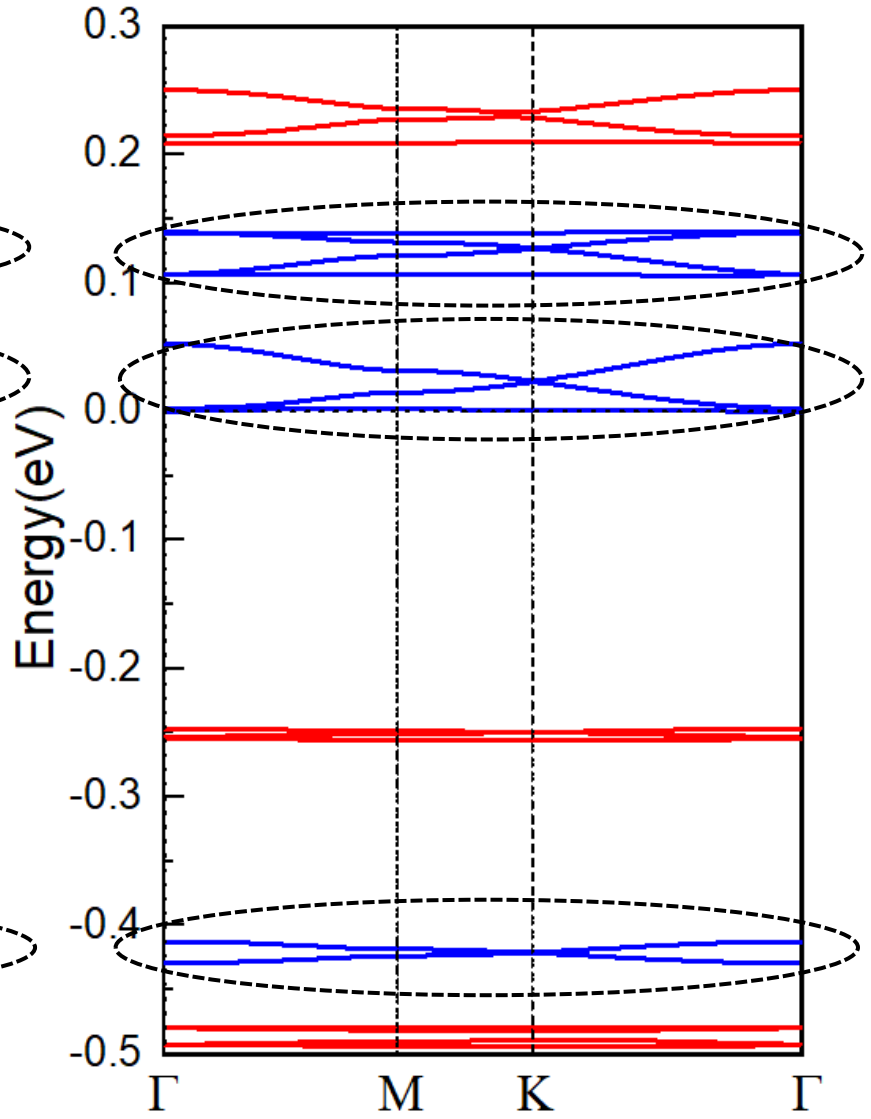

Spin up

Spin down

Tight-Binding Modeling

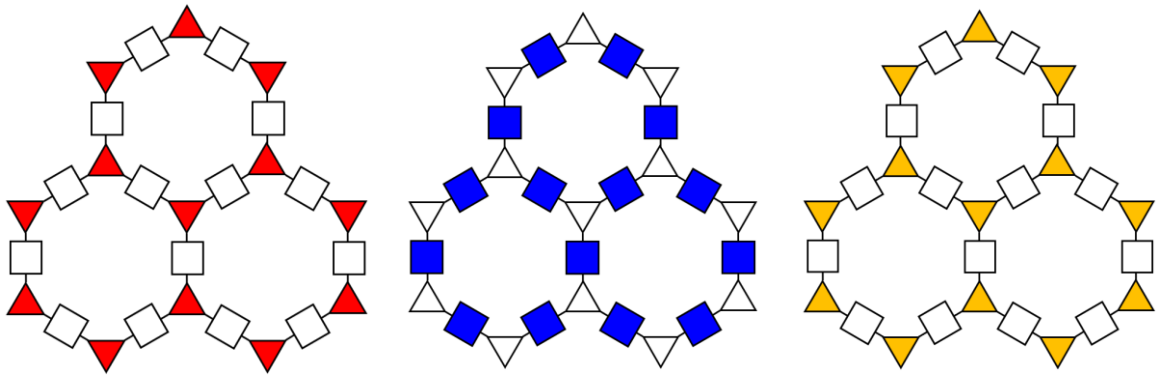

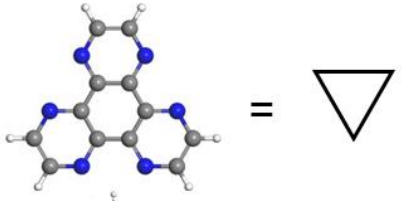

=

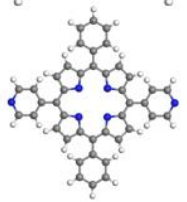

=

Without sp hybridization

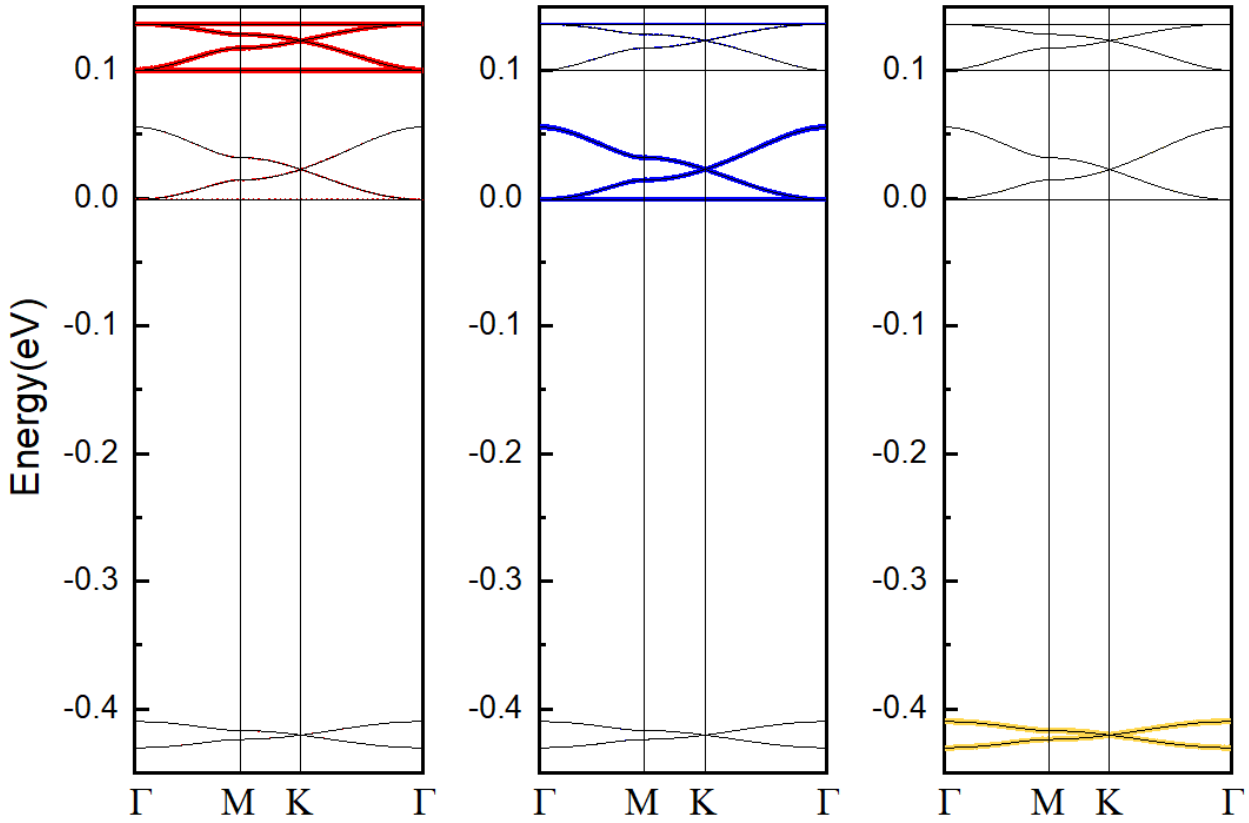

Red: HAT p_x/p_y orbital Blue: DPyP s_orbital Orange: HAT s_orbital

Red: HAT p_x/p_y orbital

Total plot

Blue: DPyP s_orbital

Orange: HAT s_orbital

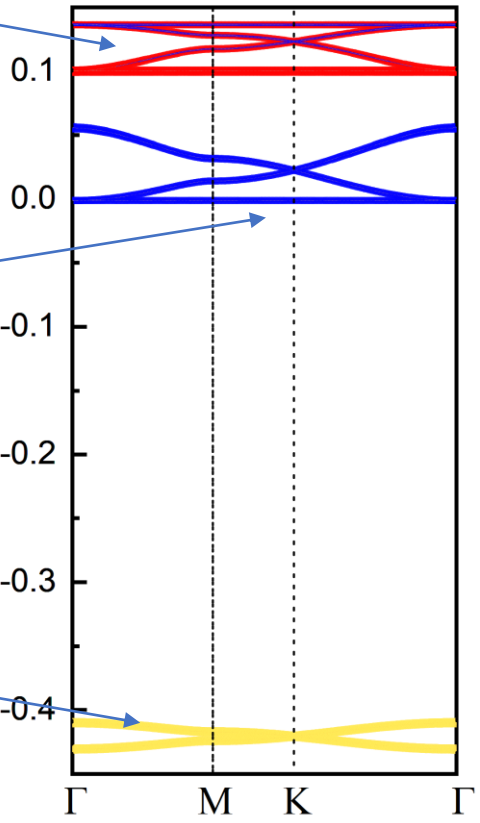

Experiment

Local density of states

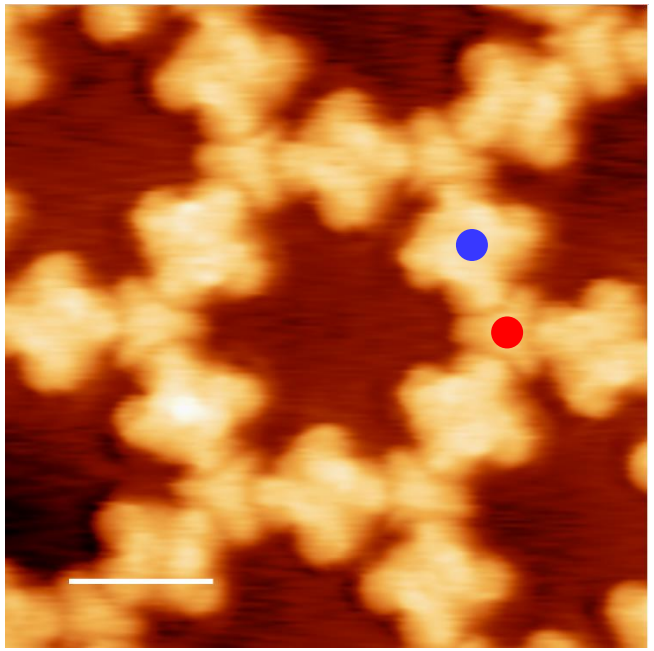

Scale bar: 2 nm

Experiment

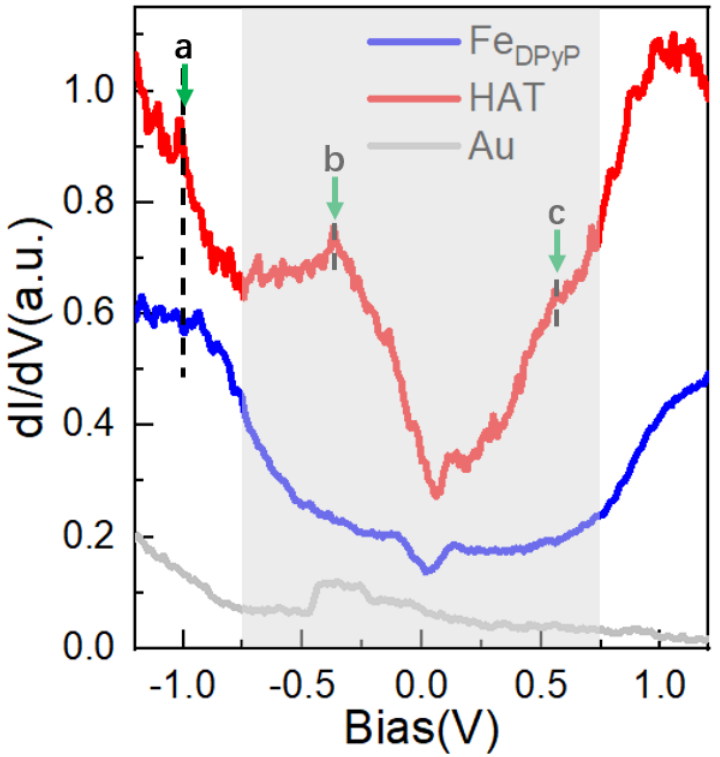

The dI/dV spectra

Calculation

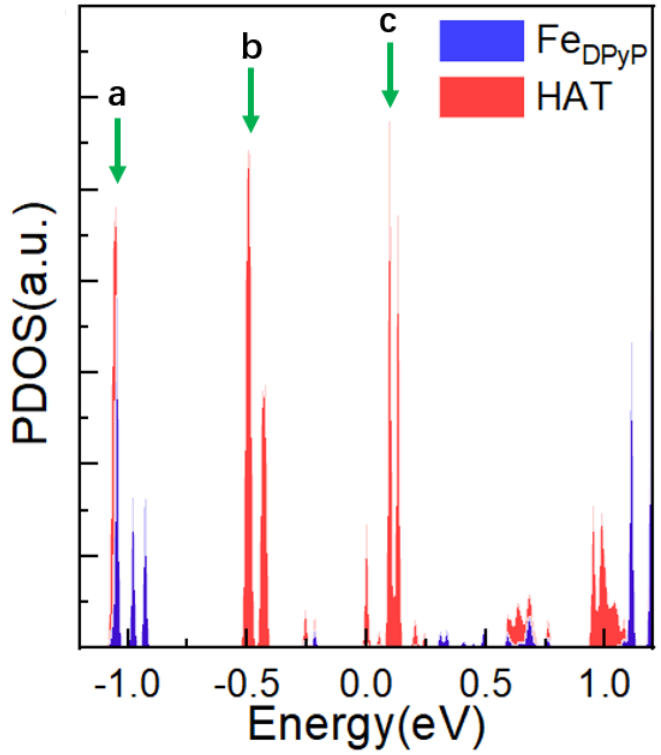

The calculated PDOS

Large-range STS measurement of
$(Fe_3{-}HAT)_2(Fe-DPyP)_3$ network

0.1eV

-0.5eV

-1.1eV

Simulation

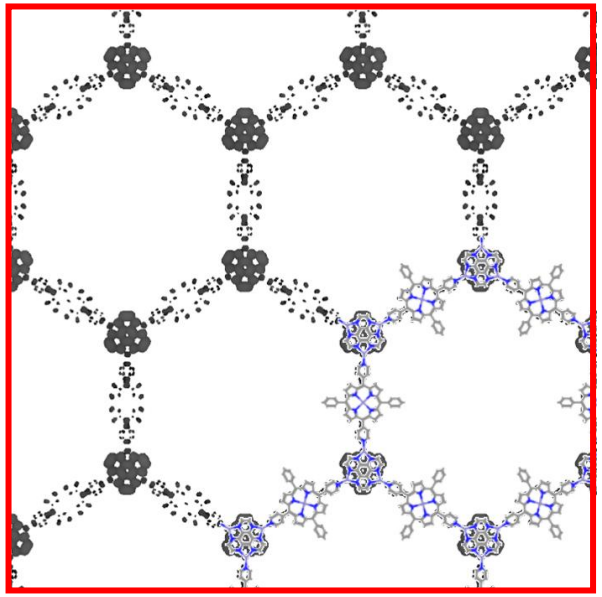

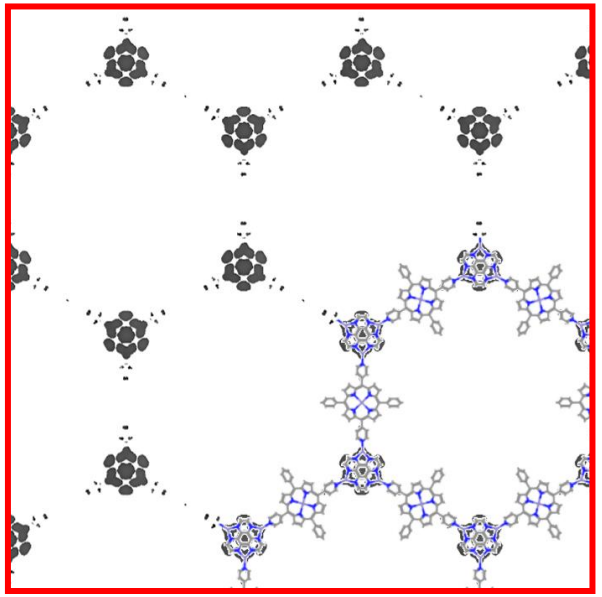

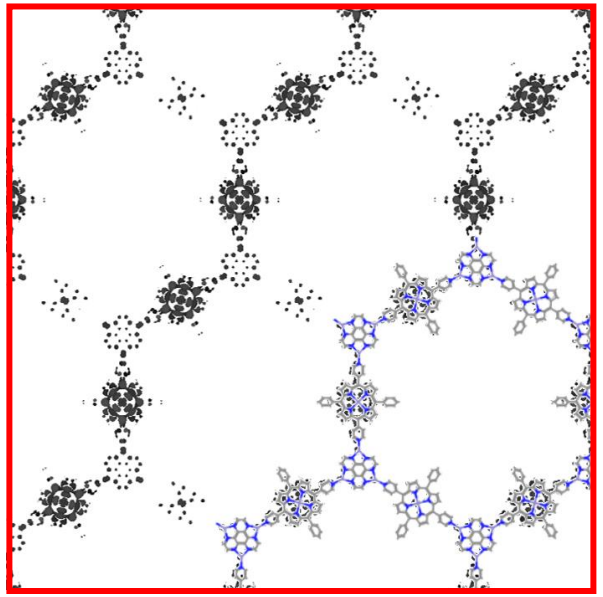

Experiment

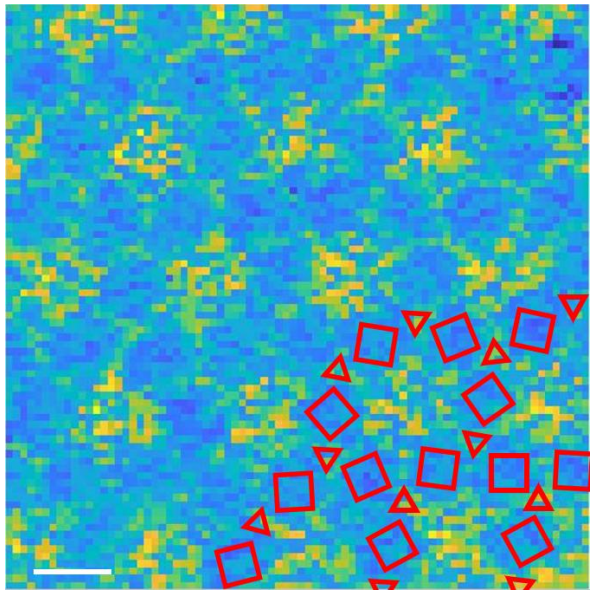

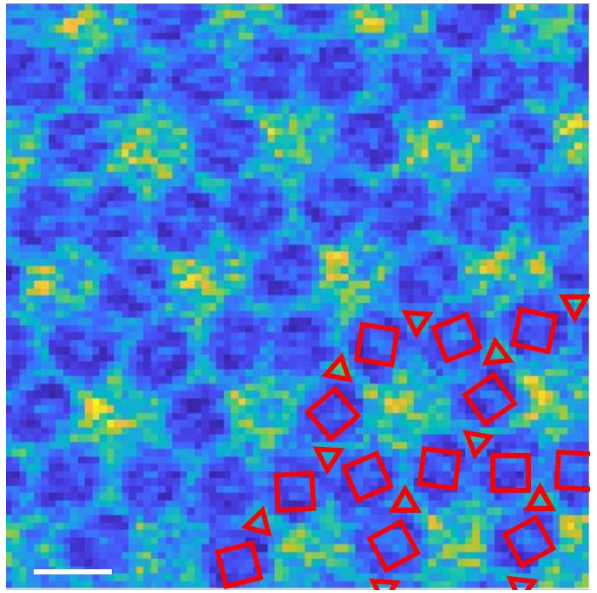

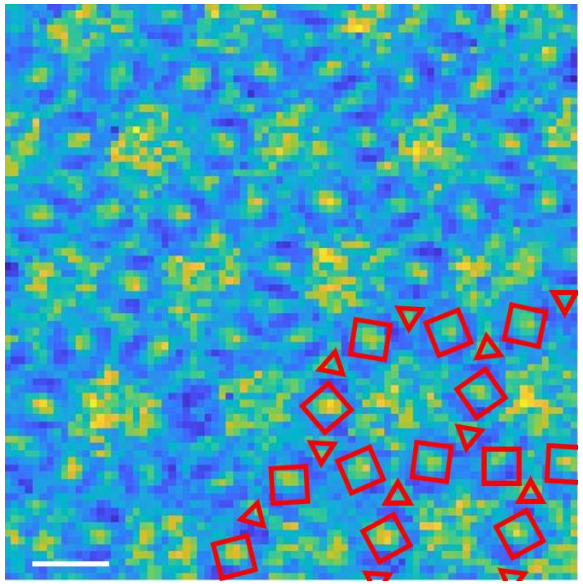

Scale bar 2nm

0.58V

-0.33V

-1.0V

Conclusions

- Monolayer of two-dimensional p-orbital honeycomb Kagome coordination network synthesized on Au(111) substrate.
- STS measurement shows a Spin-flip excitation on Fe-DPyP indicating presence of magnetic moments.
- DFT calculations show the iron magnetic moments lift the spin degeneracy of the bands.

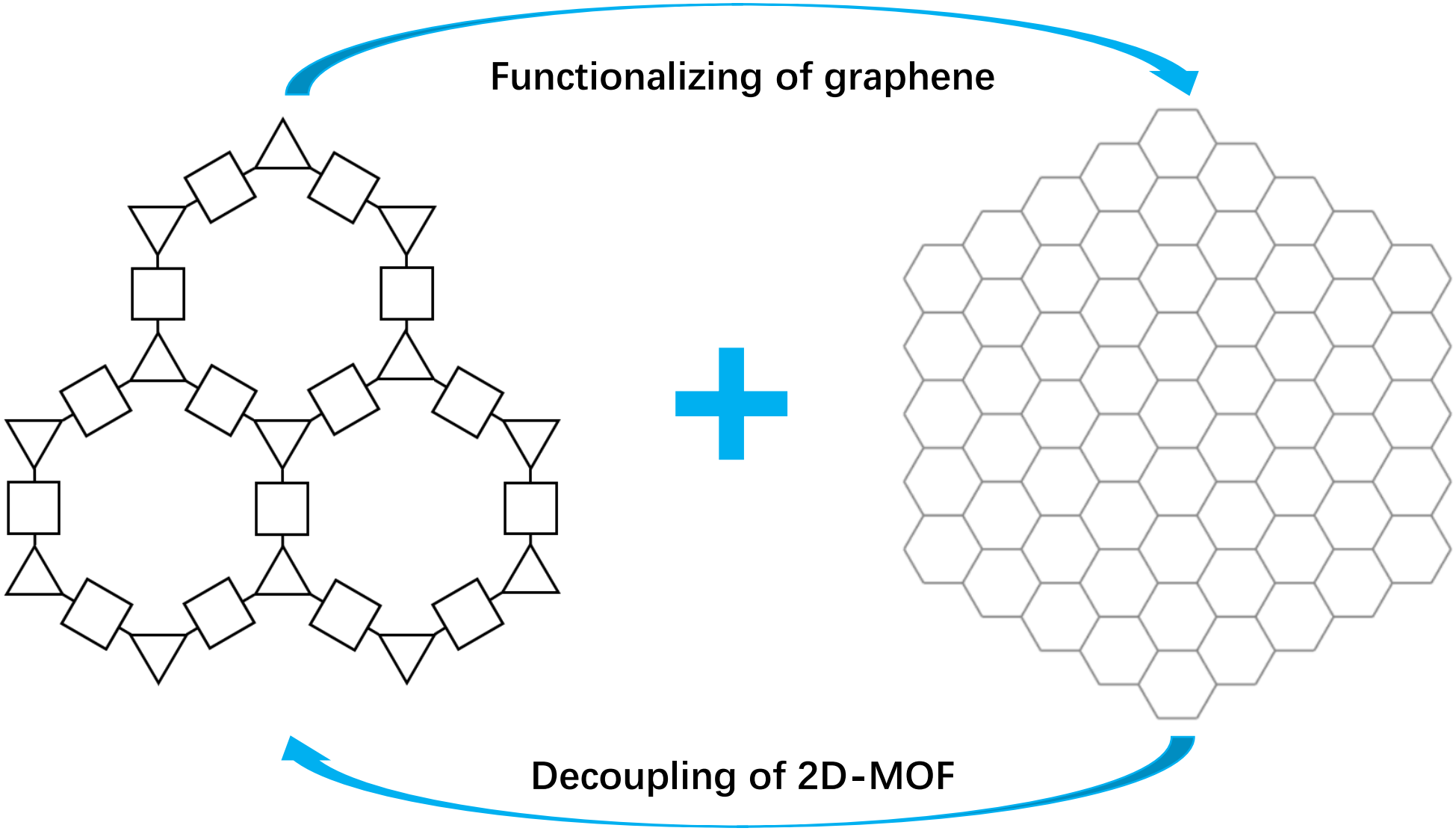
Functionalizing of graphene
Decoupling of 2D-MOF

Conclusions

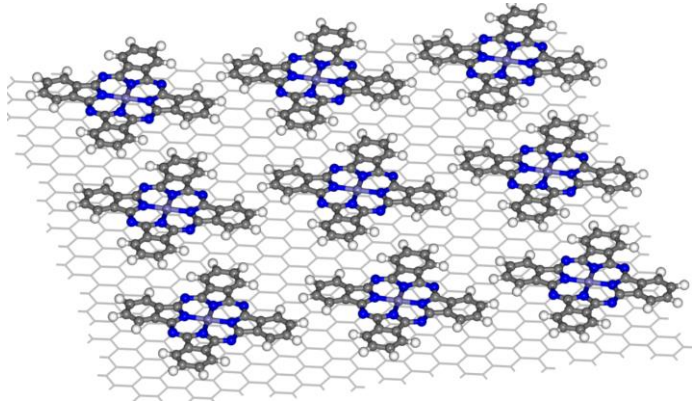

Graphene/h-BN
Hall device
+FePc

Spin Resonant Scattering

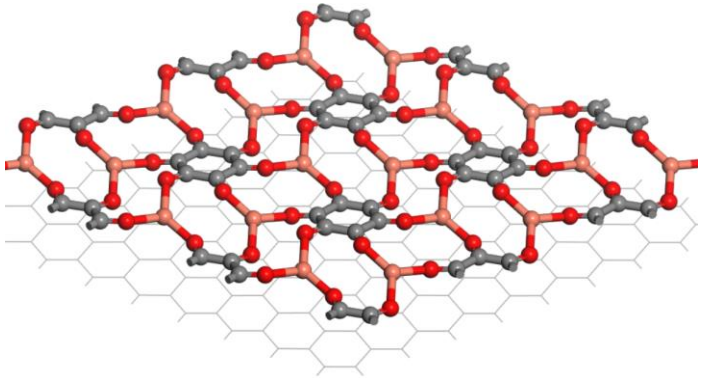

Graphene/SiC
BHO+Cu

$Cu_2(C_6O_6)$ metal-organic framework

Narrow band gap semiconductor

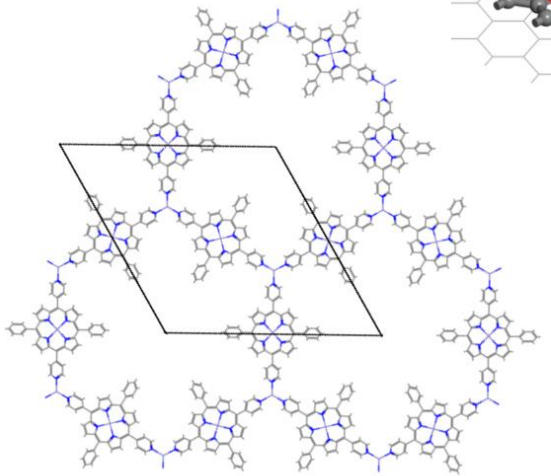

Au(111)
DPyP+Fe

$Fe_2(Fe-DPyP)_3$ metal-organic framework

Mixed Spin States

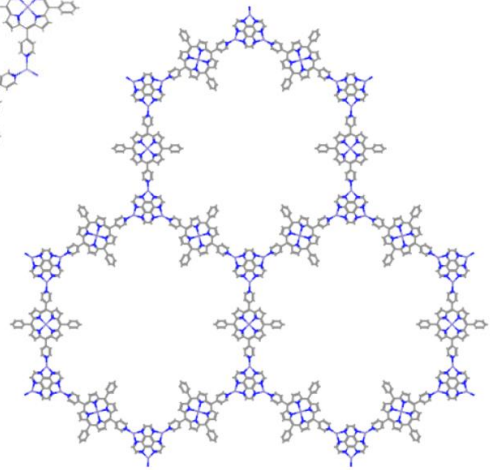

Au(111)
DPyP+HAT+Fe

$(Fe_3-HAT)_2(Fe-DPyP)_3$metal-organic framework

p-orbital Honeycomb Kagome Lattice

Acknowledgements

Supervisor：

Prof. Nian LIN

Collaborator:

Prof. Fengchuan Zhuang (DFT)

Prof. Feng Liu (DFT)

Prof. Yue Zhao (Transport measurements)

Dr. Jiaxiu Xu (DFT)

Dr. Bowen Xia (DFT)

Dr. Haiyang Pan (Graphene device making)

Colleague:

- Dr. Lei Dong
- Dr. Jing Liu
- Dr. Guoqing Lv
- Dr. Rang Zhang
- Dr. Ziang Gao
- Mr. Muqing Hua
- Mr. Songyu Mo
- Mr. Chengkun Lv
- Mr. Chengyi Chen

Thesis Examination Committee:

- Prof. Shingyu Leung (Chairperson)
- Prof. Nian LIN (Supervisor)
- Prof. Wei Xu
- Prof. Weijia Wen
- Prof. Haibin Su
- Prof. Yilong Han

Quantum Phenomena in Molecular Graphene Device and Metal-Organic Coordination Frameworks

THANKS

FOR YOUR WATCHING

HKUST Xiaobo Wang

2021.10.19